Dissertation
submitted to the
Combined Faculty of Mathematics, Engineering and Natural Sciences
of Heidelberg University, Germany
for the degree of
Doctor of Natural Sciences

Put forward by

JANICA CARMEN BÜHLER

born in: Weingarten (Germany)

ORAL EXAMINATION 6 JULY 2022

Statistical assessment and modeling of spatio-temporal patterns in speleothem records from the Last Glacial to present day

Referees: Prof. Dr. Kira Rehfeld
Prof. Dr. Werner Aeschbach

Zusammenfassung

Das Verständnis vergangener Niederschlagsänderungen ist immer noch unzureichend, trotz ihrer enormen Bedeutung für künftige Klimaprojektionen angesichts der anthropogenen Erderwärmung. Hier bewerten wir das Potenzial und die Limitationen von Paläoklimaarchiven und -simulationen vergangene regionale bis globale Veränderungen des Hydroklimas auf Zeitskalen von Jahren bis Jahrtausenden zu erfassen und aufzulösen. Wir vergleichen das Verhältnis von schweren zu leichten stabilen Sauerstoffisotopen, welches routinemäßig in Speläothemen als Indikator des Wasserkreislaufs gemessen wird, mit den simulierten Signaturen isotopengestützter Klimamodelle. Wir zeigen, dass ein Ensemble aus mehreren Modellen die hydrologischen Veränderungen zwischen dem letzten glazialen Maximum und dem mittleren Holozän genauer darstellt als ein einzelnes Modell. Der Vergleich wird durch Schwächen im Modell sowie in den Proxydaten erschwert. Speläothem-Wachstumsraten und Sauerstoffisotopenverhältnisse können, bei ausreichender zeitlicher Auflösung auf Zeitskalen, die nicht durch Karstdämpfung beeinflusst werden, als Indikator für Niederschlagsmengen in niedrigen bis mittleren Breiten dienen. Die räumlichen Muster der simulierten Sauerstoffisotopen-Verhältnisse weisen verglichen mit den Speläothem-Aufzeichnungen des letzten Jahrtausends nur geringe Abweichungen auf. Alle untersuchten Modelle unterschätzen jedoch die Variabilität auf Zeitskalen von Dekaden bis Jahrhunderten. Unsere Studie bildet die Grundlage für künftige Forschungen mit Proxysystemmodellen sowie zusätzlichen Paläoklimaarchiven und -simulationen, um die Mechanismen der simulierten und archivierten Veränderungen des vergangenen Hydroklimas weiter zu erforschen.

Abstract

Our understanding of past precipitation changes is still insufficient despite their relevance for future projections given anthropogenic warming. Here, we assess the potential and limitations of paleoclimate archives and simulations to record and resolve past hydroclimate changes on regional to global and interannual to orbital scales. We compare the abundance of heavy to light oxygen isotopes, routinely measured in speleothem records as water cycle tracers, to isotopic signatures simulated by isotope-enabled climate models. We show that a multi-model ensemble represents hydrological changes between the Last Glacial Maximum and Mid-Holocene more accurately than a single model alone. The comparison is hampered by limitations in both model and proxy data. Speleothem growth rates and oxygen isotope ratios can serve as proxies for precipitation amount in low- to mid-latitudes given sufficient temporal resolution and at timescales unaffected by karst damping. Spatial patterns of simulated oxygen isotope ratios show only small offsets compared to speleothem records for the last millennium. However, the analyzed models underestimate variability on multi-decadal to centennial timescales. Our study provides the basis for future research using proxy system models and additional paleoclimate records and simulations to further explore the mechanisms of simulated and archived changes of the past hydroclimate.

Contents

1 Introduction

Since the formation of this planet, around 4 billion years ago, weather and climate on Earth have been following the laws of nature. Physical, chemical, biological, and geological principles have formed this planet into what is now our home. Since humans roamed this planet, they needed to adapt to weather and climate conditions, wherever they settled. Changes in past climates can be linked to the major mass extinctions over the last 450 million years [255], and are hypothesized to have driven human dispersal out of Africa and into Eurasia [275]. The collapse of ancient cultures such as the Maya in Central America [141] or the Indus Valley Civilization [256] have been attributed to shifts in the past climate. Here, not only changes in temperature, but, in particular, changes in water availability might have led to food scarcity and thus to changes in politics, war, and population fluctuations [141]. Changes in the past climates are also of special interest as they provide reference to the current anthropogenic warming. High confidence statements of unprecedented greenhouse gas concentrations within the last 22,000 years [176] or medium confidence statements of global mean surface temperatures never being 2° higher than the pre-industrial state over the last 130,000 years [176] are only possible through the tireless effort and curiosity of paleoclimate researchers worldwide. The Assessment Report 5 in 2013 of the Intergovernmental Panel on Climate Change (IPCC) included a separate chapter dedicated to information extracted from paleoclimate archives [176, 41] to set reference to current changes. In the latest Assessment Report 6 [248], paleoclimate has since evolved into being woven into all chapters and provides a comprehensive view on all components of the climate system and its evolution to date [178]. In order to understand the future evolution of the current climate state, it is crucial to also look back and to understand past processes and climate evolutions [274]. Earth system experiments, where proposed hypothesis can be tested, are only available under one realization, which is its past evolution. To analyze past climatic changes that either happened before, or are on timescales longer than, the period of instrumental observations which started around 150 years ago [186], we can set up experiments using paleoclimate simulations or rely on evidence from paleoclimate archives.

Trees, ice cores, corals, stalagmites, and many other archives can store information of the past climate. These archives grow in accumulated layers where they store information of their surrounding climate. To name just a few examples - tree ring widths provide information about the growing conditions for the particular tree in a particular year, which can be translated into temperature and precipitation amount [20]; air bubbles that are trapped in the "eternal" ice of glaciers can give information on the chemical composition of a past atmosphere [240]; past sea levels can reveal past ice volume as stored in glaciers worldwide [185]. The abundance of the heavy oxygen isotope ^{18}O to ^{16}O in stable water isotopologues (SWI) is routinely measured in many palaeoclimate archives, such as stalagmite, coral, or ice core records to extract information of past climatic conditions. Isotopic ratios are usually given in δ-notation as $\delta^{18}\mathrm{O} = \left(\frac{\frac{^{18}\mathrm{O}}{^{16}\mathrm{O}}_{\text{sample}}}{\frac{^{18}\mathrm{O}}{^{16}\mathrm{O}}_{\text{standard}}} - 1 \right) \cdot 1000\ ‰$ against the Vienna Standard Mean Ocean Water [V-SMOW, 59, 140] for water

in its liquid and gaseous phases. In general, the composition of heavy to light isotopes is subject to the Rayleigh fractionation, which favours light isotopes in evaporation and heavy isotopes in condensation [140]. The isotopic composition of modern precipitation is well known [233, 125] and shows correlations to different variables [59, 304]. Positive correlation has been found to temperature, as an increase in temperature also leads to more intense evaporation. δ^{18}O and precipitation amount show a negative correlation, as the content of heavy oxygen isotopes decreases under a continuing rainfall process [304]. Other effects relate depletion in heavy isotopes (lower δ^{18}O) to altitude, continentality, or higher latitudes [59]. δ^{18}O compositions of precipitation or lake/sea water are saved in paleoclimate archives, e.g., in ice cores, stalagmites, corals, or even in the shells of crustaceans and can consequently be interpreted as climatic changes on different spatial and temporal scale. For example, temperature changes over the last 800,000 years [13], past changes in the El-Niño Southern Oscillation [43], European temperatures over the Holocene, the Last Glacial, and the Last Interglacial 120, 000 years ago [145], and intensity of monsoon systems from the Last Glacial to the Holocene[35, 195] have been extracted from various paleoclimate archives.

Speleothem records, better known as stalagmites and stalactites, form in cave systems globally under a wide range of climatic conditions. They grow as a calcite or aragonite matrix from calcium carbonate dissolved in acidic drip water saving its oxygen isotopes in accumulated layers [78]. δ^{18}O is the most widely used and best-understood proxy within speleothem records [203] and can be measured at decadal and higher resolution, with single records covering full glacial to interglacial cycles. The resulting well preserved and absolutely datable (semi-)continuous δ^{18}O time series reflect changes in cave temperature [284, 179] and the δ^{18}O composition of precipitation above the cave. The proxy signatures may, however, be overlaid by a mixture of superimposed signals, such as the δ^{18}O of the source water, transportation over large distances [20, 59], as well as large scale circulation patterns [289, 276]. Speleothem δ^{18}O is, thus, not straightforward to interpret and cannot directly be translated to past temperature or precipitation. Depending on the cave location and the local climate particularities, δ^{18}O signatures can contain information on local rainfall amount, regional hydroclimate variability, or changes in moisture sources [203, 83]. While speleothems and other climate archives are direct "witnesses" of past climatic conditions, they are, thus, only incomplete indicators when measured and analyzed, and reconstructions based on proxy records are spatially and temporally limited.

Climate models are mathematical representations of the climate system and the involved processes that are to be modeled, expressed as computer codes at different levels of complexity [215]. They can provide complete information on a climate system diagnostic or process that is incorporated in the model implementation. All processes within the model are consistent with the input model physics. In general, climate models are better in simulating surface temperature changes compared to changes in the hydroclimate, as hydroclimate is governed by processes that operate on fine spatial scales, which cannot be resolved in the models. Convection schemes and cloud physics need to be parameterized in order to obtain well represented large-scale atmospheric circulation patterns [203]. The incorporation of SWI into the hydrological cycle of many climate models provided new opportunities to trace, analyze, and evaluate the representation of the model water cycle compared to precipitation observations [277, 298]. While different models may obtain very similar diagnostics (e.g. surface temperature and precipitation patterns) under present-day conditions and compare well with observations, they can produce very different climatic responses to climate states under a different forcing background such as future scenarios of anthropogenic warming [66, 146]. For past climate periods such as

the Last Glacial Maximum (LGM), climate models produce global mean temperatures of a range of $3-6^{\circ}$ colder than the pre-industrial state. Amongst other effects, this large range of possible climate states sources from differently prescribed ice sheets, climate feedbacks arising from changes in the surface albedo, or ocean heat uptake [19]. The Paleoclimate Model Intercomparison Project (Phase 3 PMIP3 [131] and Phase 4 PMIP4 [133]) and the overarching Coupled Model Intercomparison Project (Phase 5 CMIP5 [268] and Phase 6 CMIP6 [76]) assess models under these different climatic conditions, which can reveal if the physics and the coupling between different climate subsystems in the model is simulated correctly. Through their effort, PMIP evaluations of climate models under past climate states has served to confirm the soundness of model implementation [19].

Climate models are able to provide an "out-of-sample" source to validate information obtained from paleoclimate archives. Vice versa, proxy records and paleoclimate reconstructions can be used to evaluate climate models in different climate background states. Model-data comparisons on a global scale have been made possible by the constantly growing number of available proxy measurements and large ensembles of paleoclimate simulations, and are now a commonly used method to constrain both modeled and archived climate information. Model-data comparisons can be used on very different temporal and spatial scales. For example, Liu et al. (2014) were able to identify biases in climate sensitivity in climate models, as well as seasonality biases in proxy reconstructions of the last 11,000 years that led to a perceived cooling trend from early to late Holocene [172, 165]. Comas-Bru et al. (2019) use an isotope-enabled climate model and compare the δ^{18}O signatures to speleothem records, to draw attention to generic issues in model-data comparisons to speleothem records and set potential standards for future studies [48]. Dalaiden et al. (2020) were able to find stronger relationships between surface temperature and Antarctic ice sheet surface mass balance than to δ^{18}O in modeled signatures and were thus able to assimilate more realistic reconstructions of recent Antarctic temperatures [58]. Comparisons with modeled δ^{18}O facilitate a comparison on equal ground to archives that store δ^{18}O and circumvent calibrations as a possible source of biases.

In this work, we analyze past hydrological changes as archived in speleothem records and as resolved by climate models. Model-data comparisons using isotope-enabled models provide the unique opportunity to evaluate the hydrology as resolved by different climate models as well as the extent to which variability of the hydrological cycle is recorded in archived signals of speleothem records. By combining information of speleothem records and climate models to analyze hydrological changes, the key questions addressed in this thesis are:

- What dating resolution is necessary to confidently detect speleothem growth rate changes? Do these growth rate changes indicate past hydrological changes?
- How similar are modeled and archived isotopic signatures? Can we distinguish main drivers of δ^{18}O variability?
- Can speleothem records serve as a valuable archive to detect hydrological changes on glacial to interglacial timescales? Can archived changes be resolved by state-of-the-art climate models?

Speleothem growth rates are hypothesized to reflect local changes in precipitation amount, albeit the response to hydrological changes may be non-linear and subject to karst specific processes [77]. As speleothems can cover full glacial-interglacial cycles, in particular record changes between the LGM and the Holocene, and are dated through

high precision U/Th or radiocarbon measurements [243], they are suitable to assess and constrain state-dependent precipitation changes. To extract this valuable information from speleothem records, a reliable age-depth relationship and sufficient dating resolution are necessary. However, inherent features to speleothem growth, such as growth hiatuses or large and abrupt changes in growth rates, are a challenge for current age-depth modeling methods. The estimated age uncertainties, which correspond to integrated time within one depth measurement, present additional challenge to the interpretation of the age-depth profile [217].

The introduction of an isotope-enabled water cycle to state-of-the-art climate models provides the opportunity to compare climate model diagnostics to climate archives on equal ground without additional error sources through calibration methods. Comparing these signatures in paleoclimate archives to those modeled in general circulation models can reveal valuable information on water cycle dynamics as well as uncertainties and limitations of both information sources [203]. While topography and parameterization of physical processes in climate models can complicate one-by-one comparisons, archived proxy interpretation itself is usually not straightforward, as different drivers of the isotopic signal often superimpose at the proxy location. Examining these challenges in stable close-to-present-day conditions with a high abundance of speleothem records is, therefore, crucial to detect and interpret biases in both model and data, before exploring other time periods.

Speleothem growth rate changes as well as $\delta^{18}O$ signatures provide information of hydrological changes between the LGM and the Mid-Holocene (MH). Past and future changes of the water cycle and its dynamics are far less understood and more uncertain than changes in temperature, yet just as much affect ecosystems, society, and economy [40]. While speleothem growth rates are directly dependent on the amount of available drip water [69], isotopic signatures only reflect precipitation amount changes if precipitation above the cave is mostly influenced by the amount effect [59]. The extent to which isotopic signatures in speleothems can thus serve as a proxy for precipitation amount changes on a global scale is unclear. However, multi-model comparisons between isotope-enabled models in both the LGM and the MH have not yet been evaluated. Even under PMIP3-simulations, modeled global mean temperature ranges between $3 - 6^{\circ}$ compared to pre-industrial conditions [19], which consequently results in a wide range of changes in the water cycle. Deeper insight into past hydrological changes contributes to our understanding of a changing water cycle under different climatic background states and is, thus, crucial for reliable future projections.

In summary, the focus of this thesis is to analyze climate simulations' capability to model and the speleothem records' capability to capture hydrological changes under different climate backgrounds. Using a large database of speleothem records, a large data set of reference records of hydroclimate changes, and a large ensemble of climate simulations by different climate models over different background states, we aim to thoroughly test both model and data to improve our understanding of processes and uncertainties of both. Step by step, the key questions of this thesis are addressed as outlined below:

Chapter 2 explores the age-depth relationships in synthetically modeled speleothem records with growth rate changes to assess the performance of different age-depth models under decreasing dating resolution. The findings are tested on real speleothems from the SISALv2 database to compare variations in growth rates between the LGM and the MH.

Chapter 3 compares isotopic signatures in speleothem records from the last millennium to isotope-enabled general circulation models, in particular iHadCM3, to benchmark

commonalities and differences between the modeled and archived signatures in space and time.

Chapter 4 applies the developed methods and findings on age-depth relationships and isotopic signatures in climate models and speleothem records. We investigate the potential and limitations of using speleothem records as proxies for hydrological changes on glacial and interglacial timescales, and how well these changes are resolved in climate models.

Chapter 5 discusses and interprets the findings from all previous chapters and gives an outlook on future studies.

Appendix A provides additional analysis to Chapter 2-4 that complement the results described in the respective chapters. The analysis presented in Chapter 3 in this thesis is based on previously published work in "Comparison of the oxygen isotope signatures in speleothem records and iHadCM3 model simulations for the last millennium" [24] as well as the discussion paper "Investigating oxygen and carbon isotopic relationships in speleothem records over the last millennium using multiple isotope-enabled climate models" [25], which are listed in the publication list on page 121.

2 Intercomparison of age-depth models for speleothem growth rate assessment

In this chapter, we test the skill of age models to reconstruct growth rate changes within a set of speleothem records. Speleothems are secondary cave deposits and form in accumulated growth layers in stalagmites, stalactites, or flowstone. They grow in cave systems globally in calcite and aragonite matrices from calcium dissolved in drip water. Thus, they can archive oxygen and carbon isotopes, as well as multiple trace elements as proxies of surface climate and cave processes [78]. Their great advantage compared to other paleoclimate archives are the U/Th-dated time series with unmatched precision over a range of the last 650,000 yr [241]. The high resolution in both age and climate proxy measurements makes them a suitable archive to analyze past climate variability with increased popularity over the last decades [81, 292, 70, 77].

Both age measurements and climate proxy measurements are generally taken at specific depths of the record which is later translated into an age. However, the spatial resolution of age measurements along the speleothem growth axis is usually much lower than climate proxy measurements due to the high expenditure of analysis time and the large volume of required material. While more than 100 isotope measurements per day are possible in numerous labs with no more than 20 $ per measurement, U/Th measurements are ten times more expensive and require much more time both in measurement, as well as in traveling to those labs, that facilitate the measurements [193]. Methods of different complexity for constructing age-depth models are readily available from the literature [242, 22, 107] and provide age estimates at the depth of a proxy measurement. The resulting uncertainties in the integrated time within one proxy measurements present a challenges to the interpretation of the proxy time series.

On the glacial and interglacial timescales that speleothem records cover, global changes in precipitation are influenced by the saturated water vapour pressure and thus by global changes in temperature as approximately described by the *Clausius-Clapeyron relation*. The atmosphere's capacity to hold water increases by 7 % under a 1°C warming [174], which could consequently lead to more precipitation depending on local and regional particularities. Speleothem growth rate changes are hypothesized to reflect local changes in precipitation amount [71, 112]. Higher precipitation amount in the infiltration region of the cave generally leads to more water that carries dissolved calcite into the cave, and in turn to higher accumulation rates in the cave environment [69]. Glacial to interglacial changes in hydroclimate, e.g., between the LGM (29-17 ky BP) and the Holocene (8-0 ky BP) may, thus, be recorded in speleothem growth rates. To test the hypothesis of increased speleothem growth rates during Glacial and Interglacial climate conditions, the SISALv2 database provides a large collection of speleothem records with precise dating and age-depth relationship information over the two time periods [4, 49]. However, the presence of speleothem-inherent features, such as growth hiatuses, large and abrupt

changes in growth rates [243], and the non-linear response of drip rates [278] constitute a challenge for current age-depth modeling methods. Therefore, the question remains if these changes in growth rates can be detected in typical speleothems within the database.

Here, we compare six different age modeling approaches (linear regression, linear interpolation, copRa [22], StalAge [242], Bacon [17] and Bchron [107]) and systematically test their skill in detecting and modeling growth rate changes on a large ensemble of synthetically modeled speleothem growth histories. The findings from case studies on synthetic speleothem growth rate changes are then applied to real speleothems from the SISALv2 database.

The key questions addressed in this chapter are:

- What are the strengths and weaknesses of the different age models regarding growth rate change detection?
- What is the lowest number of datings in speleothem records that is necessary for age models to confidently detect and model growth rate changes?
- Can we detect changes in growth rates in the SISALv2 database between the LGM and the Holocene?

Answers to these questions are first steps toward analyzing past hydrological changes using speleothem records from a global database and, with it, toward constraining future changes. These steps are necessary in order to test the reliability of information that we want to extract from speleothem paleoclimate archives.

After a literature review on speleothem records as a paleoclimate archive, we will introduce the SISALv2 database, the age models used in this analysis, the synthetic speleothems, and the constructed test cases. The systematic analysis of synthetic growth rate changes will reveal the minimum requirements on speleothem records for growth rate change detection, which will be applied to the SISALv2 database. The selected speleothem records will be analyzed to test the hypothesis of higher speleothem growth rates in the Holocene compared to the LGM. The identified key questions will be discussed and finally summarized.

2.1 Speleothems as paleoclimate archives

Speleothems are mineral cave deposits which form in limestone caves in karst regions under a wide range of climatic conditions. Speleothems have been found in extremely cold [157] conditions at around 80°N [187], as well as in extremely arid [191] or extremely hot and humid conditions [207]. Their occurrence is only limited by the availability of water and suitable bedrock that allows for water to drip from fractures. As a terrestrial climate archive, they are able to store climatic and environmental information on continental paleoclimate changes [20]. Several formations exist, though the most common are stalactites which grow from a dripping cave ceiling, stalagmites which grow from the cave floor, and flowstones which form underneath a thin water layer on walls and floors [77]. Stalagmites are most commonly used in paleoclimate research, as their solid internal structure of accumulated layers along a growth axis allows for the observation of different time periods [78]. Lateral shifts of the growth axis through drip-point changes on the cave ceiling as well as growth interruptions (hiatus) complicate the interpretation.

Speleothems form from drip water, where dissolved calcium carbonate from the cave bedrock precipitates to form calcite and aragonite matrices (drip-water path illustrated

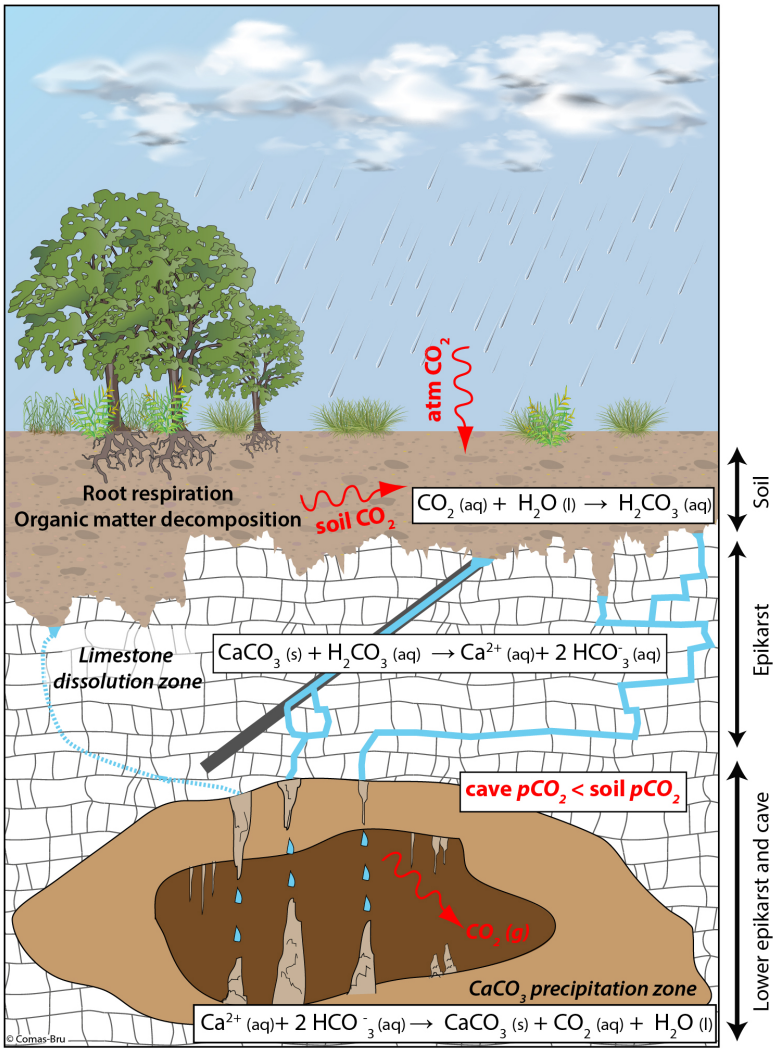

FIGURE 2.1: Formation of speleothems in cave systems. Infiltrating surface water is charged with soil gas CO_2, where the partial CO_2 pressure is larger than in the atmosphere, facilitating the carbonic acid-driven $CaCO_3$ dissolution of the host rock in the *limestone dissolution zone*. The solution travels through the epikarst and aquifer system, on different paths, where it can also mix with older residual water. Eventually, the solution reaches the lower epikarst and by chance a cave environment. The generally lower partial pCO_2 pressure conditions in the cave environment compared to that of the soil and epikarst makes the drip water degas and precipitate calcite in a fractionation process, which consequently forms a speleothem [280]. Illustration from Laia Comas-Bru [47].

in Fig. 2.1). The seepage solution not only contains dissolved calcium carbonates but also trace elements such as sulfur [91], magnesium, and strontium [78]. The most important trace element may be uranium, from which absolute age estimates for speleothems younger than 650,000 yr can be obtained (limited by secular equilibrium) [241], by measuring Uranium - Thorium (U/Th) ratios. This technique circumvents more limited dating methods like radiocarbon age calibration [180]. While uranium is soluble in water and can thus be transported in the calcium carbonate drip water solution, Thorium is considered to be insoluble. Concentrations of thorium during speleothem formation are, therefore, presumed to be zero and only accumulate over time, through uranium decay chains [126]. Dating uncertainties depend on the abundance of uranium, as well as the total age of the record. There are usually fewer dating measurements than the less costly proxy sample measurement. Appropriate age-depth models, as explained in Sec. 2.3.2, need to be constructed to assign a date to each sample, resulting in an irregular time series of the sampled proxy.

The most common proxy which is measured in speleothem archives, are oxygen isotope ratios (δ^{18}O) [180, 150] and the less popular carbon isotope ratios (δ^{13}C) [302]. Under equilibrium fractionation conditions, δ^{18}O in speleothems is only dependent on the δ^{18}O composition of the source water and the cave temperature at the time of the speleothem formation [113, 150]. Kinetic effects, which can be caused by cave ventilation and changes in humidity, may obscure the original δ^{18}O signal. Additionally, the source water is already influenced by atmospheric circulation and the climate system [59, 233]. Therefore, the amount of precipitation, its isotopic composition, the annual mean temperature, the isotopic composition of the source water, the changes to it during moisture transportation and re-evaporation, and the variability of these atmospheric events are in part imprinted in the archive.

Vegetation above the cave can alter the composition of δ^{18}O that infiltrates the soil [293] and may add a seasonal imprint, depending on the seasonal vegetation water demand. While no isotopic fractionation occurs during transpiration, seasonal potential evaporation at the cave site can cause additional fractionation of the meteoric δ^{18}O [108, 272, 290]. Transportation through the soil and epikarst level, filtering processes [60], and vadose-zone fractionation [280, 103, 231] pose further impacts to the signal. Different transit paths of the calcite solution through the epikarst may lead to varying transit times between years [145] and decades [127] at different drip sites even within the same cave. Inside the cave environment, seasonal changes in CO_2 pressure can be imprinted in the oxygen isotopic signal but also, e.g., in speleothem growth rates and may pronounce or attenuate the climate signal from meteoric precipitation composition and amount [77]. During the calcification process, interactions with the cave environment or water inclusions within the mineral are still possible and can still lead to minor changes in archived δ^{18}O.

Carbon isotope signatures are mainly determined by soil CO_2 after entering the soil layer, which is influenced by plant roots' respiration and decomposition of organic matter [302]. This CO_2 is closely related to the type of vegetation (C3, C4 or CAM [269]), which is also influenced by climatic parameters that favor specific vegetation. Speleothems in areas dominated by C3-plant vegetation cover usually have much lower δ^{13}C values, compared to C4-plant cover. Inside the karst and cave environment, calcite precipitation prior to the research site (prior calcite precipitation, PCP) can lead to substantial changes in the δ^{13}C signal and enhance variability [160, 87].

Speleothem growth rates depend on mainly two factors: how much calcium carbonate

can precipitate from one drop of drip water, and the amount of drip water. Under constant drip rate, the production of degassing CO_2 on the solid surface is determining the growth rate [69]. This production depends on the calcium concentration in the drip water, the water film thickness on the solid surface, and temperature. As such, higher calcium concentrations, thicker water films and higher temperatures lead to higher calcium carbonate precipitation [8]. Under constant water film thickness and water supersaturation, calcium carbonate precipitation depends on the drip rate and temperature. A higher drip rate under higher temperature and constant calcium concentration leads to more precipitation, which could be confirmed for many currently growing speleothems [8, 94]. In the cave environment, where concentrations can change, a higher drip rate is, however, often an indicator of short residence time in the bedrock resulting in lower calcium concentration in the drip water, and ,therefore, in lower calcite precipitation [150, 11, 6]. Recent studies find speleothem growth rates to also control kinetic fractionation and, thus, influence the recorded $\delta^{18}O$ variability. This is why they need to be accounted for in the interpretation of oxygen isotopes in speleothems with significant growth rate changes [261]. A comprehensive summary of the processes involving speleothem growth can be found in Fairchild and Baker (2012) [77].

Oxygen and carbon isotope signatures, and growth rate changes in calcite and aragonite speleothems can be influenced by a combination of all above-mentioned factors. Due to the multivariate processes impacting speleothem formation, the interpretation of the studied proxy signal is not straightforward. Systematic evaluation of $\delta^{18}O$ and $\delta^{13}C$ signatures in drip water or calcite has identified patterns of similar climate influence based on modern observations [7, 87]. Proxy System Models (PSMs; see Sec. 3.3.2), which model the input signal based on the known processes in the karst, may also help with the interpretation [75, 60].

2.2 The SISALv2 database

The Speleothem Isotope Synthesis and Analysis (SISAL) working group is an international working group, which globally collects speleothem data in a quality-controlled and cross-referenced database with rich metadata for carbon and oxygen isotope samples and dating procedures [4, 49]. The database has continually expanded from the first version [4] with 381 speleothem records from 174 cave sites to 691 individual entities from 294 globally distributed sites in the second version [49] (depicted in Fig. 2.2).

Here, we only consider data from entities which are not superseded (*entity_state* = *current*), and check for dates marked as *used*, indicating that they are known to have been used within the original chronology in the database. We omit entities, where sample or depth information are not available. The records show a large variation in their complexity and have a median coverage period of 6930 yr (min: 46.8, max: 492560) over a median depth of 399.18 mm (min: 8.4, max: 5725), with a sample resolution of 24.17 yr (min: 0.02, max: 3302.82) and 16 datings per 10,000 yr per speleothem entity. The average relative dating uncertainty per 10,000 yr is 199.7 yr (0.1 , 4400). 176 records contain at least one hiatus (the maximum being 9, median: 1). More than 80 % of datings are conducted using U/Th measurement techniques. For each U/Th-dated speleothem, SISALv2 provides the original age model (if available), and, additionally, new age models based on up to seven methods. On average, four new age models are available. Methods include linear interpolation, linear regression, Bchron [107] as adapted by Roesch and Rehfeld (2019) [230], Bacon [17], Oxcal [214], copRa (modified R version after [22] in [49]), and StalAge [242] and will be discussed in detail in Sec. 2.3.2.

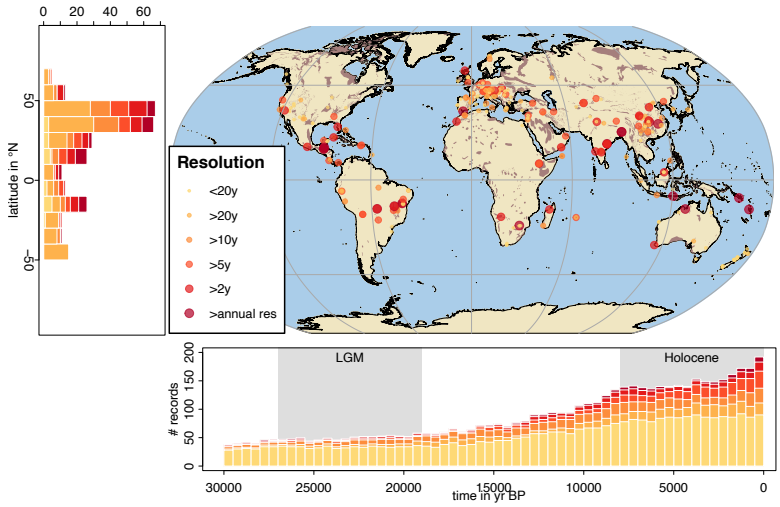

FIGURE 2.2: Latitudinal distribution, temporal coverage and site locations of all entities in the SISALv2 database [49] color-coded by temporal resolution. The brown shadings indicate karst regions [300].

The SISALv2 database has been used to analyze past regional climate changes [161, 28, 138]. As speleothem entities reproduce first-order spatial patterns of oxygen isotope variability, the database is suitable to evaluate modeled $\delta^{18}O$ across multiple time periods [48]. It has, therefore, also been employed in model-data comparisons of the Last Glacial Maximum, the Mid-Holocene, the last millennium, and the historical period using different models (iCESM: [184], iHadCM3: [24], ECHAM5-wiso: [48, 205] and GISS-E1-R: [205]).

2.3 Methods

2.3.1 Synthetic speleothems – creating test-case studies

Synthetically modeled speleothems provide the opportunity to test and assess the robustness and skill of age model algorithms on a known artificially generated speleothem. A "true" growth history is simulated and then artificial dates and proxies are sampled at specific depths. While models for speleothem growth of various complexity have been developed recently [68, 232], this analysis uses the computationally efficient synthetic speleothems as described in Rehfeld and Kurths (2014) [217]. Here, the main controlling parameters on the growth of a synthetic (or virtual) stalagmite are its growth rate λ in mm yr $^{-1}$, it's total length in mm, and the type of accumulation, which can be linear or modeled via randomly distributed accumulation rates. For this case study, the synthetic speleothems always have a fixed length of $1,000$ mm. Growth rates vary according to the case studies. To accommodate varying growth rates on a microscopical scale, gamma-distributed accumulation times are drawn at each depth, while the sample rate is kept constant. This growth history is further denoted as the "true" growth history or "true" age-depth relationship.

In real-life analyses, speleothems are dated at specifically chosen depths that will facilitate the compilation of an age-depth relationship. For example, age-measurements are often taken directly above and below a hiatus, if the hiatus is apparent from visible inspection. Dating techniques are based on U/Th, where dating uncertainties typically range from 0.1 to 0.5 % of the measured age, depending on initial concentration, overall

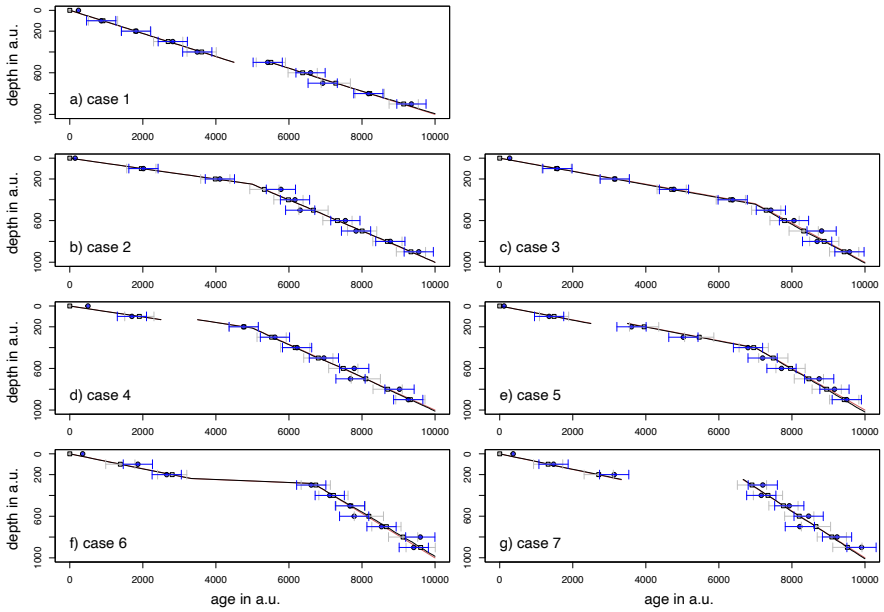

FIGURE 2.3: Example of case studies as used in the synthetic speleothem experiments. All synthetic speleothem examples cover 10,000 yr in a 1,000 mm synthetic stalagmite and have 10 datings with a precision of 200 yr. a) has a constant growth rate of 100 μm/yr with an hiatus of 1,000 yr b-g) all show a relative growth rate change of 3 at 5,000 or 7,000 yr. c) and e) include a hiatus of 1,000 yr starting at 2,500 yr. g) includes an hiatus at the same position and length, whereas f) has a very slow growth rate.

age, and contamination [77]. For the synthetic speleothems, we chose dating samples at equidistant depths and do not account for expert knowledge that would increase the robustness of an age-depth model, e.g., by manually identifying dating outliers. The center point of the assumed "measured" age distribution is hereby taken directly from the "true" growth history. The age uncertainty at the first date measurement is set to an absolute precision p and slightly increases proportional to the age. Hiatuses are modeled by a growth rate of zero.

In this study we constructed seven case studies. Speleothem growth rates are typically around 100 μm/yr [77]. On a 1,000 mm speleothem, this translates into a time range of 10,000 yr. The goal of the case studies is to find the minimal number of age measurements required to detect growth rate changes under increasing difficulty for the models. Each case is analyzed with each age-modeling method under a different number of age measurements. The age-modeling is repeated 50 times per parameter setting, where growth rates changes can vary. To avoid similar results due to dates at the same depth, we chose the number of datings in a way that they are not multiples of each other: 26, 17, 14, 10, 6, 4. The first dating is always at zero depth, to mimic real speleothems, where the first dating is at $1-10$ mm depth.

Case 1 as in Fig. 2.3a does not include a growth rate change, but an hiatus of 1,000 yr between 4,500 and 5,500 yr. This case was chosen to quantify the general performance of the age-depth models with a small difficulty of one hiatus.

Case 2 as in Fig. 2.3b includes a medium growth rate change where the second growth rate is between 2 and 4 times higher than the first one, and occurs at 5,000 yr. This means that if the second growth rate is twice (four times) the first growth rate, the growth rate

will be 66 (40) μm/yr for the first 5,000 yr, which will cover $\frac{1}{3}$ ($\frac{1}{5}$) of the depth, and then 130 (160) μm/yr for the second 5,000 years, which will cover $\frac{2}{3}$ ($\frac{4}{5}$) of the depth. No hiatus is involved in this case.

Case 3 as in Fig. 2.3c is the same as Case 2, but the growth rate change occurs at a uniformly random time between 3,000 and 4,000 yr or between 6,000 and 7,000 yr. The growth rates are chosen as in Case 2, but it is also randomly decided if the faster growth rate is at the beginning or at the end.

Case 4 as in Fig. 2.3d is as Case 2 but includes an hiatus which randomly begins between 1,000 yr and 8,000 yr and is 1,000 yr long. The growth rates, which are chosen as in Case 2, are adapted to accommodate the hiatus.

Case 5 as in Fig. 2.3e is as Case 3 but with an added hiatus similar to Case 4.

Case 6 as in Fig. 2.3f includes two growth rate changes: one at 3333 yr and another one at 6666 yr. The growth rates are slow (15 μm/yr), medium (80 μm/yr), and fast (200 μm/yr). The order of the growth rates is mixed randomly. Depending on the number of age measurements per depth, it is possible that no date is obtained in the very slow growth rate section, which adds a challenge to the age models.

Case 7 as in Fig. 2.3g is as Case 6 but instead of the slow growth rate, a hiatus of growth rate zero is added, which can be at the beginning, the middle or the end. In terms of the age-depth profile of the synthetic speleothem, this does not change a lot. However, the different age models have different ways of including hiatuses in their calculations.

2.3.2 Relevant age-depth modeling methods in speleothems

Crucial for the use of proxy measurements is the estimation of an age for each proxy measurement depth. This is accomplished by reconstructing the age-depth relationship of the speleothem through interpolation between adjacent absolute datings, which is referred to as age-depth modeling. Multiple age-depth modeling approaches of varying complexity which are based on various statistical bases have been introduced in the past decades. However, no standard approach has been established [243].

Age-depth modeling requires two data sets: the (U/Th) dated points with their respective errors (Θ_i,σ_i) and depths $\{d_i; i = 1, ..., n\}$ and usually a higher number of the depths corresponding to the measured proxy values $\{D_j; j = 1, ..., m\}$ for which age estimates are required from the model. An age model can be described by a function $d(\Theta)$ which follows these assumptions, based on physical properties of speleothem formation [22, 107]:

- *Monotonicity:* arising from the stratigraphic growth ("the deeper the older")
- *Continuity:* an age exists for every desired depth in the speleothem
- *Flexibility:* as speleothem growth rates can change with changing environmental conditions, so can the slope of $d(\Theta)$
- *Increased uncertainty between age measurements* as less information is available there

A major challenge of age modeling during the dating process are reversals and outliers (see Fig. 2.4). A reversal is defined as a violation of growth monotonicity. In general, there are tractable and non-tractable reversals (highlighted green in Fig.2.4), depending on the overlap between the age-measurement uncertainties. Outliers are dating points

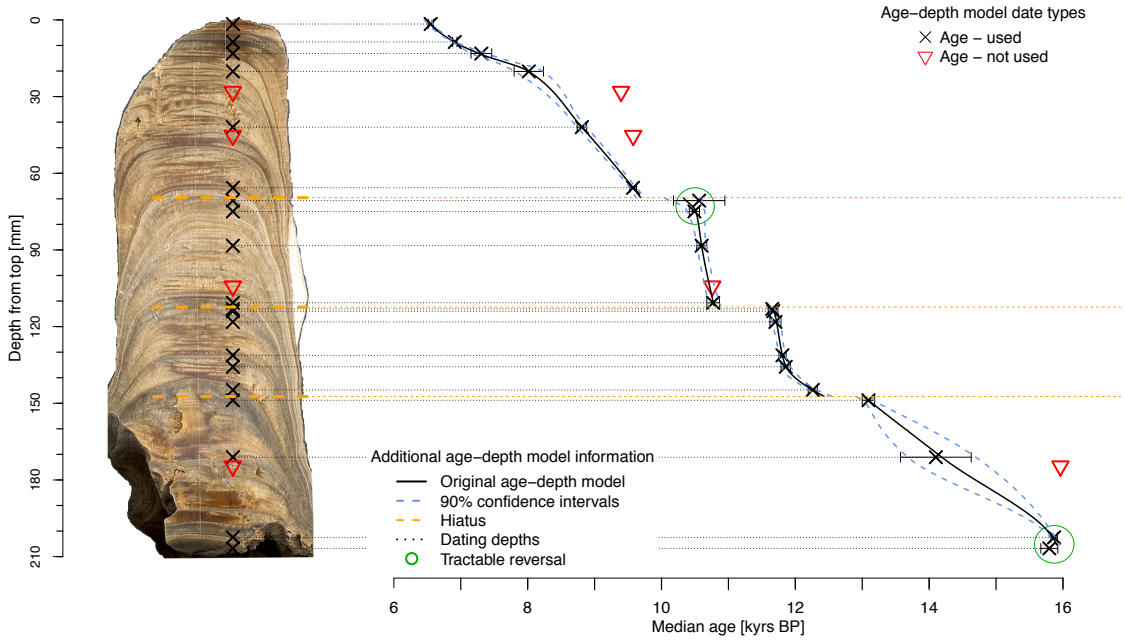

FIGURE 2.4: Example of an age-depth relationship in a stalagmite (eID 63). Age measurements are taken at specific depths (usually from top to bottom). This example has three growth hiatuses (orange dotted lines), two tractable reversals (highlighted green) and four outliers (red triangles). From the used dates, an age-depth relationship is constructed and provides age estimates between radiometric dates. Figure and caption adapted from [230], original record from [159].

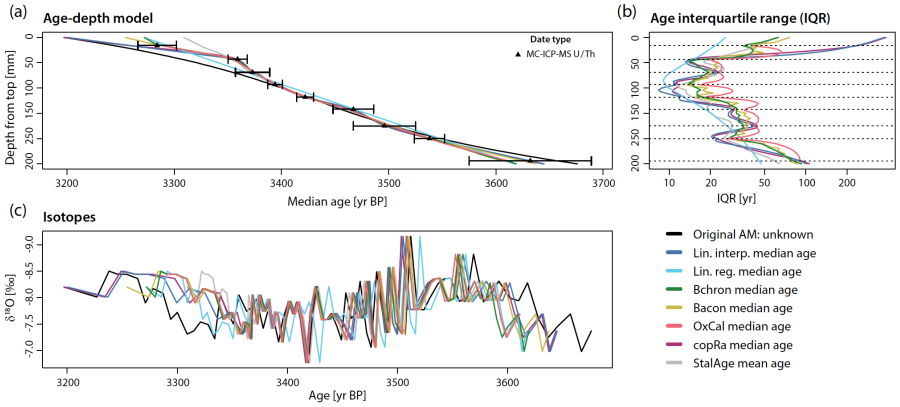

FIGURE 2.5: Illustration of how the reconstructed chronology based on the chosen age model can impact the interpretation of the isotopic signal on the example of KNI-51-H speleothem record (eID 342; [62]). a) median age estimate, b) interquartile range of the ages, c) isotopic record using the different reconstructed chronologies. Figure and caption adapted from [49].

that strongly deviate from a realistic age-depth relationship, which is why they most often cause non-tractable reversals [22].

A second challenge are growth hiatuses, which are a consequence of changes in the cave environment or the surrounding climate. Different age models handle hiatuses differently: some create an artificial date in the hiatus, while others calculate two separate age-depth relationships before and after the hiatus.

The construction of an age-depth relationship can strongly influence the interpretation of the proxy time series (Fig. 2.5). Depending on methodological choices, considerable temporal differences can arise, which complicate analyses that rely on the exact timing of events or correlation between time series. All age-depth models used in this study have been optimized for automatic use as described in Roesch (2020) [229]. This includes minimum input and interaction required by the user, and reproducibility of chronologies, e.g., by saving artificial ages that were added during the calculation or the Monte Carlo ensemble that some age models use.

Linear age-depth modeling methods

A non-weighted *Linear Regression* (LR) is used to calculate an age-depth slope from which age estimates at sample depths can be retrieved. In case of an hiatus, the model is split at the hiatus depth and two separate age models are produced. Speleothem records most often exhibit non-constant growth rates, which make simple *LR*s unsuitable for speleothem age-depth relationships. Still, this very simple *LR* will be considered as a reference model.

Linear interpolation (LI) is the next more complicated model compared to *LR*. Here, age-depth relationships are obtained through *LI* between adjacent dates. In case of an hiatus, an "artificial" date between the two adjacent dates is added to the dating table. For both the *LI* and *LR*, age estimates are calculated from a Monte Carlo ensemble, where ages of datings are sampled normally according to the age uncertainties, and checked for reversals. Linear methods such as *LI* and *LR* are used for 42% of the SISALv2 original chronologies. Both methods do not include a procedure which automatically traces

reversals, which is why the *StalAge* reversal scan is executed prior to the age-depth modeling.

copRa is a version of the age-depth modeling approach *COPRA* adapted for the statistical modeling software R [213, 229], but originally implemented in Matlab [22]. Compared to *LI*, it uses 2,000 Monte Carlo iterations fitting a piecewise cubic hermite interpolating polynomial (pchip) spline in the age-depth modeling process. While the original implementation allows for a wide range of options, based on the number detected or manually selected reversals or hiatuses. As in *LI*, we add the "artificial" hiatus age to the dating table in case of an hiatus. The automatically adapted R-version uses the *StalAge* reversal scan prior to the age-depth modeling. The original *COPRA* model is used in 6% of the SISALv2 original chronologies.

StalAge is an R-based age-depth algorithm first published by Scholz and Hoffmann (2011) [242]. It uses a Monte-Carlo approach to successively fit straight lines within given error bars on a subset of dating points. The best age estimate is calculated from the Monte Carlo ensemble and checked for reversals. In case of an hiatus, it is recommended to split the age model into two parts. In this study, we also use the "artificial hiatus age" and add it to the dating table before running the model. *StalAge* and combined methods are used in 15.3 % of the SISALv2 original chronologies. The popular usage originates from the universal application of the method, which simplifies usage for non-experts.

Bayesian age-depth modeling methods

While linear methods as described above try to fit a realistic relationship into the available age-depth measurements, the Bayesian models used in this study extract an age-depth relationship from a previously modeled sedimentation or accumulation process based on available datings and typical sedimentation rates. Bayesian models only account for 4% of the SISALv2 original chronologies.

Bchron was developed by Haslett and Parnell (2008) [107] for the study of lake sediment accumulation. Here an inverse sedimentation rate is modeled as a piecewise linear compound Poisson-Gamma process as a prior to the age model function. The sedimentation rates are a ratio of exponential and gamma-distributed random variables. This ensures independent and identically distributed sedimentation sections, with a skewness toward low sedimentation rates. Hiatuses, which would mean a sedimentation rate of zero, cannot be modeled and instead are added as "artificial" dates as in some linear methods.

Bacon was also originally developed to study deposition processes in lake sediments by Blaauw and Christeny (2011) [17] and was inspired by *Bchron* but used environmental constraints to define the model prior. This is achieved through applying a non-Gaussian autoregressive model for the sedimentation rate, which includes a "memory" from previous steps. In this way, hiatuses can be modeled by loosing memory in the autoregressive accumulation for the duration of the hiatus. Outlier probabilities are modeled by a Student-t test for each date.

2.3.3 Strengths and weaknesses of age-depth models tested on speleothems

The presented age-depth models feature different strengths and weaknesses. Roesch (2020) tested the age models on synthetic speleothems of constant growth rate and constant number of datings, but varied the number of hiatuses and the precision of the datings [229]. For the linear age-depth models, they find a low skill of the age model at both extremely high and extremely low precision. High precision increases the difficulty in fitting the model to the datings while including the hiatus at the same time. Low

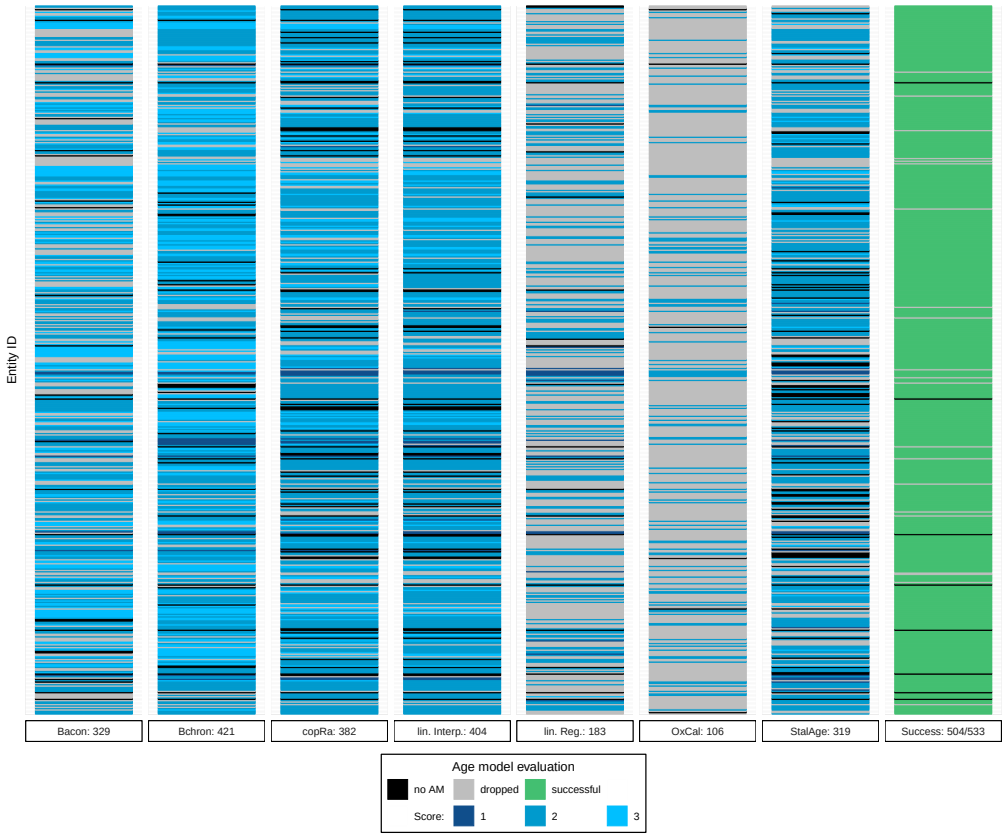

FIGURE 2.6: Evaluation of the age models computed for the SISALv2 database [4, 49]. "Entity_ids" are assigned to the y-axis. The x-axis denotes the various age modeling methods and the number of successfully produced age models. Black marks age models that cannot be computed and grey represents age models that are dropped in a final screening. The scoring of the age models is given in blue. The lighter the blue the higher the individual age model score. Green marks records for which at least one age model is successfully constructed. OxCal age-depth models are not considered in this thesis. Figure and caption adapted from [229, 49].

precision increases the possibility of reversals which causes *LI* and *copRa* to often fail. The number of hiatuses also increases difficulty and decreases coverage of the calculated and the true age-depth relationship. *StalAge* produces skillful age-depth relationships, except for extremely low precision. While *Bchron* was not tested, *Bacon* produces skillful age-depth relationships over all combinations of dating precision and number of hiatuses compared to the other models.

Testing on real speleothems from the SISALv1 database [4] reveals more differences between the models using the introduced models (Fig. 2.6). A successful model acquired scoring points if the output age-depth relationship fulfilled the theoretical assumptions on age-depth models (monotonicity, flexibility, uncertainty increase between datings; Sec. 2.3.2). Here, *Bchron* shows the highest success rate, and *LR* the lowest. The linear models also show a higher number of dropped or failed age models, which is attributed to difficulties during growth rate changes.

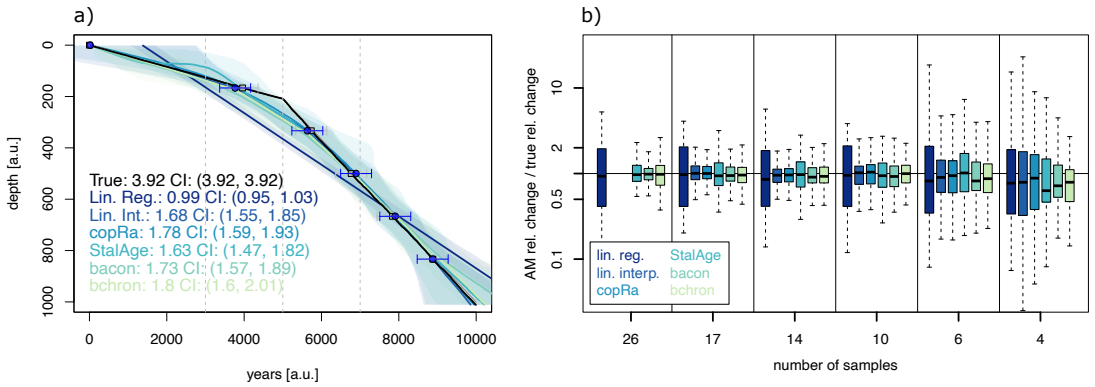

FIGURE 2.7: a) example of simulated growth rate change of 3.92 at year 5,000 with 6 datings from the ensemble on case 3. Age-depth relationships including uncertainties as calculated by different age models are depicted in the age model colors. The calculated growth rate change includes all age-depth pairs 2,000 yr before and after the true growth rate change. b) summary of all growth rate changes relative to the true growth rate change across all cases that include a growth rate change.

2.4 Results

2.4.1 Systematic assessment of growth rate change detection

We systematically assess the ability of different age-depth models to detect growth rate changes on synthetic speleothems across a decreasing number of age measurements. Fig. 2.7a shows an example of a synthetic speleothem for *case 3* and the corresponding calculated age-depth models. The date of the growth rate change constitutes also the date with highest deviation of the true ages to the calculated ages with differences between the models. Comparing the growth rate before and after the growth rate change yields different relative growth rate changes per age-depth model. We calculate growth rates in a 2,000 yr time window using linear regression over the reconstructed ages per depth. Confidence intervals are determined using bootstrapping over the age uncertainties given by the age model. Note that in all models the transition between the two growth rates is modeled more smoothly, in parts due to missing information, in parts by construction.

The summary of all relative age model growth rate changes compared to the relative true growth rate change $((gr_{AM_{after}}/gr_{AM_{before}})/(gr_{true_{after}}/gr_{true_{before}}))$ across all case studies (except *Case 1* which does not include a growth rate change) is shown in Fig. 2.7b. We summarize over all cases with growth rate changes, as these only pose different degrees of difficulty and not substantially different scenarios. For 26 datings, both *LI* and *copRa* were not able to construct an age-depth relationship for any case, including the control *Case 1*. Reversals, which are more likely under high dating density but constant precision, are detected by automatic scanning and abort the construction of an age-depth relationship. The algorithm sets the construction as "failed" if a sufficient number of Monte Carlo ensemble members cannot be constructed. For both *LI* and *copRa*, reversals are more likely than for *StalAge* as the latter includes three dates in each interpolation step.

As age-depth relationships constructed through *LR* will always show a relative growth rate change of ~ 1, the wider range of relative growth rate change ratios compared to the other age-depth models rather indicates the range of true growth rate changes that are used in the analysis. Changes in its range are due to the uncertainties of the age-depth

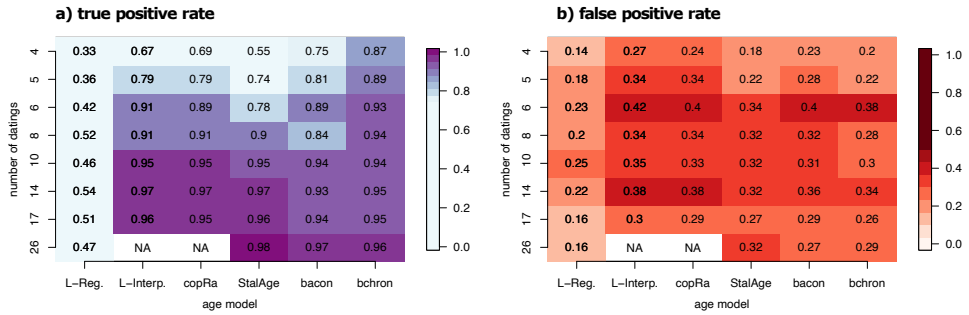

FIGURE 2.8: a) true positive growth rate detection: ratio of calculated age-depth relationships that detect a significant growth rate change in the same direction and within the same time window as the true growth rate change ($\pm 2,000$ yr). b) false positive growth rate change detection: ratio of calculated age-depth relationships that detect a significant growth rate change in a time window of constant true growth rate of at least $4,000$ yr length. We consider growth rate changes as significant if the 95% confidence interval of growth rate changes does not include 1, i.e., no growth rate change. Fig. A.2 distinguishes between cases with and without hiatus.

relationship that go into the calculation before and after the change of growth rate. For all other age-depth models (*LI*, *copRa*, *StalAge*, *Bacon* and *Bchron*), the spread of the relative changes increases under a decreasing number of datings. Here, *StalAge* mostly exhibits a wider range of relative changes than the other age-depth models. Under the extreme case of only four datings, the difference between the age-depth models is most visible, with linear age-depth models exhibiting similar ranges as the *LR*, whereas the spread of the Bayesian age-depth models is notably smaller.

For lower number of datings, the medians of the distributions shift toward smaller growth rate changes detected by the age-depth models compared to the true change. We find this, even though true growth rate changes are simulated in both increasing and decreasing direction compared to the initial growth rate to avoid biases of the direction from which the age-depth models start their calculations. This finding can most likely be attributed to interpolation methods in age model calculation favoring solutions with no extreme growth rate change.

Additional datings on real speleothems are added successively as new findings on the age-depth relationship make new datings necessary. Thus, it is most interesting under how many datings a growth rate change is detectable at all. Fig. 2.8a shows the fraction of case study experiments that detect a significant growth rate change. These are all experiments, where the 95% confidence interval excludes the case of no growth rate change, i.e., a change of 1, and the change is in the same direction as the true change. Except for *LR*, all age-depth models show high confidence of $\sim$ 90% and higher true positive detection rates of growth rate changes under eight and more datings. At six datings we still observe a high confidence of $\sim$ 90% and higher in all models except *StalAge*, which shows the lowest rate of detected growth rate changes. This is in line with the widest spread of relative growth rate change ratios (see in Fig. 2.7b). Except for *LR*, the true positive rate decreases for decreasing numbers of datings for all age models.

The constructed age-depth relationships may, however, also exhibit growth rate changes in cases when the true chronology does not include one. These are considered as false

positive detections. The rate of false positive growth rate change detection is depicted in Fig. 2.8b. For six datings, most age-depth models exhibit high rates of false positive detection (> 40 %). *LI* shows the highest false positive rate for all dating resolutions which coincides with high true positive rates under most dating resolutions. We do not find a consistent pattern across the different age models or a relation between false positive rates and the number of datings, which hints at the dominant role of background noise from dating uncertainties. Analyzing true and false positive rates against growth rate changes reveals higher true positive rates for higher growth rate changes. For false positive rates, only a small decrease with increasing growth rate changes can be found (results not shown).

Distinguishing between cases that include hiatuses and those without a hiatus shows that the presence of an hiatus strongly decreases the ability of the age models to detect growth rate changes, except for *LR*. While high confidence in detecting growth rate changes can still be found at an extremely low dating resolution of four datings with *LI*, *copRa*, and the Bayesian models, there is a strong decreasing trend in in detecting growth rate changes for eight datings or less in case an hiatus is present. (Fig. A.2). The slightly increased detection rate in *LR* originates from the calculation of the age-depth relationship in case of an hiatus, where two separate relationships are calculated - one before and one after the hiatus. This leads to an artificial detection of a growth rate change.

Summarizing, the analysis suggests an optimal number of 6 to 10 datings for an analysis on growth rate changes, depending on the chosen age model and the presence of a hiatus. This allows for an average true detection rate of $\sim$ 90 % at a maximal false positive rate of 42 %. To estimate unbiased relative changes, a dating resolution of 10 datings and higher is necessary. Too many datings, however, do not add additional estimation skill. Considering all possible cases, *Bchron*'s detection performance is best and exhibits the smallest range when comparing the extent of the change. The presence of a hiatus strongly decreases detection performance.

2.4.2 Applying the findings from synthetic speleothems on the SISALv2 database

Based on the criteria defined by the analysis on synthetic speleothems, we scan the SISALv2 database for speleothem records which cover a minimum period of 4,000 yr within the Holocene (8,000-100 yr BP) or the LGM (27,000-19,000 yr BP) and contain at least four datings within the respective time period which corresponds to the 8-10 datings needed to detect a growth rate change (four before and four after the growth rate change). We only obtain five records that meet the criteria of coverage in both LGM and an extended Holocene period between 10,000-100 yr BP (only three records within the original bounds). These records allow for a direct comparison of growth rates within one stalagmite (eID 163, 237, 305, 319, and 500 as depicted in Fig. 2.9). The records cover twice the time period of the synthetic speleothems. The depths of the speleothems vary greatly between 1,517 mm for eID 163 and 105 mm for eID500. In four cases we observe higher growth rates in the Holocene compared to the LGM, and one case with a lower Holocene growth rate. Two cave sites of the five are in Malaysia in close proximity to each other, but experience a growth rate change in different directions.

Due to the small number of available records that cover both time periods with a sufficient number of datings, we also compare growth rates across all available records that cover one of the time periods. With this approach, we obtain 124 records for the Holocene and 23 records for the LGM with at least four datings within the respective time periods and a coverage of 4,000 yr. The distribution of growth rates is depicted in Fig. 2.10. In total,

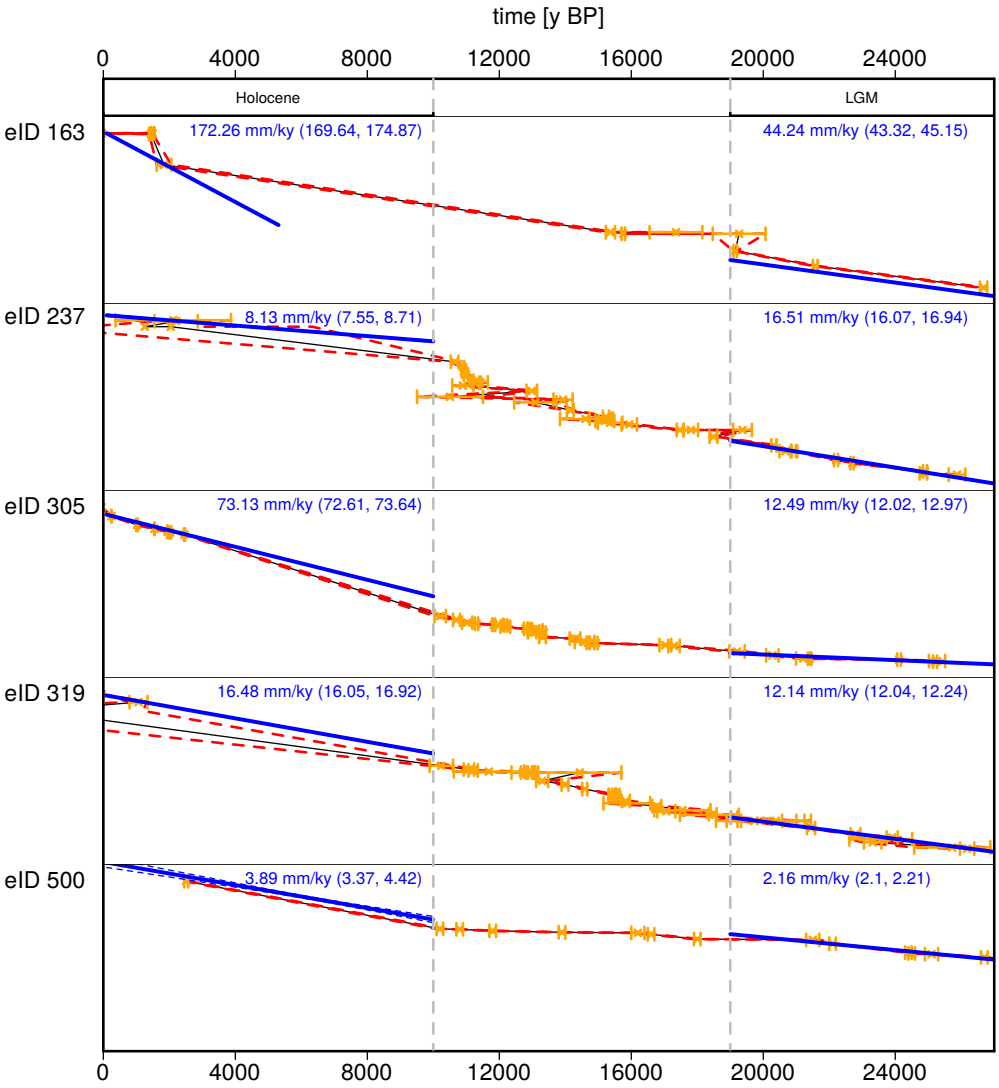

FIGURE 2.9: Age-depth relationship with growth rates in the Holocene and LGM for five entities from the SISALv2 database (eID 163 from Cango cave in South Africa [265], eID 237 from Gunung-buda cave in Malaysia [207], eID 305 from Sofular cave in Turkey [82], eID 319 from Bukit Assam cave in Malaysia [207], eID 500 from Cueva del Diamante cave in Peru [35]). The datings and their age uncertainties are depicted in orange, the original authors' chronologies in black, the chronology uncertainties in red, and the growth rates and their uncertainties as calculated in Sec. 2.4.1 in blue. All original chronologies are calculated using *LI*, except for eID237, where the age model type is unknown. To obtain a higher data coverage, the Holocene dating criteria was extended to 1,0000 yr.

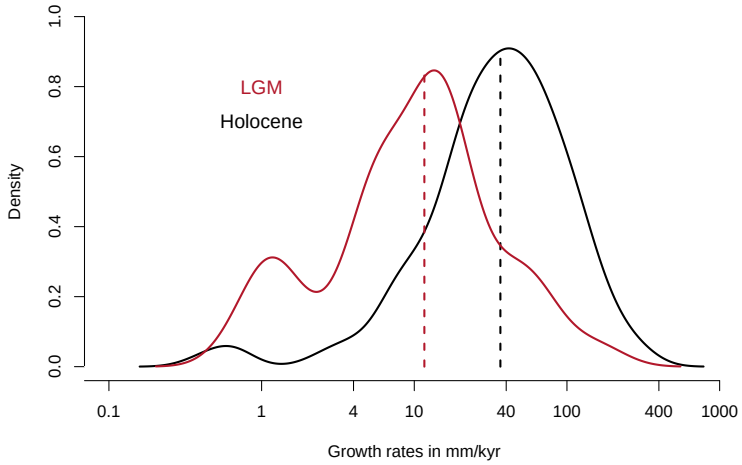

FIGURE 2.10: Aggregated density plot of growth rates for all records in the Holocene (black) and the LGM (red), with a minimum coverage of 4,000 yr and 4 datings. Growth rates are calculated as described in Sec. 2.4.1.

the median growth rate in the Holocene is three times higher than in the LGM with a median growth rate of 37.9 mm/kyr 90% confidence interval (34.6, 48.2) compared to 14.1 mm/kyr (11.1, 35.5) during the LGM. The detailed map in Fig. **??** shows the spatial distribution of the records' growth rates in the LGM and MH.

2.5 Discussion

2.5.1 Growth rate change detection in synthetic stalagmites

Our case study on synthetic speleothem age-depth relationships provided clear criteria to study growth rate changes on speleothem records. On a synthetic speleothem that covers 10,000 yr over 1,000 mm depth, we found high skill in detecting medium to large growth rate changes in both linear and Bayesian age models, except for *LR*, which is expected from its definition. Here, Bayesian models performed slightly better, however, further analysis needs to be done as to reveal the reasons. While a higher number of datings increased neither the skill of detecting true changes nor the growth change estimates, it led to aborted age-depth relationship constructions under the automatized *LI* and *copRa*. For a minimum of 8-10 datings, growth rate change estimates were still comparable to those with more datings, while true positive rates for detecting growth rate changes remained > 90 %. The presence of an hiatus strongly decreased detection rates and advised caution to use more datings rather than less. This is in agreement with the findings of Roesch (2020), who found that age models, especially the linear models, increasingly struggle to construct an age-depth relationship under an increasing number of hiatuses [229].

This study complements previous work from Scholz et al. (2012), who tested the performance of commonly used age-depth models on one specific synthetic speleothem example [243]. Since then, however, *copRa*, *Bacon*, and *Bchron* have either been newly developed or gained popularity in speleothem research, and have, therefore, not been included in their analysis. In the recently published SISALv2 database, all age models that are used in this analysis were evaluated according to their ability to produce age-depth relationships (as in Fig. 2.6). They found *Bchron* and *LI* to be the models with the highest

success rate due to their adaptability. This is in agreement with our findings, where *Bchron* shows the highest skill in detecting growth rate changes under all tested cases. Most of the individual age model performances supported previous studies. *StalAge* is known to struggle with abrupt growth rate changes [229, 243]. At the extreme end of only four datings, *StalAge* constructed an age-depth relationship which is to be expected from the way is is implemented and similar to *LR*. *Linear regression* is implemented assuming linear growth and, thus, does not allow for the detection of growth rate changes, unless under the presence of a growth hiatus. *Bacon*'s performance depends strongly on its prior distributions for growth rates [229, 17], and may thus underestimate growth rate changes more than *Bchron* (as in Fig. 2.7b). All age models underestimated growth rate changes compared to the true change. This is expected from the implementation of interpolation methods between datings that favor monotonicity and thus expect only positive growth rate changes.

Compared to the typical speleothem in the SISALv2 database, the synthetic speleothem is more than double in size, and covers longer time periods. 67 % of the records in the database fit our requirements of 10 and more datings (average of 12 datings) and are, thus, suitable to analyzing growth rate changes within the record over the period they cover. We note that the distinguished requirements rely, however, solely on the case studies with predefined depth, coverage, ranges of growth rate changes and an average number of datings per growth section. Further studies are necessary to translate the findings also to records outside of these ranges. The precision of the age measurements in the synthetic stalagmites was chosen as the median uncertainty of the SISALv2 records relative to a $10,000$ yr coverage and is thus comparable. However, this also means that the results solely relate to this constant precision. Effects that may be influenced by dating precision were not analyzed. More analysis on a range of dating precision is necessary to better constrain the number of suitable records but also to disentangle, for example, the false positive rate from the dating precision. High false positive rates are an indicator of underestimated sources of uncertainty in the models and may, therefore, be connected to dating precision. A cross-validation detection using multiple different models, i.e., calculating true and false positive rates of a set of different models may further increase detection skill at a low number of datings and, thus, increase the number of suitable records.

Generally, we found that it is possible to detect growth rate changes even with a low number of datings. The findings can be summarized in two main categories: 1) Bayesian age models performed better in detecting growth rate changes compared to linear model, in particular *Bchron*. For this age model, extremely low number of datings ($4-5$) may be sufficient to detect a growth rate change and to determine if additional datings are necessary. For linear methods, except for *LR*, six and more datings will be necessary to detect changes, especially under the presence of an hiatus. 2) When analyzing an already dated speleothem record or an ensemble of records, 8-10 datings were the minimum number of datings to confidently detect and estimate growth rate changes. If multiple age-depth relationships from different age models are available, as provided by the SISALv2 database, the number of datings may be decreased slightly. Additionally, from an age model perspective, the models need to be further improved to produce more realistic uncertainties and additional criteria need to be found that indicate false positive growth rate changes.

2.5.2 Growth rate changes between the glacial and interglacial climate

We tested a selected number of speleothem records from the SISALv2 database for growth rate changes between the LGM and the Holocene and found significant changes in all records. Applying the selection criteria from the analysis with synthetic speleothems to the database and requiring that records cover both time periods yielded five records with two times the coverage of the synthetic speleothem case studies but very different depths, which range between 105 and 1517 mm. Four of these records exhibited an increased growth rate in the Holocene and one record a decreased growth rate. However, some of the original authors' age-depth relationships that are depicted in Fig. 2.9 require more careful analysis using the additional chronologies as provided by the SISALv2 database. Due to the small number of records that covered both periods with a sufficient number of datings, we extended the analysis to a separate approach, including a total of 142 records from both time periods. On average, the growth rate distributions showed a speleothem growth that is three times higher in the Holocene than during the LGM. This is in agreement with both global and local studies on glacial-interglacial growth rate comparisons [229, 262, 190]. Stoll et al. (2013), who studied growth patterns from stalagmite in six caves in Northern Spain across the last 200,000 yr found an attenuated growth rate in the early compared to the late Holocene [262]. Changes of growth rates in high-resolution speleothem in Texas, USA, were, however, found to be not directly translatable into changes in cave water supply, as this relationship may be more complex [301]. Further studies with comparisons to climate model output and independent hydroclimate proxies are necessary to better understand how well climatic signals are recorded by speleothem growth rate changes on these timescales. A large uncertainty factor in this study originates from the low number of available records that cover both time periods. When including records that cover only one of both periods, the number of suitable records within the LGM was five times smaller than the number of records available in the Holocene. This large difference in sample size may lead to sample biases and requires further analysis, e.g., with a more regional focus. The sample size and robustness of the analysis could be increased by including the additional chronologies provided by the SISALv2 database. A larger sample size, especially in records that cover both periods, may help to distinguish spatial patterns, if they exist. This could be achieved by analyzing the sample split into larger regions of similar climate or latitude bands. As suggested for the synthetic speleothems, cross-validation between different age models may decrease the number of datings that are necessary for reliably detecting growth rate changes and, thus, possibly increases the sample size, but also reduces the number of false positives.

2.6 Summary

Concluding, we found high detection rates of growth rate changes for all age modeling techniques, expect for *LR*, if a sufficient number of datings of a synthetic speleothem is available. Bayesian models, in particular *Bchron*, performed better both in terms of detection accuracy and estimating growth rate changes. The presence of only one hiatus, a prevalent growth feature which is included in 25 % of the SISALv2 speleothems, already substantially decreased the growth rate change detection ability of age models. Whether dating a new speleothem or analyzing an already dated record, our results suggest at least six datings to detect, and 8-10 datings to quantify a growth rate change. Additional studies with special focus on hiatus length, dating precision, and cross-validation would help to better constrain selection criteria.

The results from the selection of speleothem records, that fit our prerequisites from analyzing growth rate changes in synthetic speleothems, support our initial hypothesis of higher speleothem growth rates in the warmer Holocene and lower growth rates in the colder LGM. However, whether these changes are linked to changes in cave water supply through changes in the hydrological cycle remains to be analyzed. Additional hydrological proxies both in speleothem records as well as in other archives in proximity to the cave sites, as well as precipitation patterns simulated by climate models would help to constrain past precipitation changes and subsequently confine uncertainties of future changes.

3 Isotopic signatures in the last millennium: model-data comparison as model-evaluation

In this chapter, we compare isotopic signatures in isotope-enable general circulation models (iGCMs) speleothem and ice core records as natural climate archives [1]. The model-data comparison faces many challenges both by the model and the records: spatial resolution especially in model topography as well as parameterization of simulated physical processes, make one-by-one comparisons between models but also to observations difficult [203]. On the proxy records side, archiving processes such as karst damping effects in caves [77, 150], firn diffusion [20], or the superposition of different isotopic signals at the location of the record [150], make it difficult to extract a climatic signal that can be compared to model output diagnostics. Isotope-enabled models, however, provide the unique opportunity of a direct comparison between model and data "on equal ground". While models show little coherence between ensemble runs that start from different initial states, except when forced externally, they are still able to reproduce the frequency of climatic events [42]. This allows the comparison of modeled and recorded variability, even though modeled events may not necessarily be aligned in time. Age uncertainties of proxy records as addressed in Chapter 2 are taken under consideration where applicable.

The overarching aim of this thesis is to test the ability of speleothem records to reveal hydrological changes between the glacial and interglacial cycle using $\delta^{18}O$ signatures and growth-rates as proxies thereof. In relation to this, model and data evaluation in a stable and well-known time period such as the last millennium (LM) is a prerequisite to differentiate between credible climatic information and model or data biases.

The key questions addressed in this chapter are:

- How similar are the modeled $\delta^{18}O$ signatures of iHadCM3 compared to those of other isotope-enabled models and to the speleothem and ice core records, especially regarding variability?
- Can we distinguish main climatic drivers of modeled and archived $\delta^{18}O$ signatures?
- How representative is $\delta^{18}O$ as archived in speleothem records for their region?

Answers to these questions will help to understand the constrains of isotopic signatures in model and data as an indicator of climatic changes between the Last Glacial and present day climate.

[1] This chapter is in part based on my previously published paper on "Comparison of the oxygen isotope signatures in speleothem records and iHadCM3 model simulations for the last millennium" [24] as well as my discussion paper "Investigating oxygen and carbon isotopic relationships in speleothem records over the last millennium using multiple isotope-enabled climate models" [25]

After a literature review on the current state of model-data comparison and isotopic variability as represented by both models and paleoclimate proxy records, we will introduce the climate models and the proxy data used in this analysis, as well as the statistical methods. The identified key questions will be discussed in the results and discussion section, and finally answered in a summary.

3.1 Background

Human societies and natural systems have always been sensitive to changes in past climate conditions. Under the current anthropogenic warming trend [248], knowledge of the changing mean climate state becomes more and more important to assess risks and uncertainties [41]. While a current changing mean state of the climate is well observed, many open questions remain on the direction and magnitude of potential changes to its variability [90]. Changes in variability influence the occurrence and intensity of extreme temperature and precipitation events [136], and have major impacts on ecosystems [286], society, and economy [124]. Past climate changes offer a test-bed of changes in the mean climate state and its variability and, thus, can help to better understand projected changes in the future. Instrumental records on climate variables such as temperature measurements only cover multiple decades of data with longer local exceptions [186] (Fig. 3.2). On longer timescales, we have to rely on past climate information extracted from paleoclimate archives, which are compared to state-of-the-art climate models. These models represent our current understanding on fundamental physical, chemical and biological processes of the Earth's climate against a background state of radiative forcing. Using information of both the climate archive and the climate modeling world can help in interpreting and explaining past changes and, thus, constrain uncertainties in future projections. Hydrological changes in past, present, and future are, however, far less understood and more uncertain than changes in temperature and different proxy systems archive different components of the water cycle in different ways [203].

Natural variability in the composition of stable water isotopologues (SWI, commonly referred to as stable water isotopes), has been used to track global, regional, and local changes in the hydrological cycle and atmospheric processes. It is commonly expressed in the form of the ratio between the heavier isotopologue $H_2^{18}O$ and the lighter $H_2^{16}O$, given in the δ-notation as $\delta^{18}O$ as described in Chapter 1. During phase transitions, such as condensation and evaporation, isotopic fractionation occurs, favoring heavier water isotopes in the condensed and lighter isotopes in the evaporated state. Thus, SWI constitute an effective tracer of the phase transition history of a specific water parcel as it moves across oceans, atmosphere and land [148] (phase transition and transportation as in Fig. 3.1). Relationships between the isotopic composition of precipitation and regional climate variables have already been established in the 1930s and summarized by [59] in the 1960s. These relationships describe $\delta^{18}O$ as an indicator of evaporation temperature, precipitation amount, altitude, or distance to source water. However, the isotopic composition of precipitation at one location may be governed by multiple atmospheric processes where different signals are superimposed [18].

The Global Network of Isotopes in Precipitation (GNIP) database [125] provides measurements of $\delta^{18}O$ in collected precipitation since 1961, on which monthly to decadal variability can be analyzed. Along with seawater, river or water vapor $\delta^{18}O$ databases, GNIP has been used to evaluate models for the present climate [276, 299, 49]. On decadal and longer timescales, we rely on paleoclimate archives, which store isotopic information of the past climate.

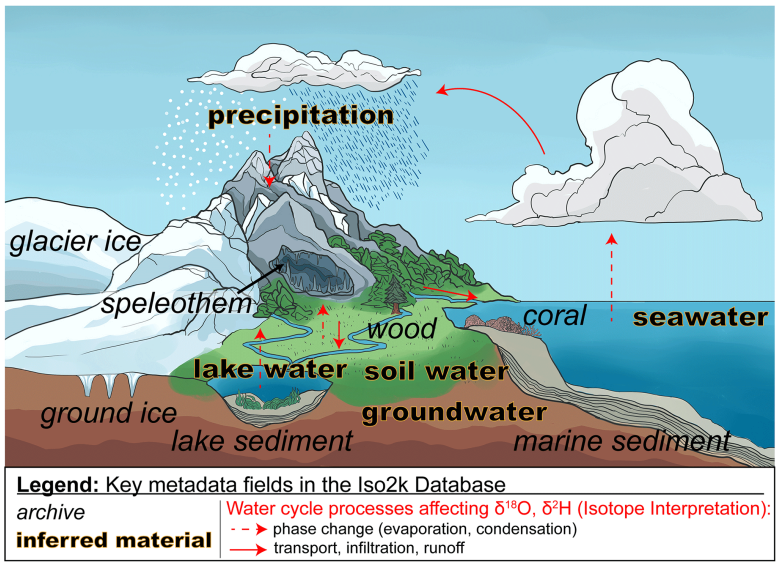

FIGURE 3.1: Schematic illustration of archives and inferred materials of the global water cycle that are included in the Iso2k database [148]. Phase transitions during evaporation and condensation, as well as transport are depicted as red arrows. Paleoclimate archives (italic text) store information in form of stable water isotope proxy data from their inferred material (bold text). Schematic from [148] and base illustration by Helen Xiu, Washington University.

Hydroclimate proxy records are very commonly analyzed and, thus, globally distributed as they can store $\delta^{18}O$ in a variety of archives such as glacier ice cores, cave deposits, corals, tree wood, lake and marine sediments [20, 148]. In this study, we rely mostly on speleothem cave deposits and ice core records. Speleothems allow sampling of a wide range of climates in the low- to mid-latitudes [157, 191, 207] and provide (semi-) continuous precisely dated time series of oxygen isotope ratios. $\delta^{18}O$ variations in stalagmite-calcite, the most common speleothem in climate research, to first order represent changes in $\delta^{18}O$ in the meteoric precipitation above the cave. The climatic interpretation of isotopic changes, however, is not straightforward [79]. For example, broad correspondence has been established between speleothem $\delta^{18}O$ and both surface temperature [181] and local precipitation strength and seasonality [182, 141, 36]. Between the surface and the cave environment, modifications on these signatures by vadose-zone fractionation [280, 103, 231], karst hydrology, cave internal conditions [77, 290, 127, 87], and differences in geochronological methods (as described in Chapter 2) can complicate paleoclimatic interpretations [22, 217].

In the high latitudes, we rely on glacier ice core records. They present the most commonly used archives of climate dynamics and provide isotopic time series dating back 800,000 yr [139]. In the polar regions, these show an almost linear relationship to temperature and with surface mass balance [177, 130]. However, the signal can be superimposed with information of changes in moisture source and condensation processes [100]. Paired with isotope-enabled model simulations, the information from a network of speleothem and ice core records can lead to an improved understanding of hydro-climate dynamics and of its spatial and temporal variability on timescales longer than the instrumental period [60, 270, 148].

Model-data comparisons have long been used to evaluate climate variability as represented in models and archived in paleoclimate records. For simulations of the past

climate, proxy data also constitutes the only available "out-of-sample" validation information for models [203]. Extensive studies analyze temperature and precipitation patterns [166, 202, 247], and how these are impacted by external forcing [5, 203]. The incorporation of stable water isotopes into the hydrology of climate models enables direct intercomparison between modeled and archived or observed isotopic ratios [297, 263, 303], instead of using uncertain and not straight forward calibrations to climate variables such as temperature and precipitation amount. These comparisons provide valuable information about Earth's climate system and its hydrological cycle [291, 60, 46, 260, 206]. For example, Sjolte et al. (2018) compared the variability of the simulated ECHAM5/MPI-OM δ^{18}O to Greenland ice cores over the LM and were able to differentiate between solar and volcanic forcing effects from their gridded reconstructions [254]. On orbital timescales ($\sim$150,000 yr), Caley, Roche, and Renssen (2014) found broad model-data similarity with small differences attributed to seasonality from the comparison of transient isotope-enabled simulation with the model of intermediate complexity iLOVECLIM to speleothem records from South East Asia [31].

The hydroclimate and, thus, isotopes in models are generally described by convection and cloud physics [259]. In the model world that has a finite resolution, these processes rely heavily on parameterizations and tunings, which differ for each model and resolution. To increase comparability between models of past, present and future, the Paleoclimate Model Intercomparison Project (PMIP) [131, 133] under the overarching Climate Model Intercomparison Project (CMIP) [268, 76] sets idealized boundary and forcing conditions to a wide range of climate model simulations. Water isotopes, however, have not been included in the CMIP or PMIP assessments so far [268, 76]. The Stable Water Isotope Intercomparison Group (SWING) compares isotope-enabled simulations to isotope observations, yet restrict their analysis to the historical period [226, 225].

Our model-data comparison aims to constrain variability of the hydroclimate proxy δ^{18}O both in models and archives. The LM provides an optimal test-bed to evaluate and better understand the proxy. It offers the opportunity to study variability on decadal and longer timescales and to decipher internal variability from externally forced variability [133]. The last millennium is characterized by stable, close-to-present-day, boundary conditions such as fairly constant greenhouse gas concentrations and sea level. Climate variability is mostly driven by volcanic eruptions but also by other natural forcings as well as solar variations [245, 202, 268, 192]. It is a key-paleoclimate period not only in paleoclimate research but also for the CMIP5 and CMIP6 experiments [268, 76]. Additionally, records of δ^{18}O such as speleothem or ice core records are abundant in this period [49, 148].

Variations in the mean state and other statistics of the climate beyond weather events are defined as climate variability [41]. This includes variations in the frequency of extreme precipitation events or variations and trends in the global mean temperature. It can be separated into variability which stems from complex internal interactions between processes in the atmosphere, ocean, biosphere and cryosphere (internal variability) [64] and externally forced variability [89], e.g., from changes in greenhouse gas concentration, volcanic eruptions, or total solar irradiance [227]. Examples for internal variability are so-called climate modes such as El-Niño Southern Oscillation (ENSO) [281], the North Atlantic Oscillation (NAO) [119, 121], or the Indian summer monsoon (ISM) [99]. Variability in climate models can be separated into the same categories (external forcing for last millennium depicted in Fig. 3.2). Archives of climate signals such as speleothems or ice core records may be sensors to both internal and external variability of the climate system. The detection ranges from climate modes on interannual to decadal

timescales (ENSO [264, 184], NAO [244], or ISM [81, 191]) to orbital timescales such as glacial-interglacial changes [294, 2].

Previous studies have suggested that modeled temperature variability is systematically underestimated on decadal and longer timescales, especially on regional scale [152]. Discrepancies are already substantial at interdecadal timescales [151] and increase toward longer timescales and lower latitudes. This can mostly be attributed to a lack of internal variability, insufficient energy cascades [152], or missing processes and feedbacks [218]. The large proxy-based changes in variability between the LGM and the Holocene [220], emphasize the lack in variability, e.g., of the PMIP3 ensemble on millennial and longer timescales. Uncertainties of the recorded signal due to archive-internal variability, may, however, also be responsible for discrepancies between modeled and archived variability. For speleothems, lag time between the surface rainfall and the cave drip water [127] as well as the usually slow response of the cave micro-climate to the surface climate, damp the signal on sub-decadal to decadal time scales. Examining the models' capability to simulate and the records' capability to capture variability on different time scales will improve our understanding of hydrological processes and uncertainties in both.

3.2 Model-data comparison using isotope-enabled climate models

The incorporation of stable water isotopes into the water cycle of isotope-enabled GCMs (iGCM) provides an additional mean to analyze the hydrological cycle in climate models and climate systems in general [298, 263, 276]. The models are able to temporally and spatially resolve isotope variability by adding $H_2^{18}O$ and HDO as an additional water cycle which considers fractionation processes during phase transitions such as melting, condensing, evaporating, and freezing. The ratio between simulated $H_2^{18}O$ and $H_2^{16}O$ as in Eq. **??** will further be denoted as $\delta^{18}O_{sim}$.

Early isotope-enabled model-data comparisons questioned established paleoclimate assumptions and clarified that $\delta^{18}O$ should not only be considered a proxy for local temperature. Isotopic signatures are additionally controlled by synoptic atmospheric circulation [263]. However, implementation between models differ and individual models show biases toward observations. Small biases, e.g., in the convection or moisture transport scheme of the model, can lead to significant over- or underestimation of isotopic depletion in specific regions [196, 21, 305, 226].

The Stable Water Isotope Intercomparison Group (SWING) formed to build systematic intercomparison and assessment between isotope-enabled models, similar to the CMIP and PMIP projects [226]. Through analysis over the historical period and with the help of observation measurements, they show that most differences between modeled isotopes arise from differences in the control of atmospheric humidity [225]. Models which realistically capture precipitation patterns in the tropics did not necessarily prove to simulate the isotopic composition of precipitation realistically compared to measured data [50]. Positive and negative mean biases in models also caution to use multiple models when comparing to paleoclimate proxy records.

The models used in this study range from AGCMs forced with SST and sea-ice distribution to fully-coupled AOGCMs. Their basic characteristics and boundary conditions are listed in Tab. 3.1. Fig. 3.2 shows the climate as represented by the different models and external forcings used in the simulations.

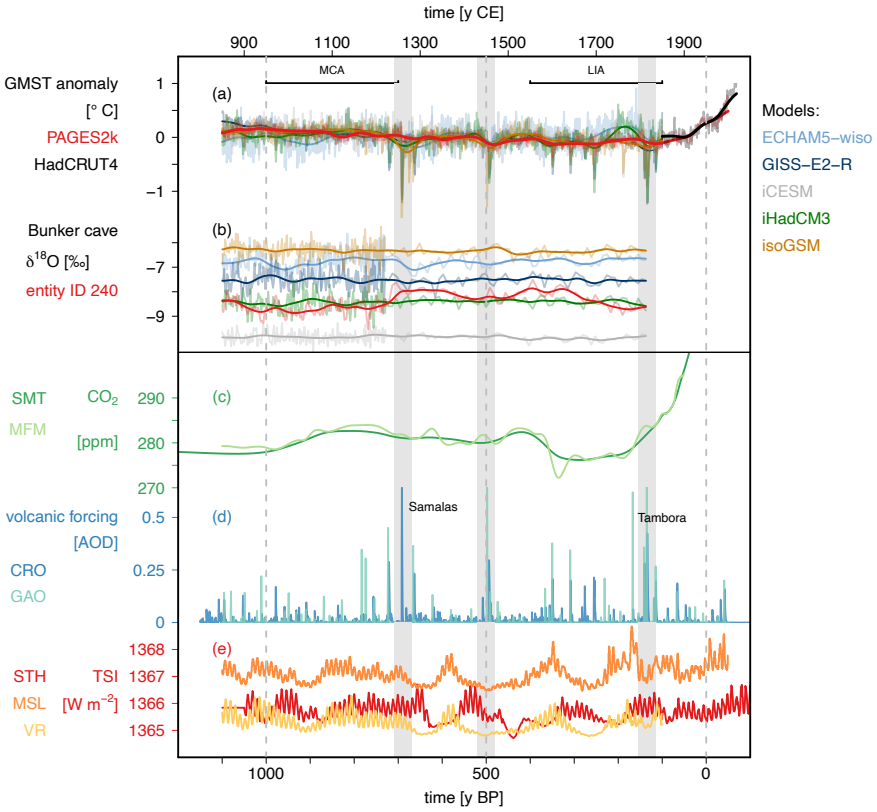

FIGURE 3.2: GMST and oxygen isotopes in precipitation as represented by different GCMs (ECHAM5-wiso (light blue), GISS-E2-R (dark blue), iCESM (grey), iHadCM3 (green) and isoGSM (orange)) under different external forcings over the last millennium: a) GMST anomaly against the 850-1850CE period for each model (in model colors), reconstructed (red, [202]) and observed temperature anomaly (black, [186]). b) infiltration weighted $\delta^{18}O_{sim}$ (in model colors) at the cave site location of Bunker cave (Germany) and $\delta^{18}O_{speleo}$ of entity ID 240 [49, 84]. Fainted lines are the time series in annual or record resolution respectively, while thick lines are smoothed values with a 100 yr Gaussian kernel bandpass and smoothing from the R-package nest (`https://github.com/krehfeld/nest` [219, 217]). The climate in models is forced by c) atmospheric CO_2 concentrations (SMT: [236], MFM: [171]), d) volcanic forcing in units of aerosol optical depth (AOD) (CRO: [56, 55], GAO: [92]), where the [92]-AOD reconstruction was estimated by dividing the sulfate loading by 150 Tg (following [5]), e) total solar irradiance (TSI) (STH: [258], MSL: [189], VR: [287]). Periods of high volcanic activity in the forcing are marked by gray bars. Figure from [25].

TABLE 3.1: Basic characterization of the last millennium simulation adapted from [25].

	ECHAM5/MPI-OM	GISS ModelE2-R	iCESM1	iHadCM3	isoGSM
Reference	[254, 298]	[163, 46, 45]	[21, 260]	[24, 276]	[305]
Years	800-2005 CE	850-1979 CE	850–2005 CE	850-1850 CE	851-2000 CE
Atmospheric resolution	$3.75° \times 3.75°$	$2.5° \times 2°$	$2.5° \times 1.875°$	$2.5° \times 3.75°$	$1.875° \times 1.875°$
Orbital Parameter	[23]	[14]	[15]	fixed to 0BP	a millennium trend is considered
GHG	CO_2, CH_4, NO_2: [171] Historical, anthropogenic: [173]) Ozone: Climatology of [208]	Transient from 850 [235]	well-mixed greenhouse gases (CO_2, CH_4, NO_2) from high-resolution Antarctic ice cores [235]	well mixed CO_2, CH_4, NO_2 and other trace gases [245, 236]	well-mixed greenhouse gases (CO_2, CH_4, NO_2) from high-resolution Antarctic ice cores [236]
Vegetation	[211] with vegetation from [131]	[211]	[211], starting 1500 CE: [122]	dynamic TRIFFID [54]	[211], starting 1500 CE: [122]
Volcanic forcing	[56]	[56]	[92]	[55]	[92]
Total Solar Irradiance	[189, 188]	[258], starting 1850: [295]	[287] with 11-year cycle added similar to [235]	[258, 295, 245]	[287], starting 1834: [158], with 11-year cycle added from [236]

3.2.1 iHadCM3 - a detailed model description and simulation overview

In this chapter, the main emphasis is on the coupled atmosphere-ocean isotope-enabled general circulation model (iGCM) iHadCM3, which has been widely used in numerous studies in different climatic states for past (late Holocene, LGM, and Last Interglacial [117, 251, 252, 117, 118]), present and future climate [250, 276, 41].

The model is a three-dimensional GCM and consists of several components. The atmosphere model HadAM3 [212] is run on a horizontal grid of $2.5° \times 3.75°$ with 19 vertical levels of 39 km depth (as represented in Fig. 3.3) and updated at time steps of 30 min. The ocean model HadOM3 [98] runs on a horizontal resolution of $1.25° \times 1.25°$, 20 vertical levels of maximal 5 km depth and time steps of 1 h. The atmosphere and ocean models are coupled once per simulated day. Additionally iHadCM3 consists of a sea ice model [285] and a dynamic land surface and vegetation model based on TRIFFID [54] with a time step of 5 yr.

In the isotope-enabled version, stable water isotopes $HD^{16}O$ and $H_2^{18}O$ are incorporated in the full hydrological cycle as two separate water tracers in the atmosphere component of the model. Evaporation and condensation in HadAM3 incorporate the corresponding fractionation processes. The ocean component has a fixed defined volume of water per gridbox, leading to isotopes being represented in fractions as tracers, similarly to salinity. Changes in the isotopic composition of the top level of the ocean through evaporation, precipitation, and runoff are experienced through virtual isotope fluxes [276].

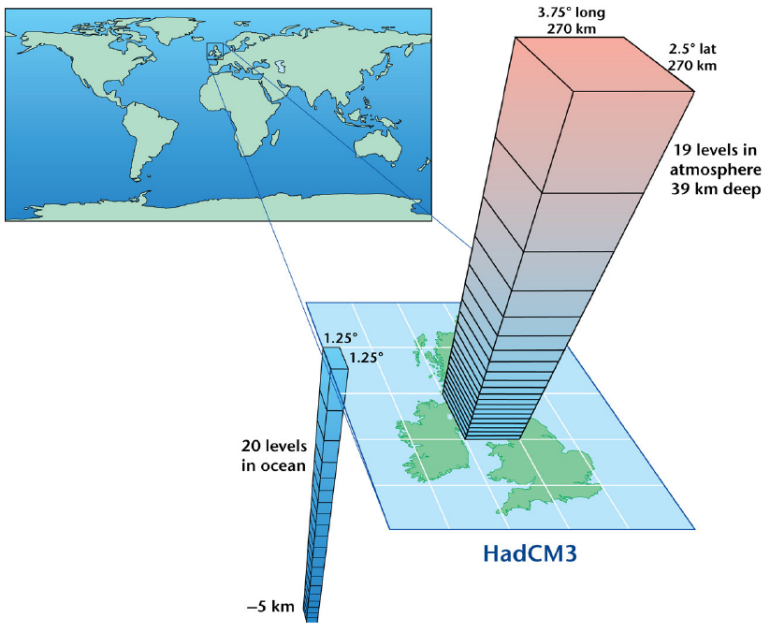

FIGURE 3.3: Schematic representation of the grid box architecture and resolution of ocean and atmosphere components in HadCM3. Figure taken from [169].

Albeit its relatively low resolution compared to other state-of-the-art GCMs, HadCM3 compares well to instrumental observations on the sea surface temperature, sea ice extent, and ocean heat content [98], while still slightly overestimating local evaporation in the freshwater hydrological cycle [204]. When focusing on the representation of isotopic signatures, the model simulates the major isotopic fractionation effects as described by Dansgaard (1964) such as the latitude effect, the amount effect, or the continental effect. Comparisons with observational $\delta^{18}O$ indicates that the main characteristics and spatial distribution of isotopic composition of precipitation are well reproduced, with only small biases due to the coarse model resolution [308, 276, 250]. Summarizing, iHadCM3 captures all important large scale climatic and isotopic features, while remaining computationally efficient to perform millennial-scale simulations including water isotopes.

In this study, we use a last millennium (850-1850CE) three-member-ensemble, identified with the LM prefix [24]. Each ensemble member follows from the same spin-up simulation, but is initialized from different years. In comparison to the multi-model ensemble, only LM1 is used.

3.2.2 Other isotope-enabled models with last millennium runs

In order to set a reference for the results obtained from iHadCM3, we also rely on other isotope-enabled models, which are shortly introduced here. For more detailed descriptions, please refer to the respective original publications.

ECHAM5/MPI-OM

Simulations of the last millennium performed with the isotope-enabled version of the fully coupled Earth System Model ECHAM5/MPI-OM (hereafter ECHAM5-wiso) [298, 132] are analyzed [254]. ECHAM5-wiso is widely used in the paleoclimate field and provides simulations over a wide range of boundary conditions, e.g., in [298, 156,

101]. As iHadCM3, the model consists of several components: an atmospheric model ECHAM5 [228] and an ocean model MPI-OM with embedded sea-ice model [175]. Isotopic diagnostics are added through the entire water cycle in both the atmosphere and ocean component [298] and show good agreement to present-day observations. For past climates such as the mid-Holocene or the LGM, the isotope climatology compares well to proxy based measurements from both speleothems and ice cores [48, 298]. The isotope-enabled last millennium simulation used in this analysis has been evaluated before in many global [25, 184, 205] as well as regional studies [254, 104].

GISS ModelE2-R

For the isotope-enabled version of the AGGCM GISS ModelE2-R (hereafter GISS-E2-R) [238, 237], water tracers and stable water isotopes were added to the full hydrology of the model: the atmosphere, land surface, ocean, and sea-ice component [239]. In this analysis, we use an ensemble member of a large set of last millennium experiments with different combinations of external forcings [46, 45, 163]. In comparison to present-day isotopic measurements, GISS-E2-R simulates changes in convection, clouds, and isotope kinetics well, except over Antarctica [239]. This last millennium run has been analyzed in numerous studies focusing on isotopic signatures in relation to volcanic eruptions [46], the position of the intertropical convergence zone [45], and to ENSO [163].

iCESM1

As the model is publicly available and open-source, the isotope-enabled iCESM1 version 1.2. (hereafter iCESM) [120, 21, 184] is one of the most-widely used climate models in the scientific community with multiple simulations existing for past and present climate states [198, 309, 308]. The last millennium fully-forced version that is used here, is out of an eight-member ensemble with experiments under different external forcings. For the isotope-enabled version, stable water isotopes are added as numerical tracers to a new parallel hydrological cycle. Present-day global isotopic signatures are well captured across the ocean, but small negative biases across the land surface exist [21] due to overestimated convection in mid-latitude oceans followed by insufficient mass transport of stable isotopes land- and poleward [196].

isoGSM

Based on a previous operational weather forecast model [134, 32], isoGSM presents the isotope-enabled version of the Scripps Experimental Climate Prediction Center's (ECPC) GSM (hereafter isoGSM) [305]. In contrast to the other models used in this analysis, it is an only-atmosphere model, forced with SST and sea-ice distributions from CCSM4 last millennium simulations [155]. The isotope-enabled version for the last millennium has been evaluated in Bühler et al. (2021) [25]. Present-day isotopic signatures and variability are captured well compared to other isotope-enabled models [226], specifically showing good agreement to oxygen isotopes measured in speleothems from East and South Asia [38, 135]. Across dry regions such as Antarctica, isoGSM underestimates isotopic depletion caused by the moisture transport scheme of the model [305, 226].

3.2.3 δ^{18}O proxy data from speleothems and ice cores

The speleothems that we use in this study are taken from the SISALv2 database, introduced in section 2.2. For the last millennium, records with sufficient resolution and reasonable dating uncertainties are available for the analysis. We only use data from

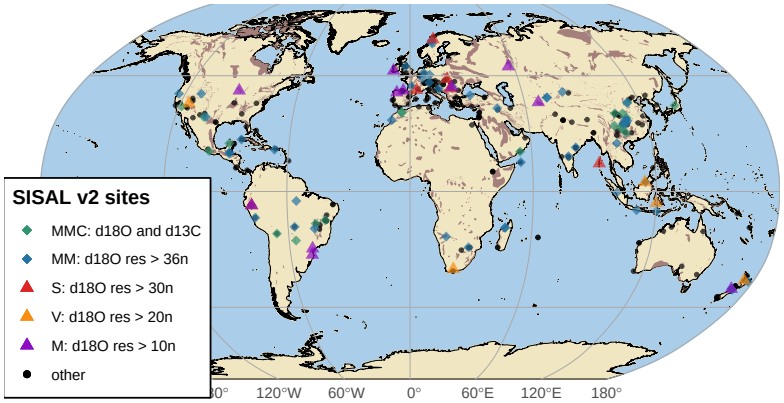

FIGURE 3.4: Site locations of the SISALv2 database on a global karst map (brown shadings from [300]). The sites with entities that fulfill the prerequisites for our analysis are marked in colored triangles and diamonds. These entities cover at least a period of 600 yr within the last millennium and have a minimum of two dating points in this period. They have at least 36 measurements with carbon measurements (green diamond) or only oxygen isotopes (blue diamond), 30 (red triangle), 20 (orange triangle), or 10 (purple triangle) δ^{18}O measurements and two dating points in this period. All other sites in the SISALv2 database are marked with a black dot. Figure and caption adapted from [24, 25].

entities which are not superseded (*entity_state* = *current*). We require a minimum time coverage of 600 yr and at least two radiometric dates or be lamina counted within the period (850-1850CE). We only consider those dates that are marked as *used*, which indicates usage in the original chronology of the record. Records that include no information on oxygen isotope samples or depth are omitted.

For our analysis, we set requirements on the records' resolution in four categories. At least ten isotopic measurements are required when comparing mean δ^{18}O offsets between iHadCM3 and speleothem oxygen isotopes (M-subset). At least 20 δ^{18}O measurements are needed, when comparing variances between model and speleothems (V-subset). For the correlation and network analysis we use all speleothems with at least 30 isotope samples (S-subset). To compare the speleothem records to the multi-model ensemble, we require at least 36 stable isotope measurements to guarantee a minimum resolution of 30 yr. The used records are depicted in Fig. 3.4 and basic characteristics, such as the number of entities and sites, are given in Tab. 3.2.

With SISALv2, the database now provides new possible age-models through up to seven methods that are obtained from the original U/Th dates (details in Sec. 2.2 and Sec. 2.3.2). Age-model ensembles are available for 69 of the 85 entities in the S-subset and used in our analysis on networks (Sec. 3.3.3). For all other analyses, we use the original age-model chronologies as given by the original authors.

On monthly to decadal timescales, the Global Network of Isotopes in Precipitation (GNIP) database [125] provides measurements of δ^{18}O and δH in collected precipitation water around the world. It was initiated by the International Atomic Energy Agency (IAEA) and the World Meteorological Organization (WMO) in 1960, and serves as a monitoring tool of the hydrological cycle since then. We only use the time series of the δ^{18}O measurement site in La Paz in Bolivia (WMO_code=8520101) which provides 126 monthly samples between 1995 and 2006.

TABLE 3.2: Basic characterization of the last millennium subset of the SISALv2 database [49].

	analysis type	requirement	entities	sites	resolution
M-subset	mean state comparison	>10 samples	104	87	18.67 yr (15.24, 22.18)
V-subset	total variance comparison	>20 samples	92	76	12.21 yr (10.15, 14.38)
S-subset	spectral and network analysis	>30 samples	85	71	9.67 yr (8.14, 11.22)
MM-subset	subset in the multi model comparison	>36 samples δ^{18}O	89	75	8.09 yr (6.87, 9.23)
MMC-subset	subset in the multi-model comparison with oxygen and carbon isotopes	>36 samples δ^{13}C and δ^{18}O	58	50	6.08 yr (4.07, 7.85)

This work also analyses ice core records from the Iso2k database [148], which was developed in the framework of community-led paleoclimate data synthesis efforts endorsed by PAGES [202, 203]. The database is a compilation of 759 previously - published records of stable water isotopes (δ^{18}O and δH) from 506 geographic locations. These stem from a variety of natural archives of stable water isotopes and include glacier and ground ice; speleothems; corals, sclerosponges, and mollusks; wood; lake sediments and other terrestrial sediments; and marine sediments. All records cover at least 30 yr over the last two millennia and range from sub-annual to centennial resolution.

Glacier ice in polar regions and high elevations forms in accumulated layers of snow that get compacted over time into chronological layers of ice. Drilled glacier ice cores can, therefore, contain up to sub-annually resolved records of past climate information, depending on the accumulation rate and laboratory measurements [216]. Dating is achieved through layer counting and the alignment with dust deposits from major volcanic eruptions [249]. Ice cores provide an archive for multiple proxies of the past climate, e.g., past atmospheric composition through trace gases in air bubbles [240], or even forest fire activities through specific biomarkers [73, 306]. Time series of stable water isotopes, δ^{18}O in particular, are most prominently used and show high correlation estimates with local temperature and surface mass balance [177, 130] but the signal can be superimposed with information of changes in moisture source and condensation processes [100]. Processes such as firn diffusion or melting in summer months smooth the variability on high frequencies [20].

We only consider glacier ice where the primary time series, i.e., the time series which the original authors based their main climatic interpretation on, were oxygen stable isotopes. We remain with 100 glacier sites that cover a time period of at least 30 yr in the last millennium (850-1850CE), 46 arctic, 36 antarctic, and 13 non-polar records.

3.3 Methods

3.3.1 Data preparation for comparison

Model data from all different models was available on monthly resolution but for different time periods as can be seen in Tab. 3.1. When we compare between different models, we restrict our analysis to the time period from 850 to 1850CE, which is considered PMIP's interval for the last millennium [268]. For the multi-model comparison, we were provided with different sets of post-processed output variables, where we focused on surface air temperature, precipitation amount, precipitation-$\delta^{18}O_{sim}$, and evaporation. Where evaporation was lacking as a diagnostic (iCESM, isoGSM, and iHadCM3), latent heat was used and converted to potential evaporation. All post-processed variables are checked for outliers by comparison with neighboring values of grid boxes in space and time. Deviations of more than five standard deviations were set to NA, which only applied to 0.001 % of values per variable and simulation. To be able to compare simulation data from different spatial resolutions, we used block-averaging to down-sample the higher resolved simulations to the resolution of ECHAM5-wiso, which was sufficient for the purpose of the analysis.

Modelled variables at record locations are extracted using bilinear interpolation as in Bühler et al.(2021) [24]. The data is resampled from neighboring gridboxes in proportion to the overlap they have with a box of the same size with the cave's location at its center. As speleothems form naturally, measurements only provide irregularly sampled time series [217]. As the SISALv2 last millennium subset with the smallest number of required proxy measurements, the M-subset has a median resolution of 18.67 yr per entity, 90% CI: (15.24, 22.18). Therefore, we down-sample the simulation data at record location to the record's reconstructed time axis by using block-averaging.

Model-data differences between individual modeled and recorded $\delta^{18}O$ are given in $\Delta\ \delta^{18}O = \delta^{18}O_{sim}$ -$\delta^{18}O_{\ rec}$ and referred to as "offset". We quantify the model-data difference by the ratio of recorded to modeled variance at the record location, denoted by Var_{rec}/Var_{sim}.

For spatial mean estimates, we reduce potential biases due to irregularly distributed cave sites through area-weighting. Following Marcott et al. (2013) [172], we calculate the gidbox-mean of all records distributed into a grid of the same spatial resolution as that of the respective simulation, which is then area-weighted across latitudes. We use bootstrapping [72] to provide 90 % confidence intervals, if not stated otherwise.

Speleothem drip water conversion

The here considered last millennium SISALv2 subset includes both calcite and aragonite speleothems. To compare $\delta^{18}O_{sim}$, which is given in V-SMOW standard, to $\delta^{18}O_{speleo}$ given in PDB-standard, $\delta^{18}O_{speleo}$ is converted to its drip water equivalent ($\delta^{18}O_{dweq}$). The empirically-based conversion is temperature dependent and specific for each mineral. That is why speleothems with mixed mineralogy were removed from the subset, as it remains unclear to which extent the applied conversion is appropriate [48]. The conversion follows a protocol set by Comas-Bru et al. (2019) and used in both Bühler et al. (2021) and Bühler et al. (2021) [48, 24, 25].

For calcite speleothems, Tremaine, Froelich, and Wang (2011) [280] provide the empirically-based fractionation formula

$$\delta^{18}O_{\text{dweq}} = \delta^{18}O_{\text{calcite}} - \left(\left(\frac{16.1 \cdot 1000}{T}\right) - 24.6\right), \tag{3.1}$$

with T in K and δ^{18}O in ‰. For aragonite, the fractionation factor from Grossman and Ku (1986) [103] follows:

$$\delta^{18}O_{\text{dweq}} = \delta^{18}O_{\text{aragonite}} - \left(\left(\frac{18.34 \cdot 1000}{T}\right) - 31.954\right). \tag{3.2}$$

For both conversions, temperature values specify the local cave temperature at the time of the fractionation. Especially in paleoclimate studies, these are often not available. Annual mean temperatures above the cave can serve as a surrogate for cave air temperatures [77]. Underestimation of mean cave temperature due to long-lasting snow-packs in very cold conditions only corresponds to ~ 1 ‰in $\delta^{18}\text{O}_{\text{dweq}}$, which is still well within the range of the multi-model ensemble. For both mineralogies, we use modeled annual mean temperatures at the cave location, down-sampled to the record's resolution. This is done for each simulation of the multi-model ensemble as well as of the LM ensemble individually and changes the time-averaged mean and the variance of the isotopic value. In a final step, V-PDB is converted to V-SMOW following Coplen, Kendall, and Hopple (1983) [52]

$$\delta^{18}O_{\text{SMOW}} = 1.03092 \cdot \delta^{18}O_{\text{PDB}} + 30.92. \tag{3.3}$$

The comparison between carbon isotopes from different mineralogies also requires a conversion, as their fractionation paths depend on the mineralogy. To this end, we convert the aragonite δ^{13}C values to their corresponding calcite values through a fractionation offset of 1.9 ± 0.3 ‰[87]. The fractionation offset adjusts for the different enrichment factors of the two minerals as empirically established in laboratory studies for minerals [231] and confirmed in the special case of speleothems [86].

The conversions for $\delta^{18}\text{O}_{\text{speleo}}$ to $\delta^{18}\text{O}_{\text{dweq}}$ is only used, when directly comparing modeled to recorded time-averaged mean values, variances, and spectra. For correlation estimates it would, however, only add an additional source of uncertainty, as the record values then already include simulation data. To this end, we denote raw values that are measured directly in the calcite or aragonite matrix by δ^{18}O, and drip-water converted values by $\delta^{18}\text{O}_{\text{dweq}}$. For the carbon conversion, the offset only changes the time-averaged mean, and has no effect on the rest of the analysis. We, therefore, use the converted values throughout the analysis and generally denote them by δ^{13}C .

3.3.2 Proxy system models or transforming model data into proxy space

Speleothemes and ice cores are amongst many other mediums which archive a specific sensor response to environmental and climatic forcings. Reading information from an archive can, therefore, include signals from different stages of signal en- and decoding. In a first step, a sensor responds to specific environmental changes. Examples are the composition of the drip water that speleothems form from, which is influenced, amongst other factors, by cave temperature, the residence time of the water [280, 127], the composition of seawater δ^{18}O, and seawater temperature during coral formation [270]. These climatic or environmental signals are emplaced into the archive. Examples for an archiving process are compaction and diffusion of snow and firn into the later

formed ice core [128]. In a final step, observations are made on the archive, which include measurement uncertainties in both age and proxy. As such, proxy systems are effective filters of a climate system [142], where the desired signal may be enhanced, damped, or integrated over time and space [75].

A proxy system model (PSM) emulates all or only parts of the sensor, archive, and observation processes. It produces a simplified representation of the variations on a prior, typically a measured climate variable or climate model output, that results in the observations, from which a signal is retrieved [75]. Therefore, it provides means to better interpret the observed signal.

Precipitation and infiltration weighting

The most basic PSM may be the weighting of a desired climate variable depending on another one. Archives that form in accumulative layers depend on seasonally influenced precipitation input such as speleothems on drip-water or ice cores on precipitated snow. Weighting each month of the input signal uniformly in an averaging process may artificially elevate input from specific months with only small total precipitation amount. Precipitation weighted δ^{18}O ($\delta^{18}O_{pw}$) and infiltration weighted δ^{18}O (precipitation minus evaporation, $\delta^{18}O_{iw}$) give a more realistic weighting on the month or season with stronger influence on specific archives. Monthly mean $\delta^{18}O_{sim}$ values are used for precipitation or infiltration weighting to obtain annual values which are calculated as:

$$\delta^{18}O_w = \frac{\sum_{k=1}^{n} \delta^{18}O_k \cdot w_k}{\sum_{k=1}^{n} w_k}, \tag{3.4}$$

with $\delta^{18}O_w$ being the weighted annual mean value ($\delta^{18}O_{pw}$ or $\delta^{18}O_{iw}$), $\delta^{18}O_k$ as the monthly simulated $\delta^{18}O_{sim}$, and w_k the corresponding monthly weights. In case of precipitation weighting, the weights correspond to the precipitation amount per month. For infiltration weighting, the weights describe the precipitation minus evaporation amount. Negative weights due to higher values of potential evaporation than precipitation in certain months are set to "0", to avoid non-physical results. As additional isotopic fractionation processes occur during evaporation from soil, some model diagnostics also include δ^{18}O of soil layers. This more realistic value for $\delta^{18}O_{sim}$ for terrestrial archives was, however, only available for few simulations. Precipitation and infiltration weighting of $\delta^{18}O_{sim}$ allowed for the evaluation of all models equally and a better comparability between the results. In the multi-model comparison, all analysis is done using $\delta^{18}O_{iw}$. For the focused iHadCM3 model-data comparison, all analyses are conducted with both $\delta^{18}O_{pw}$ and annual $\delta^{18}O_{sim}$, but only the $\delta^{18}O_{pw}$ version if not stated otherwise. Within the LM iHadCM3 ensemble, weighting and annual-averaging is done for each simulation individually to allow the examining of the dynamic response in the signal.

Speleothems: karst filtering

Before cave drip water reaches the cave environment, it is transported through the soil and karst system, where it is subject to mixing and filtering processes. We test the impact of a residence in the karst storage [93, 60] by implementing an aquifer recharge model style filter (hereafter *karst filter*). The karst filter is modeled using a simple exponential decay with characteristic timescale τ describing the mean residence time. Mathematical, the filter is given by the impulse response (Green function) $g(t) = 1/\tau \cdot e^{-t/\tau}$, for $t > 0$. We use a normalization such that $\int_T g(t)dt = 1$, where T is the filter time period [60]. We

apply the filter to annually resolved simulated $\delta^{18}O$ ($\delta^{18}O_{pw}$) and down-sample the time series to record resolution in a subsequent step.

Ice: firn diffusion

Ice cores are drilled from glaciers, which form from accumulated layers of snow. The weight of additional layers consequently form firn and finally ice. In this formation process, the isotopic signal is affected by diffusion in the firn. This post-depositional processes damp and even erase part of the encoded climatic signal [20]. Following Casado, Münch, and Laepple (2020), we account for this by applying an isotopic diffusion scheme that convolves the depth of the record with a Gaussian kernel [33, 128]. It uses a depth-dependent diffusion length [153] that is site specific depending on local temperature, accumulation rate, atmospheric pressure, firn depth, and firn density. Local temperatures and precipitation amount are extracted at the ice core location, where precipitation amount serves as a first order approximation of accumulation rate. Firn density modeling follows the Herron-Langway densification model [114]. We set a constant surface density of 350 kg m^{-3} and constant local surface pressure (650 mbar), as its impact on the diffusion length is minimal [33]. Firn depths time series are derived from the age and depth of the records.

3.3.3 Statistical tests and time series processing

Statistical tests for irregularly sampled time series are similar to those for regularly sampled ones, but require either some sort of intermediate reconstruction of the time series (interpolation) or kernel-based methods. The adapted statistical methods used on irregularly sampled time series in this analysis are explained in detail in the following.

Correlation estimates for irregularly sampled time series

The correlation estimates for irregularly sampled time series are calculated using an adapted Pearson-correlation [219, 217]. We chose a significance level of $\alpha = 0.1$, which is appropriate for both the regular and irregular time series, as it balances the considered number of samples N compared to the strictness and expected level of false positives. The corresponding p-values are estimated based on a t-distribution. The degrees of freedom are estimated from the temporal coverages $R_{x,y}$ and the persistence time $\tau_{x,y}$ as $N_{\text{eff}} = \min(\max(R_x/\tau_x, R_y/\tau_y, \text{na.rm=TRUE}), \max(N_x, N_y))$, as described in detail in the R package `nest` [219, 217]. For our analysis using the speleothem last millennium subset of the SISALv2 database, N_{eff} can be estimated between $(20, 470)$ and are generally similar to the number of measurements within a record. For regularly sampled time series, correlation estimates are calculated through Pearson's product moment correlation (using the function `cor.test` in the R package `stats` [213]).

Spectral analysis for irregularly sampled time series

The power spectral density (PSD) of a time series allows for the analysis of the variations of a signal on the frequency spectrum. It describes the distribution of power in frequency components of the time series over a finite interval of time. Integration over all frequency components of the interval yields the total variance [34]. Irregularly sampled time series first need to be interpolated to their mean resolution, before a spectrum can be computed. This is done by a double interpolation and filtering procedure as described in [151, 152, 220, 67] and was recently confirmed to be a robust spectral estimator [109]. In a final step, spectra of sufficiently high resolution can then be averaged to a mean spectrum over a

certain frequency range [149].

Spatial correlation using paleoclimate network approaches

Networks in the climate field are a practical tool to analyze spatio-temporal variability of a specific climate variable and, therefore, to investigate the dynamic and information provided by the climate system and its teleconnections [282, 283, 221]. In this study, we use a network consisting of n nodes, where n is the number of speleothem entities from the SISALv2 last millennium subset that fulfill the sampling criteria of min. 30 $\delta^{18}O_{speleo}$ measurements. The network of speleothem entities is then joined in pairs by links, also called edges, if the respective cross-correlation $\hat{r}_{i,j}$ between entity i and j are significantly different from zero. This results in a maximum of $n \cdot (n-1)$ links being formed.

To better distinguish similarities and differences between the simulated and recorded network, we split the network into eight sub-networks, using hierarchical distance-based clustering of the node locations. We manually split the cluster that includes all East Asia caves into one cluster for East Asia (all caves above 20°N) and one cluster for South East Asia (all caves below 20°N), resulting in a total of nine clusters (see Fig. A.3). For better visualization, we use the concept of "fixed link density", where only links that are above a certain threshold are visualized ($|r| > r_{5\%}$, with $r_{5\%}$ being the minimum correlation strength of the 5 % absolute strongest correlation estimates).

To increase the network analysis strength, we account for age-model sensitivity. To this end, we include all available age-model ensembles that are consistent with radiometric constraints [49] and calculate cross-correlation estimates for all possible combinations for two entities. We define a *best selection tuning* as the age-model pair with the strongest absolute correlation estimate between two entities that is also significant ($p < 0.1$).

Estimating similarity using synchronous events

Transient climate simulations, although forced with GHGs, volcanic eruptions, solar and orbital changes, do not represent a reconstruction of the climate evolution of the desired time period but rather a climate state and variability of the specific time. Through e.g., distinct volcanic eruptions, however, responses of the simulated climate system can be attributed to a specific year. When comparing similarities between simulated responses and possible responses measured in archives, we use synchronous extreme events. Especially given the irregularity of the available time series, this is a useful alternative similarity estimate to correlation estimates. The measure of strength and direction only depends on the relative timing between two extreme events [217].

In this analysis, we rely on the 5 % maxima and minima values given by the 97.5 and 2.5 % quantile ranges of the time series distribution, respectively. For the special case of volcanic eruptions, the 5 % extreme values are distinguished as those above the 95 % quantile. Two successive extreme events are treated as two separate extreme events.

We consider two extreme events as synchronous, when they are closer together than a local threshold τ. It is chosen as half the minimum time between two extreme events and their preceding or succeeding extreme event (Fig. 3.5). For this analysis, we consider only high resolution speleothems with both oxygen and carbon isotopes. The median local τ is 4.62 yr (90% CI: 4.37, 5.28), which reflects the median resolution of the selected speleothems of 6.08 yr, (4.07, 7.85). With this definition, it is still possible that the algorithm distinguished two extreme events as synchronous,

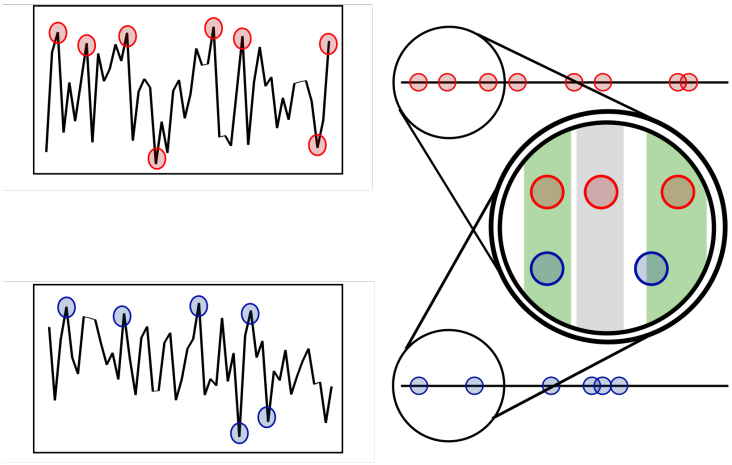

FIGURE 3.5: Illustration of synchronous extreme events. The 5% extreme events of two time series which are indicated by blue and red circles, are considered only through their relative dating (not their absolute value). The events are considered synchronous if they are within a threshold (indicated by the grey and green bars). The width of the threshold (τ) depends on the neighboring extreme events.

although their relative timing is not in relation to their resolution and the studied time scale. We, therefore, introduce a hard threshold of 50 yr, which corresponds to the median age uncertainty within the original and ensemble chronology of our SISALv2 sub-sample [49]. Two extreme events that are 50 yr apart are, thus, never considered synchronous. Age uncertainties within the analysis of synchronous events between oxygen and carbon isotopes of one speleothem entity are not considered, as both time series stem from the same age measurements and, therefore, include the same uncertainties.

For the visualization of the temporal distribution of synchronous extreme events, these are binned into 10 yr intervals, corresponding to approximately twice the median local τ. Bins only consider one synchronous extreme event per analyzed pair and additional synchronous extreme events are not counted. This avoids over-representation of high-resolution speleothems. We determine the significance of synchronous extreme events within one bin by repeating the analysis 2,000 times while randomly permuting one time series of each pair. If the counts within one bin exceed a 95% quantile threshold of the "mean background noise", the number of synchronous extreme events are considered to be significant.

3.4 Results

3.4.1 Relationship between time-averaged modeled and archived variables

In a first step, we compare the SISALv2 last millennium M-subset to the iHadCM3 LM1 $\delta^{18}O_{pw}$ time-averaged means to assess potential model biases. Fig. 3.6 shows the annual mean temperature and precipitation fields (Fig. 3.6a,b), the modeled mean $\delta^{18}O_{pw}$ with the point-wise $\delta^{18}O_{dweq}$ at the cave locations (Fig. 3.6c), and the difference between the modeled and archived time-averaged mean $\delta^{18}O$ (Fig. 3.6d). Results for the

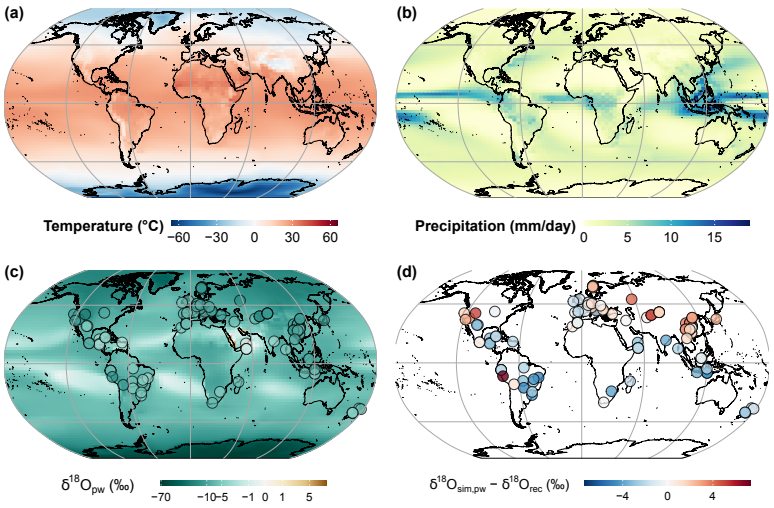

FIGURE 3.6: Characterization of the mean surface climate of the simulation (LM1): Shown are (a) mean annual surface temperature, (b) precipitation, and (c) $\delta^{18}O_{pw}$, including $\delta^{18}O_{dweq}$ at cave sites in drip water equivalents. Note the logarithmic color scale. Point-wise differences between the mean simulated $\delta^{18}O$ and proxy-based $\delta^{18}O_{dweq}$ (d) show anomalies. Figure and caption adapted from [24].

iHadCM3 LM2-3, which are generally very similar to LM1, can be found in [24]. The simulated mean $\delta^{18}O$ fields show some of the known prominent isotopic features, such as the temperature effect of the precipitation amount effect [59]. For example, the light spots above the mid-latitude ocean show high $\delta^{18}O$ in areas with high evaporation but comparably low precipitation. The darker spots around the poles, toward land masses, and toward regions of high precipitation in Fig. 3.6c show progressive depletion.

Generally, the offsets between modeled and measured $\delta^{18}O_{pw}$ show a heterogeneous pattern (Fig. 3.6d) with mostly higher depletion in the simulation. Local patterns exist with less depletion in the simulation on the big landmasses in the Northern Hemisphere. One prominent outlier is site 277 (eID = 598, Huagapo cave in Peru) visible as a dark red dot in Fig. 3.6d. It shows a strong depletion in calcite ($\delta^{18}O_{dweq} = -13.7‰$) while the simulation is not as strongly depleted ($\delta^{18}O_{pw} = -6.47‰$). This large model-data difference can in part be attributed to the large difference in elevation between the cave site at 3850 m and the model which is close to sea-level. The site 38 (eID = 113, Diva cave in Brasil) with the most negative offset of $\Delta\delta^{18}O = -4.79‰$ is not an outlier, but surrounded by sites where the simulation is more depleted than the records.

We contrast the iHadCM3 LM1 to the four other last millennium simulations, to see potential model biases. Fig. 3.7a-e show the modeled climatologies of $\delta^{18}O_{iw}$ as to the $\delta^{18}O_{pw}$ in Fig. 3.6c. Compared to the last millennium ensemble, iHadCM3 with a global mean of $-9.15‰$ (-9.29, -9.01) shows a stronger overall depletion, similar to iCESM with $-9.39‰$ (-9.51, -9.28). Especially across Antarctica, the depletion is strongest in iHadCM3, which leads to the large model range in $\delta^{18}O_{iw}$, depicted in Fig. 3.7f. Across the Arctic, iHadCM3 shows the highest $\delta^{18}O_{iw}$. In the low- to mid-latitudes, where latitudinal means across the ensemble are fairly similar, differences are mostly regional. The areas with the largest range between the simulated isotopes are across the Sahara desert, the Arabian peninsula, the Indian peninsula, and Siberia. Some of the deviations can be explained by temperature differences between the simulations (Fig. A.4), especially the global mean differences. Around the poles, the temperature difference is, however,

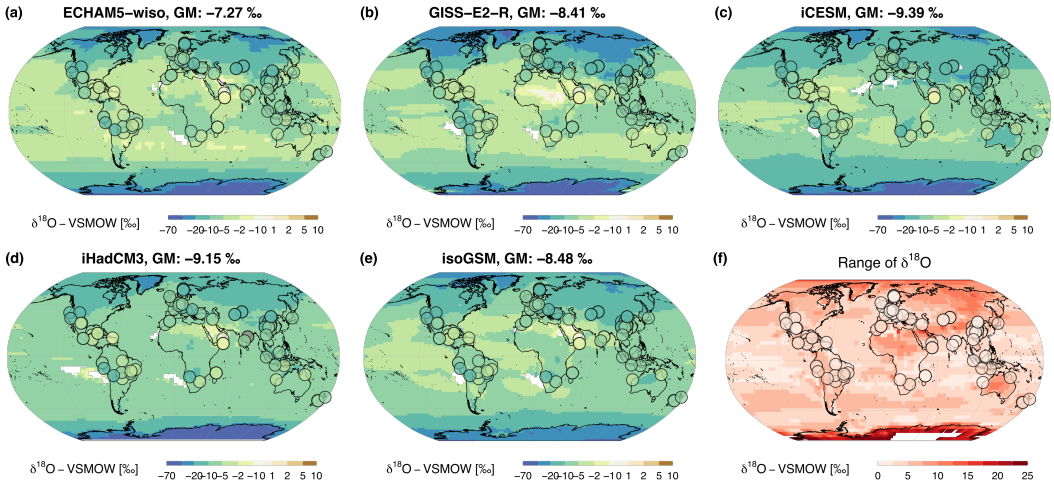

FIGURE 3.7: Simulated $\delta^{18}O_{iw}$ climatology (a-e) of the respective simulation: a) ECHAM5-wiso, b) GISS-E2-R, c) iCESM, d) iHadCM3, e) isoGSM) in the background. The time-averages mean $\delta^{18}O_{dweq}$ using the respective simulated temperatures are depicted as circles. Global means (GM) of $\delta^{18}O_{sim}$ are given in the title of each subplot. f) shows the range of $\delta^{18}O_{sim}$ between all simulations for each gridbox, as well as the range for the difference between simulation and record. Light colors indicate large agreement between the simulations, while darker colors mark areas, where the models differ strongly and the spread between the $\delta^{18}O_{sim}$ is larger. Antarctic $\delta^{18}O_{sim}$ ranges are up to 40‰, highlighting the different model performance in this region (white area in f). Figure and caption adapted from [25]. The appendix contains climatologies of surface air temperature (Fig. A.4) and precipitation amount (Fig. A.5).

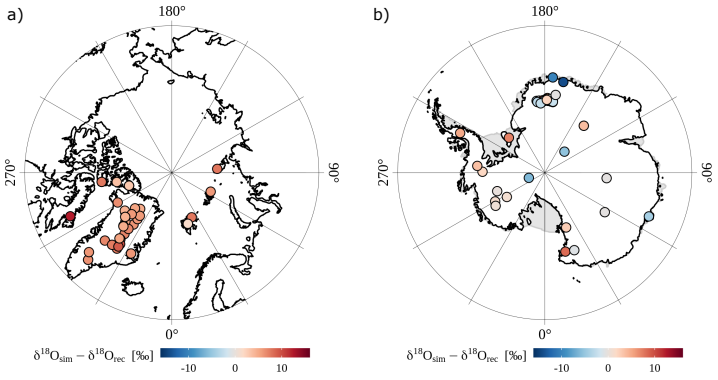

FIGURE 3.8: Comparison of the $\delta^{18}O_{sim}$ iHadCM3 LM1 and $\delta^{18}O_{ice}$. a) and b) show the point-wise differences for the Arctic and Antarctic. The grey shading depicts the Antarctic ice shelves. Figure and caption adapted from Yannick Heiser [110].

not sufficient to explain the large difference as the coldest areas are not necessarily the most depleted and vice versa.

At the speleothem locations, the highest agreement between the simulations of 2.31‰ range is obtained at site 159 Tham Duon Mai Cave in Laos [292]. The strongest disagreement of a range of 8.14‰ is at site 17 Huangye Cave in China [266]. Strong agreement between the models does, however, not coincide with high model-data match.

As the polar regions show the highest model ensemble range, we evaluate the iHadCM3 LM1 using ice core data from the Iso2k database. Differences between the modeled $\delta^{18}O_{pw}$ and archived $\delta^{18}O_{ice}$ are shown in Fig. 3.8. While there is a heterogeneous pattern for the Antarctic with a mean $\Delta\delta^{18}O = -0.73‰$ and a standard deviation of $\sigma = 4.82‰$, there is a positive bias in iHadCM3 visible for the Arctic. Here the mean is $\Delta\delta^{18}O = 6.19‰$ with a standard deviation of $\sigma = 2.03‰$ [110]. Most of the extreme differences can be attributed to elevation differences between model and record. Difference of approximately $\pm 5‰$ occur especially at very small elevation difference and can not solely be explained by them. Complex topography, especially in coastal regions can also alter the isotopic signal in ice core records through downstream transport.

Isotope data from speleothem and ice core records, as well as the comparison to other last millennium simulations suggest that isotopic signatures are well represented in iHadCM3, except for the Northern high latitudes where we find a bias toward more positive $\delta^{18}O$. Between models, most differences in isotopic composition of precipitation could be attributed to differences in temperature. These can, however, not sufficiently explain all findings.

3.4.2 Local modeled and archived variability in $\delta^{18}O$ at different timescales

To analyze similarities and differences in modeled and archived variability of the isotopic signal, we first compare the total variance in iHadCM3 LM1-3 ensemble at the cave locations to that of the 92 speleothem records in the V-subset over the last millennium. Overall, the global distribution of variance ratios between $\delta^{18}O_{dweq}$ and $\delta^{18}O_{pw}$ downsampled to record resolution in Fig. 3.9a shows higher variance in speleothem records. There are, however, local exceptions to this. The higher variance is indicated by the

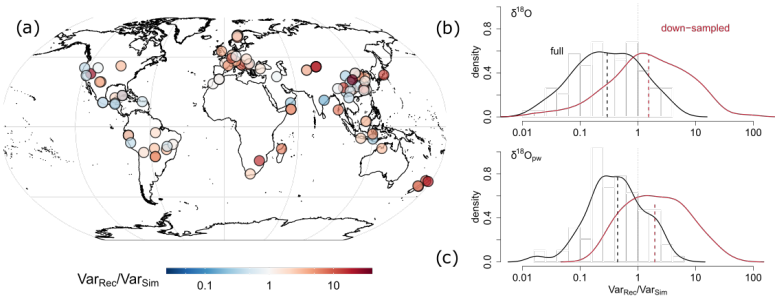

FIGURE 3.9: (a) Spatial visualization of the site-based dimensionless variance ratio V_{Rec}/V_{Sim}. The simulated δ^{18}O is down-sampled to record resolution, based on LM1. Aggregated density plots of the variance ratio of $\delta^{18}O_{dweq}$ to δ^{18}O (b) and precipitation-weighted $\delta^{18}O_{pw}$ (c) at annual resolution ("full", black lines) and at records' resolution ("down-sampled", red lines) illustrate the variance loss due to temporal averaging in the archive (uses LM1-3). Figure and caption adapted from [24].

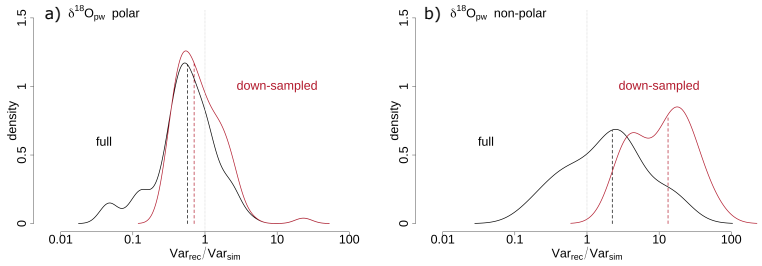

FIGURE 3.10: Comparison of variance ratios Var_{Rec}/Var_{Sim} based on the iHadCM3 LM1 similar to Fig. 3.9ab but for ice core records from Iso2k. Shown are density plots of the variance ratio of $\delta^{18}O_{pw}$ and (a) polar $\delta^{18}O_{ice}$ and (b) non-polar $\delta^{18}O_{ice}$. The dashed lines indicate the medians. Figure and caption adapted from Yannick Heiser [110].

predominant red-shading in the visualization of global distributed variance ratios. This is corroborated by the density plots in Fig. 3.9b-c showing roughly two times higher variance in the speleothem records than in the simulation (median of the histogram for $\delta^{18}O_{pw}$ at 1.8 $(1.4, 2.6)$ in Fig. 3.9c). There is a clear impact from the averaging to record resolution as can be seen when comparing the "full" and the "down-sampled" densities. While the simulated variance at annual-resolution ("full") in $\delta^{18}O_{sim}$ and $\delta^{18}O_{pw}$ is always higher than in the speleothems (variance ratio below unity), down-sampling to record resolution shows the clear discrepancy between the observed $\delta^{18}O_{dweq}$ and modeled $\delta^{18}O_{sim}$ and $\delta^{18}O_{pw}$ at the cave location.

The highest variance ratio between speleothem δ^{18}O and down-sampled $\delta^{18}O_{pw}$ is found in Jiuxian cave in China (eID 330, with a variance ratio of 49.5), the lowest in Dandak cave in India (eID 130, with a variance ratio of 0.2). For both records we find neighboring caves to show very different variance ratios. This hints at a large heterogeneity of the speleothem data from the cave environment as the modeled patterns are fairly smooth across neighboring gridboxes.

When assessing variability in the high-latitudes, we need to turn to ice core records. To increase comparability, we do not compare ice core variances to those of speleothems, but polar ice core variance (85) from the Arctic and Antarctic to those of the few non-polar

ice cores (13) in the Iso2k database. Averaging the modeled δ^{18}O to record resolution in Fig. 3.10 reduces the variance, especially for the non-polar ice cores. When comparing polar to non-polar ice cores, it is striking that while there is a general match in variance in the polar regions, a large mismatch can be detected for the non-polar ice cores. This can, however, not only be attributed to large underestimation of modeled variance, as many records covering only few decades are included in the polar dataset. Additionally, the very few non-polar records exhibit a reduced temporal resolution compared to the polar records.

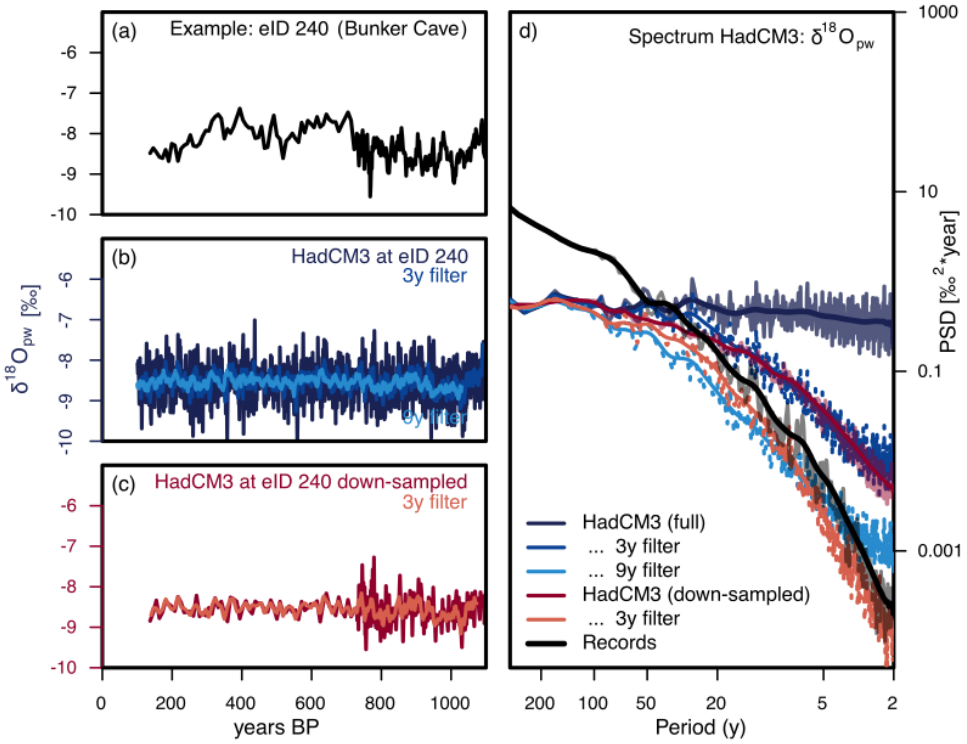

FIGURE 3.11: Time series and spectra of measured $\delta^{18}O_{dweq}$ and simulated $\delta^{18}O_{pw}$ time series as well as of their spectra. (a-c) Example time series of eID 240 in Bunker cave (Germany) [85]. (a) measured $\delta^{18}O_{dweq}$ in the speleothem, (b) iHadCM3 simulated $\delta^{18}O_{pw}$ at the cave location with two filters (3 and 9 yr) and (c) the simulated $\delta^{18}O_{pw}$ but down-sampled to the same temporal resolution as in (a) with 3 yr filter. (d) Power spectral density (PSD) of local mean spectra of simulated $\delta^{18}O_{pw}$ at the cave site in yearly resolution (blue), down-sampled to the caves resolution (red) and mean spectrum of the $\delta^{18}O_{dweq}$ of the records (black), including the karst-filtered as shown in (a-c). The spectra are area-weighted and averaged over the three simulations (LM1, LM2 and LM3). The colors for the example eID in (a-c) correspond to the colors of the mean spectra over all entities in (d). Figure and caption adapted from [24].

We extend our analysis on variability across timescales to assess the influence of low-resolution and small sample size on the comparison. The timescale dependent variance (Fig. 3.11) explores the variability of the speleothem S-subset and the iHadCM3 LM1-3 on interannual, decadal and centennial timescales over the last millennium. The spectra in Fig. 3.11d show the modeled and archived δ^{18}O variability across interannual to multi-centennial scales. It can help to better understand modeled and archived δ^{18}O

variability over different time scales and the representativity of speleothem records for reconstruction resolution. The left side of the plot (Fig. 3.11a-c) represents the time domain, while the right side (Fig. 3.11d) displays the frequency domain. For the time domain we chose an exemplary cave site (Bunker cave Germany and eID 240) to illustrate the different temporal resolutions and the effect of the karst filter, while the frequency domain shows the average spectra over the speleothem subset. By comparing Fig. 3.11a-c visually, one can already distinguish differences between the filtered and unfiltered simulation data.

We decompose the information from Fig. 3.11d: the simulated $\delta^{18}O_{pw}$ spectrum of annual resolution shows fairly constant PSD across all frequencies. This means that interannual variance (integrated PSD across interannual frequencies) is just as high as decadal or centennial variance (integrated PSD across decadal frequencies). Down-sampling to record resolution, which corresponds to a short-timescale averaging, decreases power in the higher frequency range of the simulated spectrum. Translated to the temporal domain, this means that on interannual to decadal timescales, the annual-resolved time series shows more variance than the down-sampled ones. On multi-decadal and longer timescales, both time series display a similar level of variability.

On multi-decadal and longer timescales, the $\delta^{18}O_{speleo}$ spectra show higher PSD than $\delta^{18}O_{sim}$ spectra both at annual and down-sampled resolution. This means that the speleothem records are in general more variable than the simulation on multi-decadal and longer timescales. For the higher frequencies, they show, however, less PSD than the simulation down-sampled to the same resolution. We asses this mismatch of variability on decadal and shorter timescales by testing the impact of karst processes and storage through a simple karst filter. Filters of increasing transit times τ result in increasing spectral slopes. A 3 yr filter reduces the PSD of the down-sampled simulated spectra to equivalent variance as those of the records. On longer timescales the filtered spectra eventually flatten toward the unfiltered spectra, without ever exceeding it, making it too less variable on longer timescales than the record. Spectra for all individual spectra (full simulation, down-sampled, record spectrum, and all filters) can be found in the supplemental material of Bühler et al. (2021) [24].

To set the results obtained for iHadCM3 into perspective, we repeat the analysis for the last millennium model ensemble and the speleothem MM-subset. Fig. 3.12b-c show spectral ratios between $\delta^{18}O_{speleo}$ and $\delta^{18}O_{iw}$ on annual (Fig. 3.12b) and mean record resolution (Fig. 3.12c). A spectral ratio > 1 indicates higher variance in $\delta^{18}O$, while a spectral ratio < 1 indicates higher variance in modeled $\delta^{18}O_{iw}$. For both the annual resolution and the down-sampled to record resolution case, we see that iHadCM3 shows in general a smaller mismatch on decadal and higher frequencies than the other models. This hints at less decadal and interannual variability in iHadCM3 which would decrease a model-data variability mismatch on shorter timescales. On decadal to centennial timescales, iHadCM3 has the highest model-data mismatch, indicating less variability on these timescales compared to other models. Please note that this assessment only holds for speleothem locations. Comparing area-weighted mean global variances, iHadCM3 shows higher variance over the last millennium than ECHAM5-wiso, and similar variance to iCESM, while GISS-E2-R and isoGSM still show highest variance (results from [25] not shown). The analysis suggests that variability is represented differently by models, but there is no clear dependency on the models' resolution.

Comparing isotopes within the speleothem Fig. 3.12a shows higher variance in the carbon isotope on all timescales, with more similar variability on the high frequency end. This is supported by the distribution of isotopic variance over the last millennium in Fig. 3.12d,

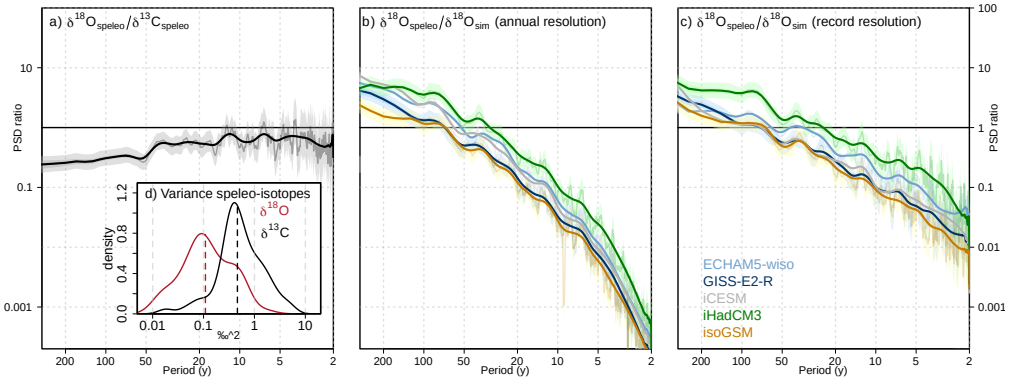

FIGURE 3.12: Spectral ratios of isotopes in speleothem and the last millennium ensemble on different timescales as shown by the ratios or mean PSD: a) spectral ratio between speleothem isotopes (δ^{18}O /δ^{13}C). b-c) spectral ratio over all cave locations for $\delta^{18}O_{speleo}$ and $\delta^{18}O_{sim}$ per simulation (model-colors). In b) we show the spectral ratios of $\delta^{18}O_{speleo}$ to $\delta^{18}O_{sim}$ down-sampled to the individual records' resolution and in c) to the simulated annually $\delta^{18}O_{sim}$. The full spectra are shown in faded colors and a smoothed spectrum in black or the model colors. d) variance of detrended $\delta^{18}O_{speleo}$ (red) and δ^{13}C (black) as measured in speleothem records. The dashed line indicated the median of the distribution. Analysis with MM-subset of SISALv2. Figure and caption adapted from [25].

where δ^{13}C shows a much higher variance with a median of 0.46‰^{2} (0.38, 0.6) compared to $\delta^{18}O_{speleo}$ with a median variance of 0.11‰^{2} (0.08, 0.12).

In a final step, we evaluate the representativity of the $\delta^{18}O_{speleo}$ as archives of δ^{18}O variability compared to other oxygen isotope archives. For this, we turn to a case study of one particular site in South America, where a speleothem entity (eID 498 from Chiflonkhakha cave), a GNIP collection station (La Paz station 8520101) and an ice core record (IC13THQU01A from Quelccaya Ice Cap) are within a 350 km radius. We use the simulated iHadCM3 LM1 $\delta^{18}O_{pw}$ values at the ice core location, down-sampled to the ice core's resolution and a firn diffusion filter (see Sec. 3.3.2), which slightly decreases variability on interannual to decadal timescales. The time periods in which the considered archives collected δ^{18}O do not necessarily overlap, especially as the GNIP station only started collection of data in 1995. Comparing the ice core spectrum to the modeled spectrum, both show a loss in PSD on interannual timescales due to smoothing processes through firn diffusion, but the ice core PSD is still higher on all timescales. The speleothem record shows lower PSD on decadal timescales than both the ice core and the simulation, but increases in PSD to the same level as the ice core variance on centennial timescales. The prominent annual peak is visible in the GNIP data. Due to the short time series, the spectra only shows PSD for the interannual timescales, where it has the same level of PSD as the ice core record. This case study hints at comparable variability across archives compared to lower variability in the simulation. However, it is yet limited to three records from three different sites.

Summarizing, we compared modeled and archived total variance ratios over the last millennium for speleothems, as well as polar and non-polar ice cores, where we found higher variance especially for the speleothems and non-polar ice cores. Assessing the variability on different time scales, variability mismatches on shorter timescales between

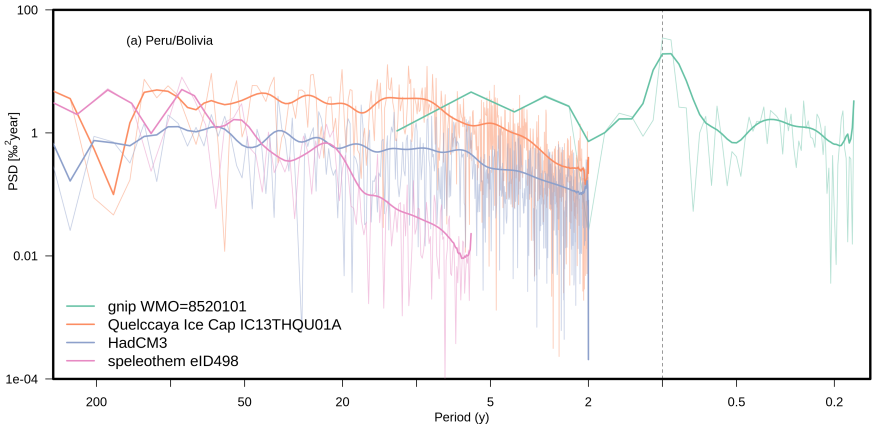

FIGURE 3.13: Comparison of the spectra for δ^{18}O records from sites in Peru and Bolivia. Records are from ice cores, speleothems, and monitored precipitation (GNIP). Shown are the PSDs for the GNIP record 8520101 from measurement station La Paz, Bolivia at 3,635 m (green), the ice core record IC13THQU01A from Quelccaya Ice Cap at 5,670 m (orange) [271], the diffused, precipitation-weighted and down-sampled HadCM3 records for the ice core site (blue), and the speleothem record eID 498 from Chiflonkhakha cave (pink) [3]. Figure and caption adapted from Yannick Heiser [110].

iHadCM3 and speleothems could mostly be explained by the lower resolution of the record and karst filtering processes. On decadal and longer timescales, a variability mismatch remained. Here, iHadCM3 was less variable on centennial timescales than the other simulations from the last millennium ensemble, while a multi-archive case study showed comparable variance between the archives.

3.4.3 Climatic drivers of δ^{18}O in time-averaged mean and variability

We assess relationships of modeled climate variables such as temperature, precipitation, and evaporation, to isotopes archived in speleothems to analyze spatial effects on speleothem time-averaged means $\delta^{18}O_{dweq}$. Fig. 3.14 shows ensemble mean climate variables at the cave location for the SISALv2 MM-subset. Cave site altitude information is included in the analysis. Separating the analysis into latitudinal bands yielded stronger relationships than a global analysis (compare to [24] Fig. 4 where results are shown for the iHadCM3 LM1 and the $\delta^{18}O_{speleo}$ measurements SISALv2 M-subset). Significant relationships are mostly found in the extratropics for all tested variables. For both temperature and precipitation, the strongest relationships to $\delta^{18}O_{dweq}$ are found in the subtropical regions. In all three regions, the relationship to temperature explains more variance than that to precipitation. Evaporation seems to play a minor role and relationships, if significant, are very weak. Especially interesting is the inverse relationship of speleothem oxygen isotopes to precipitation in the tropics compared to the extratropics, indicating different driving climate processes.

To distinguish main drivers not only for the mean state of archived and modeled δ^{18}O, but also for its variability, we correlate simulated $\delta^{18}O_{iw}$ with simulated temperature and precipitation. The mean of the gridbox correlation estimates per model to these main climatic drivers shows high agreement across the ensemble. This agreement is indicated by crossed tiles when four or more correlation estimates of the different simulations agree in sign (Fig. 3.15, individual correlation fields in the supplement material of [25]).

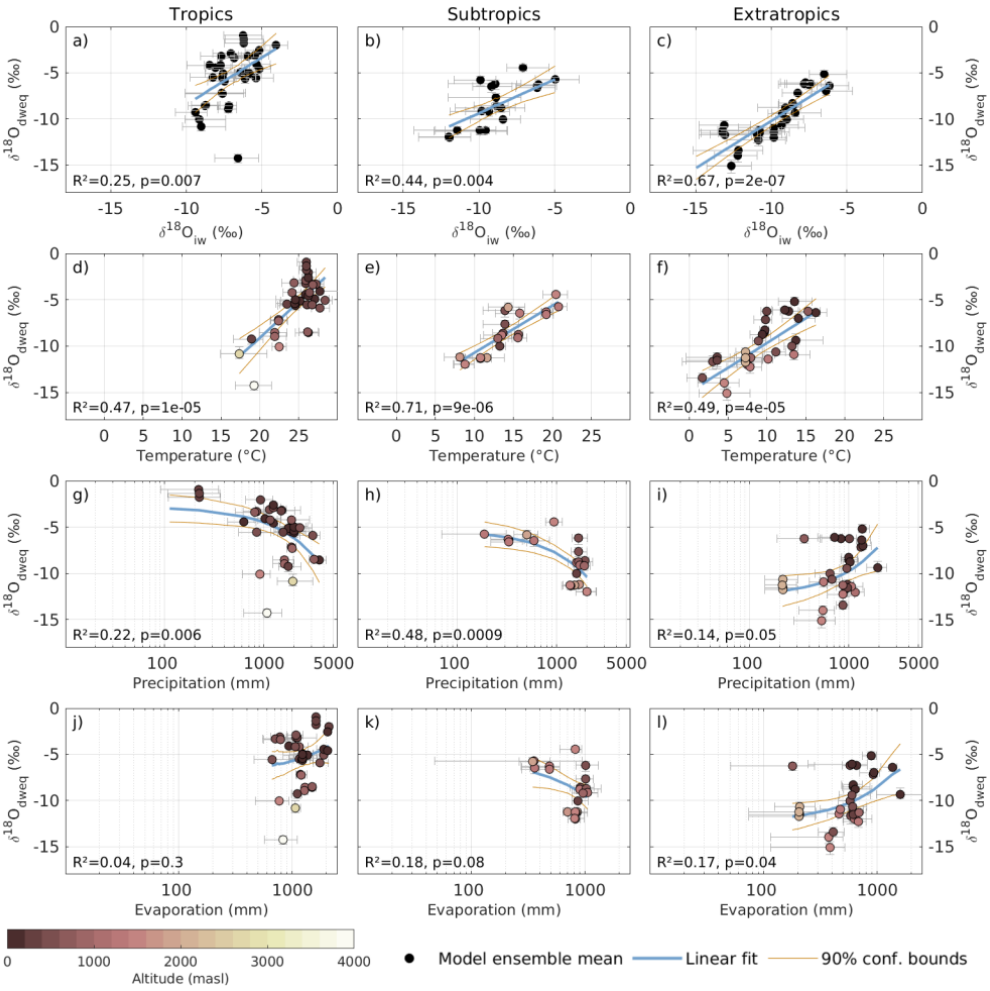

FIGURE 3.14: Infiltration weighted $\delta^{18}O_{sim}$ a-c), temperature d-e), precipitation g-i) and evaporation j-l) against speleothem $\delta^{18}O_{dweq}$ for model ensemble mean in the tropics, subtropics and extratropics. The tropical region (23.44°S to 23.44°N) is shown in left panel (a, d, g, j); the subtropical region (23.44–35°N/S) is shown in the middle panel (b, e, h, k); the extratropical region (35–90°N/S) is shown in the right panel (c, f, i, l). In d-l) altitude information is applied as shaded colors. We use $\delta^{18}O_{iw}$ for all simulations. Note the semi-logarithmic axes for precipitation and evaporation. Figure and caption adapted from [25].

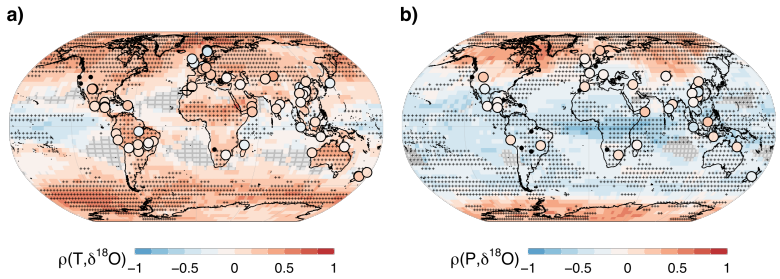

FIGURE 3.15: Correlations between simulated interannual SWI changes and a) temperature b) and precipitation in each gridbox. The background shows the mean correlation over all five simulations between annual $\delta^{18}O_{sim}$ and b) simulated annual temperature per gridbox and b) for precipitation. Crosses indicate gridboxes, where the correlation for four or more models has the same sign as the mean between all simulations. Symbols indicate the mean correlation of the simulated temperature (precipitation) to the recorded $\delta^{18}O_{speleo}$ at record resolution. Crossed circles mark locations, where more than four models agree in the mean sign of the correlation to $\delta^{18}O$. Black circles indicate the location of those speleothems in the last millennium subset that show no significant correlation to any model. Figure and caption adapted from [25].

Grey (empty) tiles indicate non-significant correlation estimates. The correlation between $\delta^{18}O_{speleo}$ and the climate variable after temporal down-sampling is also shown. The weighting generally decreases the absolute correlation estimates to both variables, when compared to correlation fields of annual mean $\delta^{18}O$ (results not shown).

For the correlation to temperature (Fig. 3.15a), we can distinguish two major domains: high positive correlation to $\delta^{18}O_{iw}$ in the high latitudes and across land masses, while we see negative correlation over the low- to mid-latitude oceans. Large-scale agreement is, however, only found across the higher latitudes and the landmasses. Correlation estimates to precipitation are more clearly separated into two domains than those to temperature: we find mainly positive correlation estimates around the polar regions, and negative correlations in the tropics and low latitudes.

The data clearly suggests that the two main tested drivers for $\delta^{18}O$ variability can be separated into two specific regions: temperature is the dominant driver in the high latitudes, where absolute correlation estimates are higher compared to precipitation. Precipitation is the dominant driver in the low latitudes, even for the land masses, where absolute correlation estimates to precipitation are highest.

Comparing the correlation fields of the individual simulations (supplement material of [25]) to that of the averaged fields in Fig. 3.15 does not reveal different processes that govern the isotopic cycle at a certain region within the simulations. We find that all simulations show similar patterns, with only small differences, e.g., ECHAM5-wiso shows slightly higher absolute correlation estimates for both temperature and precipitation across the Sahara desert than the rest. Only iCESM differs strongly from the rest. While the general patterns are similar, the absolute correlations are much higher compared to the other models.

For the speleothem records, no clear driver is distinguishable. We tested for correlation between $\delta^{18}O_{speleo}$ and the simulated climate drivers down-sampled to record resolution. We do find more significant correlation estimates to temperature across all simulations.

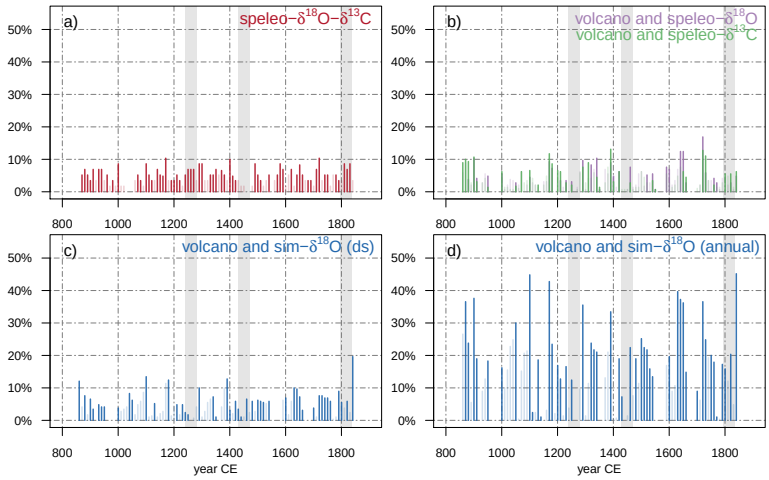

FIGURE 3.16: Synchronous events: a) the synchronous extreme events between $\delta^{18}O_{speleo}$ and $\delta^{13}C$ (red), b) the synchronous events between the speleothem isotopes (oxygen purple and carbon green), and volcanic eruptions as reconstructed by [55] or [92] (depicted in Fig. 3.2d), c-d) the synchronous extreme events between simulated $\delta^{18}O$ values at the cave locations of all simulations in down-sampled to record resolution and annual resolution respectively. Where occurrence of synchronous extreme events is significant with $\alpha = 0.05$, the bars are shown in dark colors, non-significant in transparent colors. The four light grey bars in the background of each plot show areas of high volcanic activity. Figure and caption adapted from [25]. The same figure but to the respective solar forcings can be found in Fig. A.8.

However, we also find that correlation estimates increase with decreasing resolution, indicating that this could also be a methodological bias.

Variability in models originates from internal variability and the response to external forcing. Modelled $\delta^{18}O$ is likely influenced by both. For example, the signatures of modes of variability such as ENSO (an atmosphere–ocean coupled mode of variability), ISM [99], and NAO (a quasi-periodic spatial pattern of sea level pressure changes in the Northern hemisphere Atlantic ocean) are reflected in modeled isotopic signatures (Fig. A.6). The imprint of external forcing from volcanic eruptions is visible in the $\delta^{18}O$ patterns, mostly through the covariance to temperature, which responds strongly to volcanic eruptions (Fig. A.7a-c). Changes in solar forcing (Fig. A.7d-e) are not inferable from modeled temperature, precipitation, and isotopic signatures. To test if speleothem records as well as speleothem locations in the simulation are potential sensors of external forcings, we analyze synchronous extreme events between $\delta^{18}O_{speleo}$ or $\delta^{18}O_{iw}$ at speleothem locations, and volcanic eruptions as reconstructed by [55] and [92].

Fig. 3.16 shows the temporal distribution over the last millennium of synchronous extreme events at speleothem locations. In Fig. 3.16a, we test for synchronous extreme events between oxygen and carbon isotopes to examine, if extreme external events will be archived in both signals. Despite the high number of significantly correlated oxygen and carbon isotopes (85% of records with both isotopes show significant correlations $> |\pm 0.15|$), a global response to large volcanic eruptions (indicated by grey bars) are not visible. A maximum of 10 % of speleothems shows synchronous extreme events between both isotopes at the same time over the last millennium. Both isotopes are also analyzed

individually on synchronous extreme events to volcanic eruptions as reconstructed by [55] and [92] (Fig. 3.2d) and $\delta^{18}O_{speleo}$ as in Fig. 3.16b. Here, up to 20 % of speleothems with oxygen isotopes exhibit extreme events synchronously to a volcanic eruption in the reconstruction, while the share is only up to 15 % of speleothems for carbon isotopes. As the number of counts depends strongly on the available proxy measurements in the time period, we cannot determine a constant random count level for all bins. Instead, significance of extreme events is calculated for each bin individually as described in Sec. 3.3.3.

To check if the location and resolution of speleothems is sufficient to resolve extreme events such as volcanic eruptions and their following temperature response, we compare simulated $\delta^{18}O_{iw}$ at cave locations to volcanic eruptions. For comparable extreme event signatures between the simulations, each modeled $\delta^{18}O_{iw}$ is checked against the respective forcing used in the simulation. While up to 50 % of annually resolved $\delta^{18}O_{iw}$ exhibit extreme events at the same time as extreme volcanic forcing (Fig. 3.16d), the number decreases to the level of recorded speleothem isotopes when the resolution is reduced to that of the speleothems (Fig. 3.16c). As already visible in Fig. A.7d-f, solar forcing is not strongly imprinted in modeled climate variable signatures. Our analysis on synchronous events between modeled and archived oxygen isotopes and solar variations only confirmed the negligible solar effects on $\delta^{18}O_{sim}$ and $\delta^{18}O_{speleo}$ within the last millennium.

3.4.4 Network analysis at different spatial levels

We assess the spatial representativity of speleothem records by computing statistical similarity between $\delta^{18}O$ signals within a cave ("site-level-correlation") and across nearby caves (regional or gridbox-level correlation). The networks in Fig. 3.17 represent such measures of spatial similarity. Fig 3.17a-d show the simulated signal at cave locations (annual resolution and down-sampled), while Fig. 3.17e,f show the speleothem networks for the S-subset with 85 entities. For better visibility, we only show the 5 % strongest absolute links.

For the simulated $\delta^{18}O_{pw}$, the highest correlation estimates are found at close proximity for both resolutions. This can be explained by the fact that $\delta^{18}O_{pw}$ records for different entities within one cave or within one gridbox will only differ in their temporal resolution in the case of down-sampling and will be the same for annual resolution. The mean absolute correlation for the 5 % strongest significant links in the down-sampled modeled $\delta^{18}O_{pw}$ in Fig. 3.17c is $c = 0.42\ \ (0.41, 0.43)$. Comparing the simulated networks at different resolution only reveals an additional scattering in link strength at distances longer than $2,000$ km for the down-sampled resolution.

The speleothem records show links across a wide range of distances, while no observable relation between correlation and distance or to large scale spatial patterns. Especially at the local scale, correlation estimates are much weaker than for simulated $\delta^{18}O_{pw}$. The mean absolute correlation for the 5 % strongest significant links between $\delta^{18}O_{speleo}$, as shown in Fig. 3.17e,f, is $c = 0.52\ \ (0.52, 0.53)$. Computing the networks using ensemble age models and selecting the age models that maximize the absolute correlation between sites only amplifies absolute correlation estimates but does not change the correlation-to-distance relationship. The age-model-sensitivity test performed on the simulated down-sampled $\delta^{18}O_{pw}$ still shows strong correlation estimates at short distances. Yet they are weaker than those from original chronologies. Sensitivity tests were only performed for 69 entities within the S-subset, where age model ensembles based on U/Th-datings were available [49].

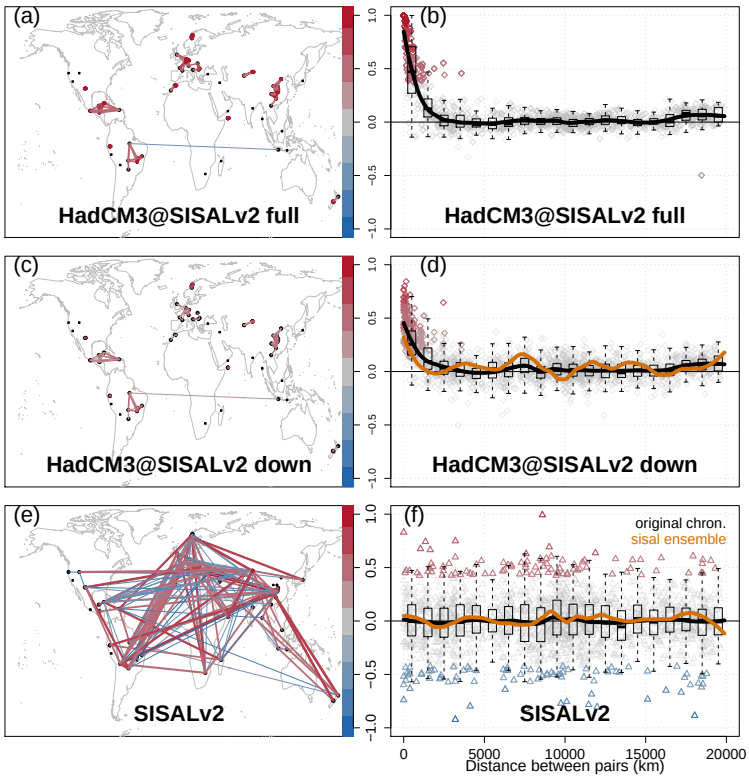

FIGURE 3.17: Network spanned by the 5 % strongest absolute correlations of simulated iHadCM3 LM1 $\delta^{18}O_{pw}$ at the SISALv2 S-subset cave sites (a) full, i.e., annual resolution, c) down-sampled). All model-based between-site-correlations are shown in the distance-binned boxplot b,d). e) network visualizations and f) distance-binned boxplot of the cross-correlations between SISALv2 S-subset site $\delta^{18}O_{speleo}$ for the original age models. The color values indicate the 5 % strongest correlations in network and boxplot. The LOESS smoother (span = 0.2) in the boxplots indicate the correlation for the original chronology (black) as well as the absolute highest correlation through selection of age-models (orange). Figure and caption adapted from [24].

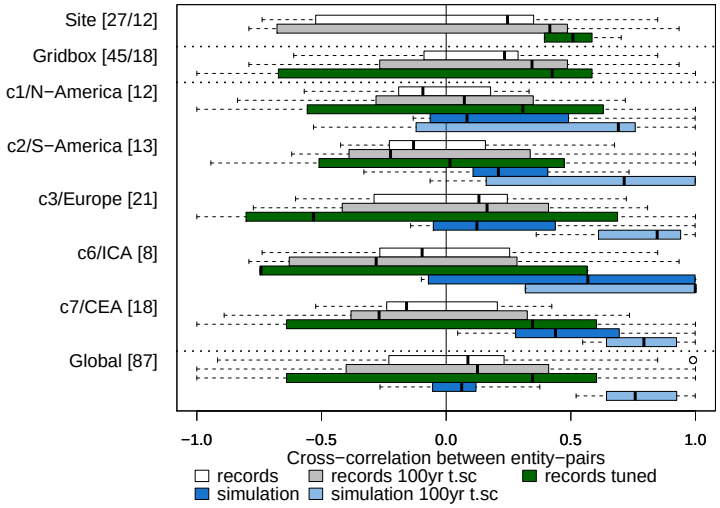

FIGURE 3.18: Cross-correlation on site, gridboxes, clusters and global scale for speleothem records and the locally interpolated model output for $\delta^{18}O_{pw}$. 12 (18) sites (gridboxes) contain more than one speleothem entity with a total of 27 (45). At each aggregation level the correlation estimates between all entities is shown for $\delta^{18}O_{speleo}$ (white bars), and the down-sampled model output $\delta^{18}O_{pw}$ of LM1-3 at cave locations (blue bars). Different temporal scales (original resolution and 100 yr-timescale (t.sc)) are compared as well as the age-model ensemble that gives the highest absolute correlation (dark green bars). Clusters are indicated with the number of speleothem entities in brackets, where c4, c5, c8, and c9 are not included because they contain too few entities. c6/ICA is the India and Central Asia cluster, c7/CEA is the China and Eastern Asia cluster. For more information on the clusters, see [26]. Figure and caption adapted from [24].

When focusing on cave-site or gridbox correlation, correlation estimates between speleothem entities strongly increase when using a 100 yr Gaussian smoothing filter and when selecting age-models under the sensitivity test (Fig. 3.18). On a global scale, the Gaussian smoothing strongly increases the simulation-based network correlation estimates, while it only slightly increases those in the proxy based-network. Extending the analysis to a regional scale of clusters, we find mostly positive correlation estimated in the simulation, while anti-correlations can be also found in the speleothem data set (example for Europe in Fig. A.9, more clusters in the supplement material to [24]).

3.5 Discussion

3.5.1 δ^{18}O climatology model-data comparison

The isotope climatology as represented in the iHadCM3 agree well with the mean state of the measured speleothem $\delta^{18}O_{speleo}$ (Fig. 3.6) with an unweighted mean offset of Δ δ^{18}O = 0.1‰(−4.6, 4.4) to the M-subset and -0.68‰ (-1.18,-0.18) to the MM-subset. Both offsets are small compared to the area weighted variance of $\sigma^2 = 0.78‰^2$ $(0.77, 0.8)$ of the global simulated mean $\delta^{18}O_{pw}$. Isotopic mean patterns are well reproduced in the Antarctic compared to local ice core records (Fig. 3.8, Δ δ^{18}O = -0.73‰ (2.00, 0.54)). However, in the Arctic we detected a positive offset Δ δ^{18}O = 6.19‰ (4.52, 6.68), which is especially large considering only $\pm$2‰ between extreme values in Arctic ice cores such as NGRIP over the last millennium [183]. Globally, measured as well as simulated δ^{18}O follow general isotopic principles as described by Dansgaard (1964), with more depletion toward higher latitudes and toward larger landmasses (Fig. 3.14a-c and Fig. 3.6c) [59].

The last millennium ensemble, however, shows a difference of 2.12‰ in the global mean between models, which we can mostly attribute to the differences in global mean temperature of 1.8 K. Similarly, many regional differences in $\delta^{18}O_{sim}$ (Fig. 3.7f) are likely due to modeled differences in temperature (Fig. A.4f). For example, the warm bias in ECHAM5-wiso in the high latitudes is known to lead to an underestimation of isotope depletion [299, 298] and a cold bias northern latitudes in GISS-E2-R is suggested to cause more depletion there [237]. Differences in isotopic representation in the high latitudes can, however, not only be attributed to differences in temperature. For instance, the less depleted Antarctic $\delta^{18}O_{sim}$ in isoGSM is an artifact of the numerical scheme used in its moisture transport [305], which is also visible in extremely dry regions. iCESM generally overestimates fractionation during re-evaporation processes, which results in stronger depletion globally [21]. Even though iHadCM3, GISS-E2-R, and iCESM show similarly cold temperatures in the Antarctic, iHadCM3 shows mote depleted mean isotopic signatures, which is realistic compared to historical ice core data (Fig. 3.8f and [276]). This suggests that the Antarctic isotopes modeled by iHadCM3 may be more consistent with reality than the multi-model mean.

At the cave locations, differences between modeled isotopes are visible in the offsets between models and record, where iCESM (the globally coldest and most depleted model) shows the strongest negative offsets compared the speleothem records and ECHAM5-wiso (the warmest and least depleted model) shows the strongest positive offset (Fig. A.10). While the median spread between the simulations at cave locations yielded 4.51‰ (3.96, 4.79), the median offset to the simulation was -0.38‰ (-0.8, -0.23). The use of a multi-model mean may be sufficient to average out strong local single-model offsets. Even though the global mean $\delta^{18}O_{sim}$ may be comparable, local and regional temperature and $\delta^{18}O_{sim}$ values deviate strongly between the models. While isoGSM displays the lowest offsets between $\delta^{18}O_{sim}$ and $\delta^{18}O_{speleo}$ (Fig. A.10), additional

processes between meteoric water above the cave and drip water may again influence this mean offset, and further studies including modeled $\delta^{18}O$ in soil will help in model evaluation.

Global studies that have evaluated $\delta^{18}O_{speleo}$ isotopic signatures and its climatic drivers using iGCMs already exist [48, 184], where regions with shared climatic features showed stronger relationships. For example, temperature zones, where annual mean $\delta^{18}O$ or $\delta^{18}O_{iw}$ weighted by infiltration amount is more similar to $\delta^{18}O_{speleo}$, were identified [7], highlighting the importance of seasonality and karst-recharge models in the comparison. Our relationships between time-averaged $\delta^{18}O_{speleo}$ and modeled climate variables are also stronger and more distinct when analyzed in separate latitude bands (Fig. 3.14), and in regions with high data density and similar climate patterns (supplement material in [25]). We observed strong temperature dependency of $\delta^{18}O_{speleo}$ in all latitude bands for the MM-subset, but also the offset between iHadCM3 LM1 and M-subset is temperature dependent (Fig. A.11). On the speleothem side, this shows the influence of fractionation and other cave internal processes on $\delta^{18}O$ in drip water. On the model side, a coarse orography may result in elevation and, thus, temperature and $\delta^{18}O$ differences between records and model. These elevation differences explain many of the strong outliers, especially in the tropics (Fig. 3.14a,e,i,m). Notable is the inverse relationship between $\delta^{18}O_{speleo}$ and precipitation in the tropics and subtropics that changes to a positive relationship in the extratropics. This is in line with the precipitation amount effect described by Dansgaard (1964) [59]. The typically higher precipitation amount in the tropics leads to depletion in the isotopic signal. In the extratropics, the observed relationship to precipitation might be due to the selection of sites, as most sites that are more depleted are also at higher elevation. They may experience the elevation effect, where higher elevated sites show more depletion, and not necessarily a general relationship to precipitation that holds for the extratropics.

On a global and latitude band scale, $\delta^{18}O_{speleo}$ shows strong relationships to the tested climate variables and represents regional climate more clearly than other proxies in speleothems. Trace elements and carbon isotopes are typically proxies for the local conditions of the cave. Only if they correlate with $\delta^{18}O$, the cave conditions are considered as representative of regional climate. Relationships between carbon isotopes and the same climate variables as in the comparison to $\delta^{18}O$ were found to be much weaker or not significant, except in the extratropics, where we found a significant inverse relationship to temperature. This is often the case when interpreting carbon isotopes, where acting processes need to be more tightly constrained and distinguished from potential anthropogenic impact [27, 12]. Local expert knowledge on, e.g., the cave covering vegetation needs to be available to confidently decipher carbon signals in speleothems [25, 87]. An elevation relationship, clearly visible in the $\delta^{18}O_{speleo}$ signal in our analysis, has been claimed for carbon isotopes as well [129], but is not visible in our results, due to low data density for carbon isotopes in higher altitudes.

Overall, iHadCM3 shows realistic mean isotopic signatures at proxy locations. Compared to the last millennium model ensemble, it shows small offsets to the speleothem records, and high agreement with ice core data, especially in the Antarctic. Nevertheless, biases, such as positive offsets in the Arctic, could be detected. Using the multi-model mean, latitudinal isotopic signatures are identified that agree with the fundamental isotopic relationships as described by Dansgaard (1964) [59].

3.5.2 δ^{18}O variability at inter-annual to centennial timescales

We found no evidence that the total variance $\delta^{18}O_{speleo}$ or the variance ratio between simulation and record is related to the mean offset between simulation and record or other tested variables such as temperature, precipitation, elevation, or cover thickness of the cave (results from SF4 in supplement material to [24]). Total variance as measured in speleothem and polar ice-cores and as simulated by iHadCM3 at cave and ice core locations is generally consistent (Fig. 3.9 and Fig. 3.10a). While temporal averaging to record resolution has little impact on the typically highly resolved polar ice-cores, inter-annual to decadal variability in $\delta^{18}O_{pw}$ at cave locations is decreased, which affects the differences in variance. Slow growth rates and limited sampling resolution lead to averaging effects, which result in lower variability on shorter timescales. Furthermore, mixing processes in the soil and karst strongly decrease variability on these timescales, where soil δ^{18}O shows much lower variability than precipitation δ^{18}O [267]. Overall, the variance over the last millennium in the speleothem records is 1.8 $(1.4, 2.6)$ times higher the simulated down-sampled variance (Fig. 3.9). The large variance offsets between non-polar ice cores and the iHadCM3 simulation can mostly be attributed to the low number of records that cover only a short period of time (Fig. 3.10b).

Considering local variability at the cave site locations, the simulated $\delta^{18}O_{sim}$ time series show less variability on centennial timescales than the speleothem records, even at the same temporal resolution. Particularly on a regional level, this is consistent with Laepple and Huybers (2014) who find local model-data discrepancies to increase with increasing timescale [151]. Under the assumption that speleothems archive climate variability correctly and that the δ^{18}O-climate relationship is not timescale-dependent, the increasing discrepancies at centennial timescales indicate underestimation of longterm climate variability in model simulations. The high heterogeneity in the variance estimates of the speleothem records, however, conflicts this assumption. Instead, the little regional consistency hints at a strong influence of the karst environment and the seasonality on meteoric δ^{18}O [181]. Speleothems may also be capable of enhancing climate-driven changes of δ^{18}O by cave-specific processes, which remains to be verified in future studies. The small similarity between nearby caves may also be explained by age-uncertainties that are not covered in the age-model ensemble. Here, multi-proxy approaches can shed new light on the dominating processes. For example, carbon isotopes show significant correlations to oxygen isotopes within the same speleothem in 86% of the MMC-subset, while being more variable (Fig. 3.12d). This amplified variance is, however, not only influenced by hydrological changes, but also by land surface processes such as soil formation or vegetation changes. Considering more terrestrial archives as well as other proxies within speleothems, such as trace elements, may help to further disentangle the climatic and environmental signals. On inter-annual to decadal timescales, where the isotopic signal in oxygen and carbon is mostly smoothed by the karst system, higher variability in δ^{13}C (as in Fig. 3.12a) may result from the stronger isotopic fractionation for carbon compared to oxygen in precipitated calcite [210, 105].

Compared to other models, iHadCM3 shows the lowest variability on all timescales at the speleothem locations. This means that especially on decadal and longer timescales, the model-data mismatch is highest, even though all models show a substantial underestimation of $\delta^{18}O_{iw}$ variability on these timescales. For unweighted δ^{18}O data, different models show higher variance than for the weighted $\delta^{18}O_{iw}$ (results not shown), highlighting the complexity of the hydrological cycle in the models. Cave locations are, however, not reflective of regional modeled δ^{18}O variability on a global scale. Although simulations with higher variability at cave locations tend to show higher variance globally, some

geographical regions such as very dry places with high $\delta^{18}O$ variance are represented differently in models altering the globally averaged variance. Additionally, the spatial resolution of the models does not seem to affect the variability of isotopic composition in precipitation.

By introducing a simplified karst-filter which delays the simulated down-sampled signal by a realistic transit time of 3 yr, we obtained spectra of equivalent power on decadal and shorter timescales. Cave reaction times with increasing drip water rates after precipitation events can range between minutes to days or months[224]. Actual transit times denote the time it takes for water from one precipitation event to reach the cave environment, which heavily depend on the karst hydrology. Tritium measurements can determine these transit times for caves, ranging from years for the Bunker cave in Germany [144] to decades for the Villars cave in France [127]. The 3 yr karst filtering installed for this analysis is similar to low-pass filtering in drip water modeling in other studies that produce and use transit times of $2 - 10$ yr [290, 60, 167].

The impact of the filter is most pronounced on timescales below 50 years, reducing the variance of the resolution-adjusted $\delta^{18}O_{sim}$ by 34% $(20, 43)$ (on timescales > 50 yr by 4.0% $(3.3, 4.4)$). As the filter has little to no effect on the centennial timescales, the total variance over the last millennium is only reduced by 14% $(9, 27)$ compared to the unfiltered down-sampled variance.

Variations in transit time change the impact of the karst filter on different models. Therefore, short-term estimates of $\delta^{18}O_{sim}$ variability representation remains limited. Expert knowledge on local cave hydrology and monitoring data is needed to disentangle effects from the model or the archive. Multi-archive studies that compare variability as stored in multiple archives and observations within close proximity to modeled signals already extract information on global temperature variability on different timescales from multiple sources [202, 61]. Our single case study in Fig. 3.13 already reveals similar levels of $\delta^{18}O$ variability in ice and calcite on centennial timescales. These are of equal power as the observations on decadal timescales. However, we obtained very different levels of smoothing on decadal timescales depending on the archive or the PSM used. Systematic case studies using different archives types provided by the Iso2k database [148] may add valuable information on isotopic variability on different timescales within the last millennium and reveal biases in models and archive types. Furthermore, it enables the evaluation of the complete hydrological cycle when incorporating ocean-based proxies such as corals or marine sediment cores.

Overall, we found that all models underestimate $\delta^{18}O_{iw}$ variability on centennial timescales. iHadCM3 displays the largest model-data mismatch at speleothem locations on these timescales. On decadal and shorter timescales, smoothing effects by the karst filter as well as temporal resolution of the records explain most of the model-data mismatches.

3.5.3 Representativity of $\delta^{18}O$ at different spatial scales

We found little spatial representativity and similarities between individual speleothems on different spatial levels ranging from same site, within the constraints of one modeled gridbox, or across larger spatial regions, as defined by the clusters (Fig. 3.17 and Fig. 3.18).

By selecting an age-model that increased the total correlation between two speleothems where age-model ensembles were available, we obtained stronger positive correlations on site and gridbox level. This age-model tuning increased the correlation by roughly a factor of 2 and also the signal-to-noise ratios by a factor of 3. On a regional level,

as represented by the clusters, as well as on a global level, no improvement could be observed. Other "tuning" options, such as considering only the 50 % links between records of closest proximity globally or within a cluster, or considering only those 50 % records with the smallest mean offset or closest variance ratio, showed no improvement. Fig. 3.17 showed that "tuning" for down-sampled simulated $\delta^{18}O$ is generally useful, however, better selection criteria are necessary.

We do not only find weak correlations between sites but also large heterogeneity in $\delta^{18}O$ variance between neighboring caves. From a climatic point of view, this strong between-site variability in $\delta^{18}O$ can be attributed to controls of regional atmospheric circulation where fractionation occurs along the moisture trajectory through rainout [150]. However, the heterogeneous temporal resolution of speleothems as well as non-climatic overprints can influence the archived $\delta^{18}O$ variability on centennial timescales. This heterogeneity could be further investigated by comparing the $\delta^{18}O$ and $\delta^{13}C$ signal recorded within the cave to vegetation, climate, and landscape evolution archives in the region. In a global analysis, we were not able to identify common climatic drivers for both isotopes [25], but additional information on vegetation cover and monitoring studies may bring more insight. Representativity tests on glacial-interglacial timescales across Western Europe noted coherent $\delta^{18}O_{speleo}$ trends, which are less prominent in the Holocene [161]. Compared to the glacial-interglacial cycles that some speleothems are covering, the last millennium is both very short and relatively stable, where climatic change might not be strong enough to be fully captured by speleothemes [95]. Extending our analysis to longer timescales, as soon as longer transient isotope-enabled simulations become available, may shed a different light on representativity on longer timescales. One promising approach to disentangle archived based processes that hinder possible spatial representativity lies in multi-archive studies. Four this, our first approach for a single location as in Fig. 3.13 needs to be extended to more available locations and combined with pseudo-proxy experiments.

3.5.4 What drives $\delta^{18}O$ variability in models and in speleothems?

Each of the considered simulations supported the distinction of temperature and precipitation amount as climatic driver of $\delta^{18}O_{iw}$. Temperature variability is the dominant driver of $\delta^{18}O_{sim}$ variability in higher latitudes and across land masses, while precipitation variability dominates in the lower latitudes (Fig. 3.15). Absolute correlation estimates are higher when using the unweighted $\delta^{18}O$, since weighting favors the season with the highest amount of possible infiltration water. Correlation estimates between simulated variables and speleothem $\delta^{18}O$ were, however, less conclusive, even after accounting for seasonal sensitivity (results not shown). Drip water monitoring comparison studies between caves worldwide combined with observation data such as [7] already helped to better characterize seasonality of individual caves. Further studies, which also compare monitoring data to model data output can lead to a deeper understanding of the climatic signal captured by speleothems and may enhance comparability between caves.

Large-scale climate patterns of circulation such as NAO [289] or ENSO [276] reflect internal variability of the climate system and modulate hydroclimate variability across the globe. Signatures of these modes are also visible in $\delta^{18}O_{sim}$ in the iHadCM3 simulation (Fig. A.6), and in speleothem records of specific regions as recently shown by [184]. Although the modeled ENSO strength affected $\delta^{18}O_{sim}$ only weakly, they were able to reconstruct past climatic modes using speleothem networks and teleconnections.

Variability of $\delta^{18}O$ can also be a consequence of externally forced variability. During the last millennium, external variability is mostly driven by variations in volcanic eruptions

[245, 192, 162]. The climate response to these volcanic eruption, i.e., the mostly uniform post-eruption cooling response or small changes in precipitation patterns, is imprinted in the global $\delta^{18}O$ signatures and visible in small regional changes (Fig. A.7a-c). The response to solar forcing does not show any clear patterns (Fig. A.7d-f).

Climatic changes in temperature and precipitation due to aerosol forced cooling can be detected in carbon isotopes [223], in growth rate changes [9], or in trace element measurements such as sulfur [91]. However, these techniques usually require sub-annual resolution of records. In our analysis of 58 $\delta^{13}C$ and 89 $\delta^{18}O_{speleo}$ records, we found no significant increase in extreme events that coincide with major volcanic eruptions. While annually resolved modeled $\delta^{18}O_{sim}$ from the last millennium ensemble pointed toward a potential detection at 50 % of speleothem locations, both down-sampled $\delta^{18}O_{sim}$ and speleothem isotopes only recorded up to 20 % of the locations. Compared to the average resolution of the MMC-subset of 6.08 yr (4.07, 7.85), volcanic eruptions are short-lived events. The ability to capture such events strongly decreases with decreasing resolution. Karst-mixing effects which further damp a possibly archived climatic response to a volcanic eruption, may further decrease the ability to detect such events. The attribution of specific peaks in speleothem data to volcanic eruptions requires additional caution because of age-uncertainties and non-climatic changes such as human settlements at the cave location [9].

As expected from the comparatively small solar variations (Fig. A.7, analysis of large magnitude solar events yields much weaker detection than for volcanic eruption (Fig. A.8). Solar variations on inter-annual to millennial timescale are, however, mostly cyclical compared to a more randomized occurrence of extreme volcanic eruptions (compare Fig. 3.2). Our results were, therefore, not surprising when regarding the methods used and are not in contradiction to studies that use spectral analysis to investigate the influence of solar variations on speleothem records capturing monsoon signatures [191, 168, 53, 296].

Overall, we successfully distinguished two main regimes for climate drivers of $\delta^{18}O_{sim}$ variability: temperature variability dominates in the high latitudes and over land masses, while precipitation variability dominates in the low latitudes. Signatures of climate modes of variability may overlap the signal, especially in regions experiencing high influence of these modes. We found that speleothem resolution in $\delta^{18}O$ is too low to detect external variability originating from volcanic eruptions. However, our results do not contradict detection of other external forcing that occur on longer timescales given this resolution.

3.5.5 Limitations

Simulated isotope variability in iGCMs is predominated by the model's climatology and its implementation of hydrological cycle. While most of our results relate solely to the three member initial-condition ensemble from the iHadCM3 simulation, we seeked to compare them to other iGCMs. This enabled the detection of common biases such as the underestimation of variability on longer timescales. Our last millennium ensemble consists of PMIP2/PMIP3 generation models, however, updated versions are already available. Additional runs with new-generation models, including isotopic tracers, require substantial computational costs. Our multi-model last millennium ensemble allowed to assess the temporal and spatial representation of s$\delta^{18}O_{sim}$ across models. As parameter and tuning choices, especially in the cloud and convection scheme, have a strong imprint on $\delta^{18}O$ signatures already within one model (for example [196] for iCESM, [80] for GISS-E2-R), a multi model ensemble under multiple model set-ups is needed, to further systematically explore and constrain modeled $\delta^{18}O_{sim}$.

The large multi-model last millennium ensemble also provides an optimal test-bed for offline data assimilation methods, as suggested by [58] or [253]. Speleothems as a terrestrial archive in the low- to mid-latitudes might be a promising addition to archives that are already used in reconstructions, such as ice cores and marine sediment cores. Because of their precise U/Th-dating and available age-model ensembles [49], they are particularly suitable. Vise versa, offline data assimilation is a promising tool to further explore complex governing processes of $\delta^{18}O_{speleo}$ variability.

Another major uncertainty arises from the temperature-dependent drip-water conversion, that is necessary when comparing calcite and aragonite based $\delta^{18}O_{speleo}$ measurements to $\delta^{18}O_{sim}$ diagnostics in models. We used annual mean simulated cave temperatures as a surrogate for actual inside-cave air measurements. These could strongly reduce biases originating from simulations. A modeled bias of $\Delta 1^{\circ}C$ at the cave location would result in a change in $\delta^{18}O_{dweq}$ of approximately $\Delta 0.2‰$, which is still well within the model-ensemble range. In extreme climates, a bias of $\Delta 1‰$ in the $\delta^{18}O_{dweq}$, however, accounts for a temperature change of $4.5^{\circ}C$ at the coldest simulated cave location ($3.1^{\circ}C$ in Norway), and a change of $5.5^{\circ}C$ for the highest simulated annual mean cave temperature ($32.5^{\circ}C$ in the tropics).

Our multi-model data comparison focuses on infiltration weighted $\delta^{18}O_{iw}$ compared to the drip-water-converted $\delta^{18}O_{dweq}$. Some PMIP3 generation models, however, already include $\delta^{18}O$ in soil layers [21, 260], accounting for additional fractionation processes during re-evaporation on the land surface as well as smoothing processes with older water. A comparison between speleothems and these model diagnostics might be more realistic than solely precipitated $\delta^{18}O$. Including evaporation processes in the weighting of $\delta^{18}O$ is not sufficient to explain model-data mismatches in high-evaporation regions.

The use of additional archives hints at their potential for the analysis of the hydrological cycle using $\delta^{18}O$, based on the multi-archive case study (Fig. 3.13). These showed a model-data mismatch on centennial variability to both speleothem and ice core $\delta^{18}O$-archives. However, there are many more potential archives and proxies that might help deciphering the governing processes of the hydrological cycle or as well as karst- and cave-internal processes [137, 246, 201, 279]. A global multi-proxy approach, where $\delta^{13}C$ is analyzed alongside $\delta^{18}O$, however, did not add much information to the interpretation of $\delta^{18}O$ [25], but may offer deeper insight with expert knowledge for one cave alone [88, 10]. The analysis of the full hydrological cycle in coupled isotope-enabled models includes seawater $\delta^{18}O$. For its evaluation, ocean-based archives such as corals or marine sediments are needed and also available in the Iso2k database [148].

We deliberately restricted this study on a regional to global analysis on speleothem $\delta^{18}O$ signal. Thus, influences and processes known for individual cave systems were not considered. For example, Kluge et al. (2013) accounted for kinetic fractionation changes over time through measurements of clumped isotope that require specialized laboratories [145], and Jean-Baptiste et al. (2019) were able to extract transit times through tritium measurements of dripwater in Villar cave [127]. Considering these and other local factors will improve our understanding of individual speleothem records, but it is difficult to scale quantitatively and systematically. Nevertheless, standardized monitoring datasets from globally distributed cave sites might help to understand the filter and fractionation processes involved. This could enhance PSMs informed by the monitoring and local expertise throughout the database, which in turn enables further model-data comparisons of data assimilation-based reconstructions.

Speleothems are capable of covering complete glacial-interglacial cycles. Compared to the climatic changes on millennial to orbital timescales, the last millennium is considered to be a relatively stable time period [268]. The strongest changes are due to volcanic eruptions, occurring on timescales that most speleothems cannot resolve. On longer timescales, speleothems may still be a good archive to capture large-scale changes [95].

3.6 Summary

Concluding, we found that isotopic signatures in iHadCM3 agree well with those presented by speleothems and ice cores, with a slight positive bias in the Arctic. Compared to other models, general signatures are similar, although with substantial offsets between the models. These are mostly attributable to temperature differences. Considering total variance and variability on interannual to decadal timescales, we found that resolution adjustment and the effects of a convolution karst filter or a firn diffusion model were sufficient to bring simulated and observed $\delta^{18}O$ spectra into good agreement. Still, total variability in the speleothem and ice core records is much higher than in all simulations, especially on centennial timescales. This supports previous findings that climate models currently do not capture appropriate variability with increasing timescales [152]. Here, iHadCM3 shows the lowest variability at cave locations. No relationship was found between the spatial resolution of the models and their variability of the isotopic composition of precipitation. Considering two complement archives that cover different geographic regions, with similar time span and type of resolution, already increased our understanding of how isotope variability is stored in different archives. Multi-archive studies, including additional archives that were not considered in this study, may reveal the underlying concepts influencing the capability of paleoclimate archives to capture and resolve isotope variability.

Temperature variability was identified as a large-scale climatic driver for $\delta^{18}O_{sim}$ variability in the high latitudes and over land masses while precipitation variability is the dominant driver in the low latitudes. This holds for all simulations, even though regional differences exist. In contrast, main climate drivers for $\delta^{18}O_{speleo}$ on a regional scale are difficult to isolate, as multiple climatic signals may overlap. Global variations from solar and volcanic forcing could not be detected in $\delta^{18}O_{speleo}$ time series, not even in a multi-proxy approach using $\delta^{13}C$. Through pseudo-proxy experiments, many archive limitations were attributed to the low resolution of the data-set compared to the timescale of the expected response to solar or volcanic forcing.

Low spatial representativity of individual speleothem entities is implied by low signal-to-noise ratios for isotopic signatures in speleothem records. While age-model tuning improved the coherency over a site and gridbox level, we still found high heterogeneity in variance on regional scales. Here, expert knowledge on local cave processes, environmental history, and, in particular, the availability of monitoring data are crucial to aid interpretation of the climate signal. Enhanced proxy system models that include inner cave and karst processes as well as additional model data diagnostics such as soil-$\delta^{18}O$ may need to be taken under consideration. However, monitoring data for evaluation and potential calibration of these proxy system models are currently only available for a few sites (for example [280]). Some parameters, such as transit times, are generally difficult to measure [127].

Summarizing, we see limitations of speleothem $\delta^{18}O$ as a proxy and tracer of the hydroclimate. Overlapping climatic and environmental signals, the low proxy resolution,

and karst damping processes are the main reasons. Nonetheless, we successfully identified processes that drive variations in isotopic signatures across spatial and temporal scales. iHadCM3 represented the last millennial climate fairly well and the comparison to other models pinpointed mean biases and too low variability at speleothem locations. Our findings can help to constrain hydrological changes from modeled and archived signatures in other climate background states such as the LGM.

4 Hydrological changes between the Last Glacial and present day

In this chapter, we compare the hydrological changes between the Last Glacial Maximum (LGM) around 21,000 years ago and the Mid Holocene (MH) around 6,000 years ago as represented in climate models and recorded by climate archives. We use the archived changes in speleothem growth rates and δ^{18}O between the LGM and the MH and the hydrological changes as modeled by iHadCM3. For this, we apply the developed requirements on age measurement resolution to determine speleothem growth rate changes in Chapter 2, and the findings on the iHadCM3 model evaluation in Chapter 3. We set these changes into perspective to the changes recorded in a large compilation of other hydroclimate archives and additional climate simulations. As such, we include lake levels of closed basin lakes [307] and pollen records from lake and marine sediment cores [1, 234], and the mean changes in the PMIP3 simulation ensemble [19, 209] in the analysis.

The key questions addressed in this chapter are:

- Can δ^{18}O serve as an indicator of past changes in precipitation amount in models and speleothem records?
- Are archived changes of hydroclimate proxies sufficiently reproduced in model simulations? Do we have sufficient information from archives to discriminate between simulations?
- Does precipitation and isotope variability on decadal to centennial timescales depend on the background state? Do we see differences between modeled and archived variability?

This chapter combines the tested methods and findings with the data from the previous chapters in order to analyze glacial-interglacial hydroclimate changes. Understanding these past changes, how and where they are archived and to what extent they are reproduced in climate model simulations, is crucial to climate research as it allows us to estimate, constrain and confine uncertainties in future projections of hydrological changes.

After a brief literature review focusing on past hydrological changes and their study using diverse paleoclimate archives, we introduce the available climate model and paleoclimate proxy data, as well as further methods. The data is used to answer the identified key questions in both the iHadCM3 simulation and the PMIP3 ensemble in comparison to a large compilation of past hydroclimate records. Finally, we discuss and summarize the results.

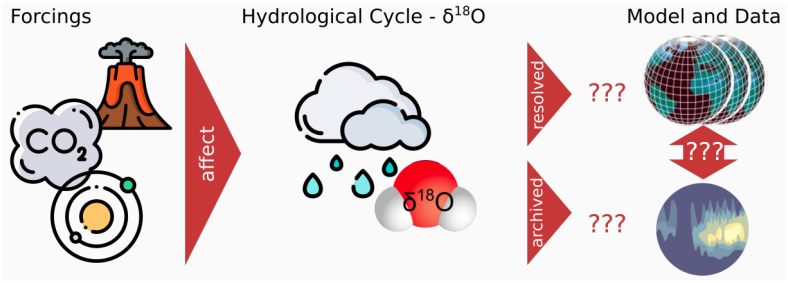

FIGURE 4.1: Schematic illustration of the hydrological response to climate forcings and its representation in model and data. The key question is how these changes are resolved in paleoclimate simulations and how they are archived in paleoclimate archives such as speleothems. Water molecule Sakurambo, Wiki Commons, Public domain, Volcano: https://www.flaticon.com/authors/smashicons, Orbit, CO2, cave: https://www.flaticon.com/, Models: modified from Rehfeld,2019.

4.1 Background

Changes in water availability under current anthropogenic warming pose a great threat to ecosystems and societies globally and affect not only drinking water security, but also the energy, transport and agricultural sector [40]. Variations in hydroclimate and their changes under different climatic backgrounds in past, present and future are, however, far less understood than changes in temperature [41]. Globally, modeled precipitation amount increases by 1-3 % for every 1 °C of warming, but strong regional differences exist [44]. For large areas, the "dry gets drier, wet gets wetter" paradigm is a simplified summary of these changes [111]. Mostly, it is only valid across the ocean [39], while moisture and water availability changes over the land surface are more complex [102]. For reliable projections on future changes that impact human societies, it is therefore crucial to increase our understanding of how the hydroclimate changes.

Paleoclimate model simulations under different climatic background states provide examples of possible hydroclimate changes and offer the possibility to study a complete representation of the climate system consistent with model physics. Paleoclimate archives of hydrological changes such as pollen extracted from lake sediments, lake levels of closed basin lakes, or speleothem growth rates and $\delta^{18}O$, are direct observers of the past climate, and can serve as reference points in model evaluation. Different climatic backgrounds, represented by different climatic forcings such as GHG concentration, orbital and solar configurations, volcanic eruptions, ice sheets, or topography affect the hydrological cycle and its tracer, the isotopic composition of precipitation $\delta^{18}O$, as illustrated in Fig. 4.1. The comparison between changes as resolved in climate models and recorded by paleoclimate archives can help to better characterize the past hydrological changes and thus constrain future hydroclimate risks.

Pollen records have long been used to analyze past vegetation. The limiting factors of vegetation growth can be translated into precipitation reconstructions [20]. The changing arboreal pollen fraction, i.e., the proportion of tree and shrub compared to herb and grass pollen, has been identified to mostly reflect changes in precipitation amount between the LGM and the MH [1, 116, 288]. Lake levels of closed basin lakes across the world serve as an indicator of changes in inflow and evaporation, and thus regional and local moisture availability [123]. Information on changing precipitation patterns from closed basin lakes is widely used in evaluation studies of other climate archives, e.g., speleothem records [96] and climate models [307]. Based on a large compilation

of lake level records, Zhang et al. (2020) recently found reasonable agreement between precipitation changes in PMIP3-CMIP5 models and recorded lake level changes. For speleothems, only regional and local analysis of hydrological changes exist. Changes in $\delta^{18}O_{speleo}$ concentration are often attributed to changes in monsoon patterns [81, 191, 168, 194]. The precipitation amount principle as described by Dansgaard (1964) states negative correlation of $\delta^{18}O$ with precipitation amount. While precipitation generally favors heavy isotopes, the content of heavy oxygen isotopes decreases with continuing rainfall [304, 59]. Decreasing $\delta^{18}O$ signatures in low- to mid-latitude speleothem records may thus reflect increasing precipitation amount. Drivers of $\delta^{18}O$ variability are, however, subject to many overlapping processes [24] and interpretation of $\delta^{18}O$ signals in speleothems is not straightforward.

In this chapter, we examine the extent to which speleothem records from the SISALv2 database [49] can be used to analyze hydroclimate changes using changes in $\delta^{18}O$ signatures and growth rate changes. Combined with a compilation of other archives of hydrological changes, the recorded changes are used to evaluate forced and unforced simulations under LGM and MH conditions with the iHadCM3 GCM. This model has been widely tested in both climatic states and used to assess climatic changes between the time periods, with a focus on temperature variability, ocean salinity and atmospheric dynamics [118, 74, 252]. Precipitation pattern changes in iHadCM3 from the LGM to the MH have not yet been quantified. Contrasting our findings to those obtained from the PMIP3 ensemble mean, will help to identify modeling biases in the iHadCM3 model and outliers in climate archives, where precipitation amount may not be the dominant driver.

4.2 Data and Methods

4.2.1 Simulation data: iHadCM3 and PMIP3 ensemble

In this study, we use six simulations from the iHadCM3 GCM that is described in detail in Sec. 3.2.1, with the boundary conditions for LGM and MH following the PMIP3 protocol [236]. The LGM experiments represent conditions from 21,000 years ago and are run with 185 ppm CO_2, and orography corresponding to a 120-140 m lower sea level and larger ice sheets in North America and Fennoscandia compared to the last millennium and present-day [19, 209]. Orbital configurations follow Berger (1978) [15] and lead to higher NH-winter insolation and lower NH-summer insolation in both hemispheres compared to the last millennium, which results in a reduced seasonal insolation contrast. The simulations exist as a solar and volcanic forced and an unforced version. Due to the absence of high-resolution solar and volcanic forcing reconstructions for the LGM, the same configuration are used as in the last millennium runs described in Sec. 3.2.1. Additionally, two LGM runs without transient solar and volcanic forcing but with higher and lower CO_2 levels (150 ppm, 210 ppm) are used. The MH runs have boundary conditions that represent conditions from 6,000 years ago, with 265 ppm CO_2, and pre-industrial orography [209]. The orbital configuration has higher obliquity and eccentricity compared to the last millennium, which results in higher NH-insolation in the NH-summer, higher SH-insolation in the SH-spring, and lower insolation in all other months [199, 222]. For the MH, one run with and one without transient solar and volcanic forcing exist.

Compared to the last millennium runs used in Chapter 3, the forced LGM run presents $(5.62 \pm 0.42°C)$ lower global mean surface temperatures (GMST) and 10 % less global

mean precipitation rates (GMPR). The forced MH run has $(0.45 \pm 0.4°C)$ lower temperatures and 0.5 % less precipitation. A table with detailed differences between all simulations used in this analysis can be found in Tab. A.1.

As reference, we use the ensemble mean climate state for precipitation from 15 available model simulations for the MH and 9 for the LGM, which are included in the PMIP Phase 3 ensemble [19, 209] and used in Rehfeld et al. (2020) [222]. Compared to iHadCM3, the resolution is interpolated to a common ($1° \times 1°$), which is why it is down-sampled to the iHadCM3 resolution ($2.5° \times 3.75°$) in case of a direct comparison.

4.2.2 Speleothems and other archives of hydroclimate changes

Speleothem Data form the SISALv2 database

For the analysis of growth rates and growth rate changes, we use the same subset of the SISALv2 database as in Chapter 2. Covering both the LGM and MH, we use the speleothem entities eID 163 from Cango cave in South Africa [265], eID 237 from Gunungbuda cave in Malaysia [207], eID 305 from Sofular cave in Turkey [82], eID 319 from Bukit Assam cave in Malaysia [207], eID 500 from Cueva del Diamante cave in Peru [35] as depicted in Fig. 2.9. We additionally include the same records than in Sect. 2.4.2 which cover either the LGM or the MH. These are 124 records for the Holocene (8,000-100 BP) and 23 records for the LGM (27,000-19,000 BP), which contain at least four datings within a minimum time window of 4,000 yr.

For the analysis of δ^{18}O changes in the records that are available in either time period, we use the criteria suggested by Comas-Bru et al. (2019) in their ECHAM5 model evaluation using speleothems records since the LGM [48]. They suggest to use the intervals $6,000 \pm 500$ yr for the MH and $21000 \pm 1,000$ yr for the LGM. We added requirements of at least 500 yr coverage and a minimum of five δ^{18}O samples and one dating. For records that cover both time periods, we require a coverage of at least 15,000 yr within a period between $21,500 - 3,000$ BP, a minimum of 20 δ^{18}O measurements and two datings. 23 records that cover both time periods with sufficient number of samples and dating resolution remain.

Lake levels

Lake levels of closed basin lakes serve as an indicator of changes in the balance between precipitation minus evaporation, i.e., of changes in the regional moisture balance [123]. Their volume is, to first order, controlled by the available precipitation that falls in its catchment area, and the evaporation of the lake [96]. Compared to open lakes that can compensate an increased inflow by an increased outflow, closed basin lakes can only respond to regional climate changes with volume changes and, thus, changes in their surface area. However, the interpretation in terms of regional hydrological climate is not straightforward [147]. Lake level increases can be due to an increase of rainfall or a decrease of evaporation [123] and may also reflect non-climatic factors. Depending on the lake's geometry, an increased inflow can lead to a larger surface area, and in turn a much higher evaporation increase. Lake levels are thus always a spatial and temporal integration of local evaporation and precipitation that can be modeled if geometry, input, and output are known [203].

In this study, we compare lake levels from the LGM and the MH with simulated precipitation fields in order to determine, if changes are realistic. We use lake level records as selected in a recent hydroclimate study comparing LGM and MH by Zhang et al. (2020) [307]. The authors provide lake level changes for each records. The records

cover both time periods with reasonable dating control and are indicators of moisture changes. The 52 records distributed globally at low- to mid-latitudes show a lake levels decrease in 60 % of the cases and an increase in 40 %.

Pollen

The vegetation of a specific region is a strong indicator of its climate. Plant types can be limited by water availability, temperature and length of the growing and winter season, radiation, and CO_2 concentration [57, 106]. On long timescales, the combination of these factors controls the natural vegetation composition in a region. Pollen are emitted each year by plants in order to reproduce. Where pollen have been preserved, e.g., in lake sediments or peat bogs, they can serve as a proxy for past vegetation and its changes [20]. Vegetation reconstructions from pollen records are possible under the assumptions that pollen grains are 1) distinguishable for a particular plant genus or species, 2) produced in large quantities and distributed widely, 3) resistant to decay, and 4) reflect the vegetation at the time of deposition [20]. Past climatic conditions can then be inferred from vegetation reconstructions by determining the limiting factors that govern the occurrence of a specific plant type [16, 37]. As a typical record contains pollen from more than tens-to–hundreds of individual taxa, the climatic interpretation is mostly based on a dimension reduction of the signal. One commonly used univariate signal in the arboreal pollen fraction (AP), which is the fraction of tree and shrub pollen in the record. As such, AP typically represents the tree cover at a specific time and location. Still, comparison between individual records remains complicated due to variations in their temporal averaging scales, different pollen transport ranges, and variations in pollen productivity [1]. Therefore, we rely on relative changes in AP fractions to compare between sites, instead of quantitative analyses. Not all AP changes are forced by climatic changes - fires, insects, infestations, or anthropogenic interferences, as well as changes of the archive itself can complicate the interpretation.

Lake sediment records rely on radiocarbon dating and are thus less precise compared to speleothems, especially the further they extend back in time. Additionally, their temporal averaging scales, which define the resolution, are typically on the order of 10^2 years, while speleothems may have a much higher resolution. Their main advantage compared to speleothem $\delta^{18}O$ is the more localized signal of the pollen, which is less influenced by long distance atmospheric processes. Their hydrological interpretation is thus better constrained than that of the $\delta^{18}O$ signal in speleothems. The analysis of Adam, Weitzel, and Rehfeld (2021) suggested that large-scale AP changes in the low- and mid-latitudes over the last deglaciation can be mainly attributed to precipitation changes [1].

Here, we use the globally-harmonized AP fractions as in Adam, Weitzel, and Rehfeld (2021) from the ACER pollen and charcoal database [234, 1]. Their selection of 63 records covers the period from the LGM to the MH (22,000-6,000 yr BP) with an average resolution of 228 yr. We only analyze the relative sign of the AP change between the LGM and MH, for which we average the AP in the LGM and MH time window as defined for the speleothems.

4.2.3 Joint and separate approach of speleothem evaluation

Proxy coverage in the LGM is much lower than in the MH, and even fewer records cover both time periods. For pollen and lake level records we only included records that cover both time periods. However, for the speleothem records, temporal and spatial availability over the deglaciation is much more sparse. In a "joint" approach, we consider those records that have continuous coverage throughout both time periods. As long as

calibrations to specific climate variables stay constant over time, relative changes in the mean state and variability ratios can be extracted directly and independently of such calibrations. However, as stated above, only five speleothem growth rate change and 23 δ^{18}O records meet the respective requirements on dating and sample resolution.

Record availability is much higher in a "separate" approach, which also considers records that cover only one of the two time periods. To generate estimates of changes in the mean state and variability, we derive mean estimates of δ^{18}O and its variability for six specific regions. The regions are defined by hierarchical distance-based clustering. The growth rates and δ^{18}O share four of the regions, which are North America, South America, East Asia, and Australia including Indonesia/Malaysia. The regional clusters around Europe, Africa and Western Asia change depending on the availability of records. For the comparison with simulations, we extract simulation data at the positions of speleothem records that are available in the respective time period. Regional averages are then calculated in the same fashion as for the speleothem records.

4.2.4 Cohen's κ coefficient

When comparing how well the simulated changes match the recorded changes, Cohen's κ coefficient provides a means of measuring the degree of agreement between proxies and simulations [154]. In addition to measuring accuracy alone, i.e., the rate of agreement between two sets, it also takes into account if agreement occurs by chance only. It is defined as

$$\kappa = \frac{p_0 - p_e}{1 - p_e}, \tag{4.1}$$

where p_0 is the probability of agreement between the two sets, and p_e the probability of expected agreement between independent probability distributions with the same marginal distributions. κ statistics of < 0.2 indicate poor to slight, $0.2 < \kappa < 0.4$ fair, $0.4 < \kappa < 0.6$ moderate, $0.6 < \kappa < 0.8$ substantial, and $0.8 < \kappa < 1$ almost perfect agreement between two sets [154]. Interpreting κ is however not as straightforward, as the categories suggest and must always be considered under a specific research question. Whenever we state κ in this analysis, accuracy will always be stated alongside.

4.3 Results

4.3.1 Local and regional changes in modeled δ^{18}O and precipitation

We first compare the changes in isotopic composition of modeled precipitation in iHadCM3 between the LGM state and the MH state to δ^{18}O changes in speleothem records. Although only few records contain a continuous time series throughout both periods, we use the separate and joint approach to find differences and commonalities (Fig. 4.2a). The modeled and archived changes are in reasonable agreement with 59 % of joint records ($\kappa = 0.3$, indicating fair agreement) and 50 % of the separate regions showing a change in the same direction. However, the joint speleothems show slightly larger changes of -0.64 ‰$(-1.39, 0.17)$ than the simulation. For the separate approach, the difference between speleothem and model is even larger with -1.49 ‰$(-2.32, -0.77)$.

While the simulated global mean δ^{18}O variability in the MH does not change compared to the LGM (Fig. A.12), distinct regional patterns of increased variability in δ^{18}O are visible in the simulation (Fig. 4.2b). The speleothem records show higher variability in

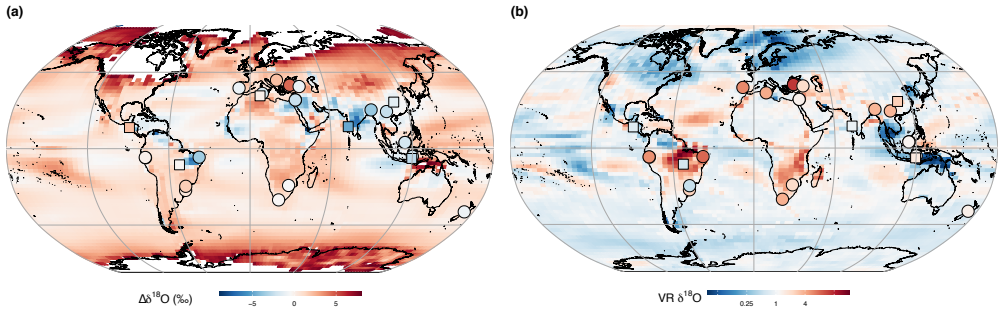

FIGURE 4.2: a) Changes in isotopic composition of modeled precipitation and in speleothem records are depicted as $\Delta\delta^{18}O = \delta^{18}O_{MH} - \delta^{18}O_{LGM}$. Red (blue) colors indicate less (more) depletion in the MH compared to the LGM. The simulated values are in the background. Circles indicate joint speleothem records, squares constitute separate regions at the mean location of all included records. The very high latitudes show changes of $\Delta\delta^{18}O > 8$ ‰and are excluded for better visibility in the low- to mid-latitudes. b) Variance ratio (VR) patterns between the MH and LGM are depicted as $VR = \frac{var(\delta^{18}O_{MH})}{var(\delta^{18}O_{LGM})}$. Red (blue) colors indicate higher (lower) variance in the MH compared to the LGM.

almost all records for the MH. This may be due to sample resolution and will be studied further in Sec. 4.3.3. The speleothem records covering LGM and MH show an increase in mean variance of 3.8 (2.86, 4.97) while the separate speleothems only show an increase of 1.11 (0.7, 2.01) and the simulation of 2.04 (1.01, 4.04).

Generally, the simulation and the speleothem records show reasonable agreement in the direction of change, even though there are complex patterns in the low- to mid-latitudes and only few speleothem records were available. The question whether the speleothems can be an indicator of precipitation amount changes remains.

Changes in precipitation are reflected in $\delta^{18}O$ changes in specific regions in the simulation. Fig. 4.3 illustrates the concurrent changes in precipitation and $\delta^{18}O$ between the LGM and the MH. In regions with high precipitation, $\delta^{18}O$ of precipitation decreases, as described by the amount effect by Dansgaard (1964) [59]. According to this effect, two main regions can be distinguished at a global scale. In the low- to mid-latitudes, $\delta^{18}O$ reflects changes in precipitation through the amount effect. Here, red (blue) indicates less (more) precipitation in the MH compared to the LGM, and $\delta^{18}O$ shows less (more) depletion, which is in line with the amount effect. In the high latitudes, we mostly see more precipitation in the MH, but also less depleted $\delta^{18}O$ values (green). Here, the $\delta^{18}O$ signal is most likely superimposed by the temperature effect, where colder temperatures lead to more depleted $\delta^{18}O$. Some isolated regions in the low- to mid-latitudes show more depletion in $\delta^{18}O$ with less precipitation in the MH most likely due to complex shifts in circulation. Across all latitudes, the relationship between precipitation changes and changes in its isotopic composition still reflects the amount effect, although to different extents. In latitude bands between 45°S - 45°N, the relationship is dominated by the amount effect, while in the higher latitudes, the precipitation - $\delta^{18}O$ relationship is not significant (Fig. A.13). The analysis suggests to use only low- to mid-latitude $\delta^{18}O$ archives, preferably from 45°N to 45°S, when analyzing precipitation changes.

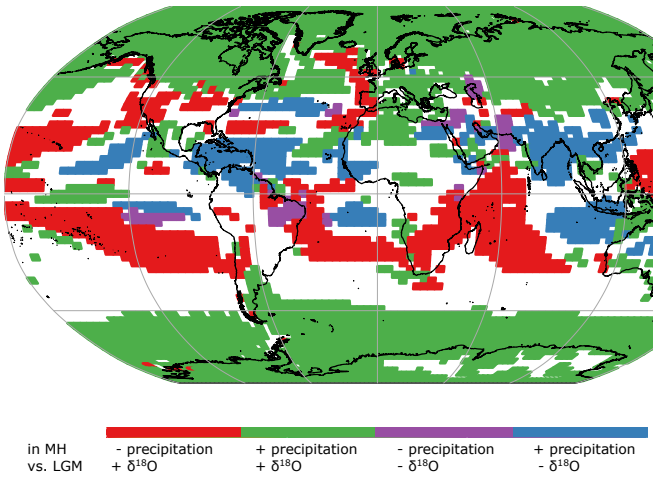

FIGURE 4.3: Relative changes of precipitation and δ^{18}O between the MH and the LGM. Colors classify regions with concurrent changes in both variables. For example, red shows a decrease in precipitation and higher δ^{18}O, i.e., less depletion, which indicates a lesser role of the amount effect. Changes of less than 10 % are marked as white. Red and blue colors indicate where precipitation changes coincide with δ^{18}O changes following the amount effect, while green and purple colors show regions, where precipitation and δ^{18}O changes do not align with the amount effect.

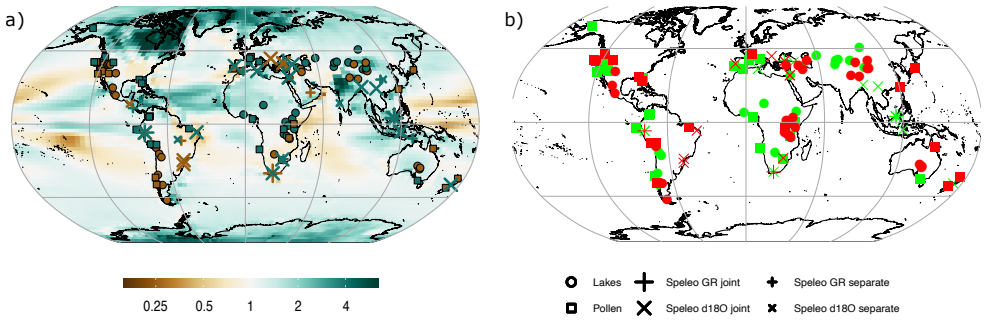

FIGURE 4.4: a) Change in mean annual precipitation between the MH and LGM in iHadCM3 and as indicated by hydroclimate proxies. The background shows the simulated mean precipitation change of the MH respective to the LGM state. Ratios above one indicate higher precipitation rates in the MH compared to the LGM. The symbols indicate the climate archive (Lake levels, AR pollen records, speleothem growth rates and δ^{18}O in a joint and separate approach) and are colored in the direction of the hydrological change. b) shows the match or mismatch in the direction of the change between the simulation and the proxies. Green symbols indicate that the change in archive and simulation is in the same direction (both increase or decrease), while red symbols indicate different directions in archive and simulation (one shows a precipitation increase, while the other one shows a decrease).

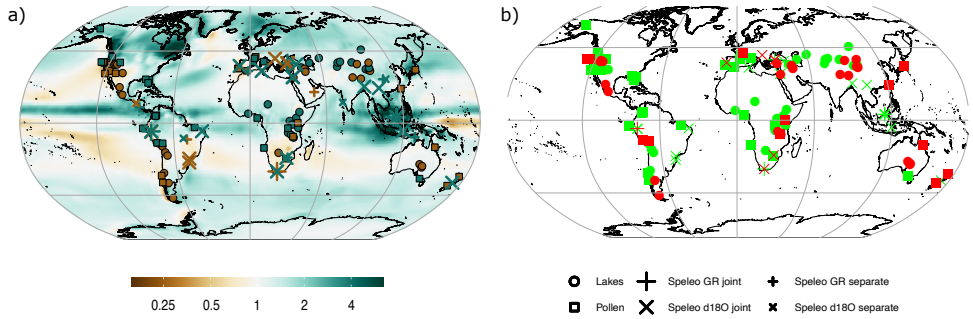

FIGURE 4.5: As Fig. 4.4 but using the PMIP3 ensemble mean precipitation difference between the MH and the LGM.

4.3.2 Comparison of modeled and archived changes of precipitation

Using the δ^{18}O records as indicators of precipitation change, we analyze the similarity between archived and modeled hydrological changes from the LGM to the MH. Due to the small number of available speleothem δ^{18}O records, we add more climate archives of hydrological changes, namely speleothem growth rates, past lake levels, and arboreal pollen records. The relative changes in the iHadCM3 simulation as well as in the proxy records are shown in Fig. 4.4a. Fig. 4.4b shows where the direction of the change as archived in the different records matches the simulated direction of change. We find 48 % match between the records and the transient solar/volcanic forcing MH to LGM iHadCM3 change. The proportion does not increase substantially using other simulated changes such as the unforced MH to LGM change or changes to the colder or warmer LGM simulation. We find $\kappa = 0.03$, which indicates agreement that is not significantly different compared to agreement by chance. While agreement for lake levels and the speleothem records is very low, pollen records alone show a slightly higher than random agreement with $\kappa = 0.13$. No distinct regional pattern of agreement and disagreement is found between the records and the simulation.

Comparing the recorded changes to mean precipitation changes of the PMIP3 ensemble (Fig. 4.5) yields both higher accuracy and agreement. We find 60 % of the recorded changes match in direction with the simulated changes and an agreement of $\kappa = 0.3$. For pollen records only, the agreement increases to $\kappa = 0.37$. Here, global patterns are more distinguishable. Disagreement between simulations and records are most common in "transition" regions, where positive and negative changes are close together such as on the west coasts of both North and South America.

We compare the changes as simulated by iHadCM3 and by the PMIP3 model ensemble and their respective agreement to the direction of recorded changes in Fig. 4.6. The match between both simulations at the proxy locations is high, with an accuracy of 82 % and a moderate agreement of $\kappa = 0.48$. However, there are distinct regions where the PMIP3 ensemble better reproduces archived changes than iHadCM3 and only few records, where iHadCM3 performs better. Fig. 4.6 shows higher agreement of PMIP3 especially in many East African records, which is a region that is modeled to experience much dryer conditions in the iHadCM3 simulations. In eastern South America, the PMIP3 ensemble reproduces the complex changes better than iHadCM3. Some "transition" regions are better resolved in PMIP3, such as on the North and South American west coast. However, there still remain examples, where both iHadCM3 as well as the PMIP3 ensemble do not model changes in the same direction as the records, such as Europe, central Asia or the Eastern Pacific area.

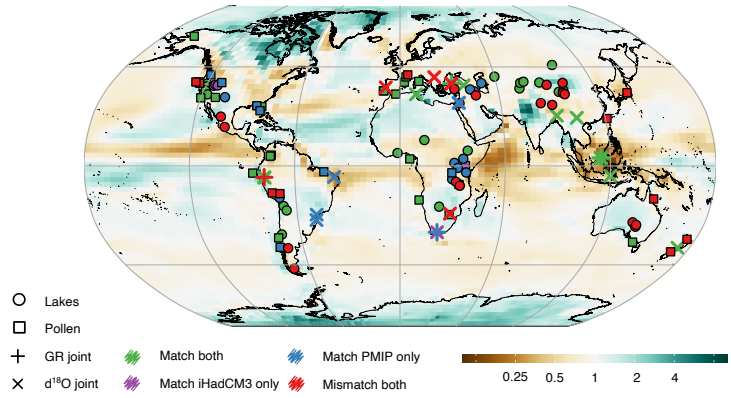

FIGURE 4.6: Relative difference between the iHadCM3 LGM to MH change to the PMIP3 change as $\frac{MH_{iHadCM3}}{LGM_{iHadCM3}} / \frac{MH_{PMIP}}{LGM_{PMIP}}$. Brown colors indicate a dryer change in iHadCM3 than in the PMIP3 ensemble (iHadCM3 LGM wetter at similarly wet MH, or dryer HadCM3 MH at similarly wet LGM) while green colors indicate wetter changes in iHadCM3 than in the PMIP3 ensemble (iHadCM3 LGM drier at similarly wet MH, or wetter HadCM3 MH at similarly wet LGM). The symbols indicate the type of hydroclimate archive as in Fig. 4.4 and Fig. 4.5. The color of the symbols indicate if the simulated changes match with the recorded changes. Green indicates where both iHadCM3 and the PMIP3 ensemble match, and red where both mismatch. Blue and purple indicate a match to only one of them.

4.3.3 Decadal- to millennial-scale variability of δ^{18}O

We analyze time-scale dependent variance in the MH and the LGM in the forced iHadCM3 ensemble and the speleothem records, to better explore variability in δ^{18}O for different climate background states. Fig. 4.7 gives an insight into variability of the joint records that cover the whole deglaciation, as well as the records that only cover either time period and modeled signatures at their cave location. On decadal and longer timescales, the MH and LGM recorded and simulated δ^{18}O variability all fall into a similar range of power spectral density and thus match the power of the joint records that cover much longer time periods. We used no detrending on the joint records to remove the strong trend of the deglaciation, as we only look at variability up to a period of 500 yr.

On multi-decadal and shorter timescales, differences between the recorded and simulated spectra in different climate states become visible. The modeled spectra show higher variability than both MH and LGM records on decadal and shorter timescales. Generally, the recorded variability in the LGM is lower than in the MH. This apparent state-dependency of variability on decadal timescales can, however, partly be attributed to differences in resolution. Fig. A.14 shows the recorded and modeled MH records at the same average resolution as the LGM records, which decreases variability on multi-decadal and shorter timescales. Fig. A.12 shows no difference between the average regional simulated spectra at annual resolution. While the simulated global mean δ^{18}O variability is much lower than the local and regional variability, it is still of similar magnitude in both MH and LGM time periods.

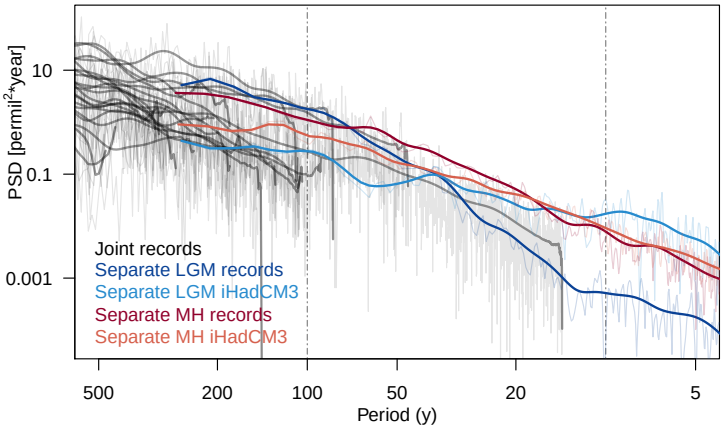

FIGURE 4.7: Variability on different timescales for speleothem record δ^{18}O and iHadCM3 simulated δ^{18}O at the speleothem locations in both the LGM and the MH. The simulated values are downsampled to the respective speleothem record's resolution.

4.4 Discussion

4.4.1 Hydrological changes in the low- to mid-latitudes as reflected by speleothems

In our study, we found fair agreement between the direction of isotopic changes as modeled by the iHadCM3 forced LGM and MH runs and the speleothem δ^{18}O records, both in the joint and separate approach. However, recorded changes are on average larger than modeled ones by -0.64 ‰$(-1.39, 0.17)$ in the joint and by -1.49 ‰$(-2.32, -0.77)$ in the separate approach. Comparing modeled precipitation changes to modeled isotopic changes reveals that changes in isotopic signatures can only be interpreted as precipitation changes in low- to mid-latitude regions, specifically in regions between 45°N and 45°S, with local exceptions. The joint SISALv2 subset only contains records within these regions and not outside, which are further considered as records of precipitation amount in the global analysis.

We aggregated the speleothem δ^{18}O signal, the speleothem growth rate changes from Sec. 2, a lake level set, and an arboreal pollen fraction database to a large set of hydroclimate proxies. Using this compilation, we evaluated the precipitation amount change between the LGM and MH state and compare it to that simulated by iHadCM3. The simulated precipitation changes show the expected poleward shifted dry regions in the subtropics [143]. These circulation drifts are also visible in the PMIP3 ensemble mean changes and in the pattern of the proxy records on the west coast of North and South America. While precipitation changes may be driven by circulation changes, a thermodynamic control cannot be excluded and needs further detailed research focusing on the extent of the Hadley cell and equator-to-pole temperature gradients.

The iHadCM3-simulated and recorded patterns only match by 50 % and show agreement indistinguishable from agreement by chance. The PMIP3 ensemble performs much better in reproducing the recorded changes with an accuracy of $\sim$ 60 % and a fair agreement ($\kappa = 0.3$), which is in line with recent model-data comparisons using lake levels only

[307, 170]. All simulations are able to reproduce some of the changes on the west coast of North and South America. There, the PMIP3 simulations shows a more poleward shift of transition zones between more and less precipitation compared to iHadCM3. Both iHadCM3 and the PMIP3 ensemble reproduce a wetter west Africa which is in line with the available records, as well as wetter changes in South East Asia. The PMIP3 ensemble shows much higher agreement with records in Eastern Africa. There, iHadCM3 simulates a dryer LGM to MH transition, but most lake level records report higher lake levels. In Eastern South America, PMIP3 again outperforms iHadCM3 in precipitation amount change accuracy compared to the climate proxies. If assuming a more depleted δ^{18}O equals more precipitation in the MH, then all three continuous speleothems in this region only agree with the PMIP3 ensemble. In contrast, the direct comparison of isotopic signature changes between LGM and MH shows agreement between these three records and the simulated patterns in iHadCM3. Thus, the higher agreement between proxy records and PMIP3 simulations must be treated with caution and requires more detailed analysis using additional isotope-enabled models.

Records most prominently do not match the simulated changes in both iHadCM3 or PMIP3 in the Mediterranean, East Asia, Australia, and New Zealand. The low accuracy between the simulated precipitation and the East Asian and New Zealand pollen records has also been found in a recent study on vegetation changes over the last deglaciation [1]. The AP pollen fractions from Japan and Taiwan were less representative for the vegetation changes between LGM and MH than in other regions, which could lead to spurious signals that are not representative of regional precipitation changes [1]. The closed basin of Eastern Asia is dominated by the East Asian monsoon climate as well as the arid central Asian climate. Lake levels in this region show different direction of changes even at very close proximity. These differences can not be resolved by either iHadCM3 or the PMIP3 ensemble and may be due to local particularities which superimpose the large-scale changes. This is in agreement with the findings from Zhang et al. (2020) [307].

While pollen records show a 80 % match to all simulations in Europe, 60 % of the speleothem δ^{18}O signal do not match with the changes in any simulation. In alignment with the findings on co-varying precipitation and isotopic composition changes as shown in Fig. 4.3, this indicated that δ^{18}O as archived in European speleothems is less likely to be influenced by changes in precipitation amount. Individual studies on these European speleothems (eID305 [82], eID428 [51], and eID 587 [63]) also distinguish (sea surface) temperature and changes in moisture source δ^{18}O concentration as main drivers of changes for these δ^{18}O records. Compared to the simulated changes, these records clearly show the latitude-limit of interpreting speleothem δ^{18}O as a proxy of hydrological changes. Future studies including more hydroclimate proxies in the mid- to high-latitudes, such as accumulation rates in ice core records or the recently published harmonized fossil pollen database LegacyPollen 1.0 [115], could help to interpret speleothem δ^{18}O in other regions, where the dominant δ^{18}O driver is unclear. This would help to divide hydroclimate from non-hydroclimate proxies.

Generally, isotopic signatures match well between iHadCM3 and the speleothem records. This suggests that most mismatches between simulated precipitation and speleothem d18O can be explained by different climatic drivers in δ^{18}O. However, the number of speleothem records that are available for the joint approach is very small compared to available continuous pollen and lake level records. The separate approach increases the sample size, it combines large regions where overlapping effects on different records may be averaged out. Even though the records add valuable information in areas where few to no lake level or pollen records are available, such as Eastern South America or

Indonesia/Malaysia, more records are necessary for a coherent global analysis. Lake level and pollen records are, however, not sufficiently resolved to study variability changes. Analysis of state-dependent variability of precipitation in the tropics is, thus, only possible using speleothem records.

This model-data comparison used the proxy records only to analyze the direction of changes in precipitation amount. Quantitative analysis on these changes that directly infer changes in precipitation amount may give deeper insight, especially in areas where the direction of change is small. However, calibration of every record is necessary for this type of analysis, which would introduce an additional error source. Extending the analysis to the higher latitudes, accumulation rates in ice core records could provide an opportunity for a quantitative analysis of changes in precipitation. Although we used different sets of LGM and MH climate state simulations for iHadCM3 and include them in the comparison, we always considered one simulation only. Including additional isotope-enabled climate models could help to better understand the concepts and underlying physics of precipitation changes in the models.

As in Sec. 2 and Sec. 3, we considered a regional to global view on the archived signal. Local particularities that influence lake levels, pollen records, or cave systems, are not included in the analysis. Accounting for these may give deeper insight into hydrological influences on specific records, but proxy system models that are applicable and accurate on the regional-to-global level are mostly missing. Therefore, incorporating these local differences is beyond the scope of this study.

4.4.2 State dependency of modeled and archived δ^{18}O variability

We found state-dependency of δ^{18}O variability as archived in speleothem records using the joint and separate approach. The 23 records in the LGM show lower variability on multi-decadal and shorter timescales compared to the 124 records in the MH, which can only in part be explained by the different temporal resolution. On multi-decadal and longer timescales, the records show similar variability. This contrasts to a study by Rehfeld et al. (2018) who find declining millennial-scale temperature variability in a global compilation of temperature proxies from the LGM to the Holocene [220]. However, we note that temperature variability does not directly translate to precipitation variability nor to variability in isotopic signatures. Additionally, we only have a small number of records available in the LGM and are restricted to the low- to mid-latitudes. Further analysis using multiple archives of δ^{18}O is needed to confirm if the here found state-dependency of variability in isotopic signatures is limited to the tropics and subtropics, or even to speleothem records only.

Simulated δ^{18}O variability does not reproduce the state-dependency found for δ^{18}O archived in speleothem records. Here, the local, regional, and global spectra of both time periods show very similar power (Fig. A.12), with little to no changes under forced and unforced runs (results not shown). Our findings on simulated variability are in agreement with Ellerhoff et al. (2022), who analyzed temperature variability in the LGM and pre-industrial climate state, and only found state-dependency of variability in the high latitudes ($> 65°$N/S) [74]. On centennial and longer timescales, the variability in the models is underestimated compared to those archives in speleothem records, in line with the findings in Sec. 3 and previous studies that compared archived and modeled variability [74, 24, 152, 151].

4.5 Summary

In conclusion, we found that δ^{18}O signatures as well as growth rate changes in speleothem records in low to mid-latitudes can be a valuable indicator of glacial to interglacial precipitation changes. Speleothem records from Europe and poleward of 45°N/S should only be interpreted with caution. However, the small number of available records that cover both time periods limits the informative value, especially in regions with high data coverage of other archives.

We found only poor to slight agreement between the iHadCM3 simulated changes and those archived in the available compilation of hydroclimate records. Comparison to the PMIP3 ensemble revealed dry biases in Eastern Africa in the iHadCM3 changes as well as less poleward shifted transition zones between wetter and drier regions. The influence of the meridional circulation patterns as modeled in different climate states may give deeper insight into dynamically driven changes in both precipitation amount and isotopic signatures, and need to be analyzed in detail in future studies.

We investigated state-dependency of variability in δ^{18}O as archived by speleothem records, where MH records show slightly higher variability than LGM records. This state dependency could not be reproduced by the iHadCM3 LGM and MH runs. Analyzing δ^{18}O variability from different climate archives over these time periods can help in deciphering climate induced variability from observed variability in climate archives.

Our analysis provides a first approach for constraining global past precipitation changes using δ^{18}O and growth rate changes in speleothem records and a starting point for further analysis. Additional hydrological proxy records from higher latitudes could give further insight into how to interpret speleothem records in these regions. Analyzing simulated changes and ensemble of isotope-enabled models could reduce single model biases and reveal drivers of individual records. Furthermore, as hydrological changes between the LGM and the Holocene display complex spatial patterns, using them as a reverse analog for future changes is regionally dependent [170]. Thus, the findings also need to be analyzed in comparison to future climate scenario conditions. Approaching hydrological changes between the Last Glacial and present day from all the suggested angles, will in the end help to constrain past precipitation changes and subsequently confine uncertainty of future changes.

5 Discussion and Outlook

In this work, we presented and evaluated methods to extract information on past hydroclimate change from speleothem records and isotope-enabled climate model simulations. Understanding these past changes, how they are recorded in paleoclimate archives and resolved in general circulation models, is crucial to confine uncertainty of future changes under the current anthropogenic warming trend [248]. The central questions that we addressed in this thesis added step-by-step more information to the overarching question on past hydrological changes: Can growth rate changes in speleothem records be detected sufficiently reliable, and do these changes reflect hydrological changes? How similar are modeled and speleothem-archived δ^{18}O signatures over the LM, and what drives their variability? Can growth rate changes and δ^{18}O signatures in speleothem records serve as a proxy for hydrological changes between the LGM and the MH, and are these changes reflected in climate models? These questions are discussed and summarized in the following:

Intercomparison of age-depth models for speleothem growth rate assessment

Detection of speleothem growth rate changes both in synthetically modeled speleothem age-depth profiles and in real speleothems from the SISALv2 database was the main focus of Chapter 2. As growth rate changes are hypothesized to reflect changes of water availability [71, 112], requirements for confident growth rate change detection were necessary. Using a large ensemble of synthetically modeled speleothems with different scenarios of growth rate changes, we found clear requirements for detecting growth rate changes. A minimum of $8-10$ age measurements, i.e., datings, within a desired time period yielded 90 % true positive rates under an acceptable ratio of false positives and growth rate change estimates that were comparable to those estimates with more datings. Six datings may, however, already be enough to detect a growth rate change with high confidence and can indicate where additional datings might provide valuable information. In general, we found Bayesian methods to perform slightly better than linear methods. The presence of already one hiatus strongly decreased the detection skill of true changes and increased false positive detection rates. Applying the found results to speleothems from the SISALv2 database confirmed the hypothesis of higher growth rates in the Holocene compared to the LGM. However, only five records in the database met the criteria of sufficient number of datings, and when comparing all records within one time period, the SISALv2 database contained five times as many records within the MH compared to the LGM.

Future improvement of the detection skill under a smaller number of required datings could be achieved through expanding the analysis into several directions. Additional experiments on synthetically modeled speleothems with variations of the precision, but also with special focus on hiatus length and position, may further increase our understanding of the different performance of the age-depth models. Using the strengths

of all age-models, cross-validation methods between the age-models may substantially increase detection skill overall, which may in turn decrease the number of necessary datings to detect growth rate changes. Under less strict requirements, more records in the speleothem database would be available for analysis of growth rate changes as proxy records of hydrological changes.

Isotopic signatures in the last millennium: model-data comparison as model-evaluation

The incorporation of stable water isotopes into the hydrology of climate models finally lowered the "language barrier" between climate models and paleoclimate proxy data. Chapter 3 evaluated similarities and differences in modeled and archived isotopic signatures in the LM. The idea was to identify possible biases in both model and data in a stable close-to-present-day climate with high data density, before venturing into climates of different background states and fewer available records. Isotopic signatures as simulated by iHadCM3 compared well to those recorded in speleothems and ice cores, however, the comparison to other LM simulations revealed substantial offsets between different models. On multi-decadal to centennial timescale, not only iHadCM3 but all studied iGCMs underestimated speleothem variability. Precipitation amount could be distinguished as the main driver of δ^{18}O variability in the low to mid-latitudes in all models, which suggests that δ^{18}O archived in speleothem records in these regions can be used as a proxy for hydroclimate change. Many discrepancies and limitations of speleothem records as paleoclimate archives could be attributed to their low resolution compared to the observed processes. As such, they were not able to resolve thermodynamic cooling in response to volcanic eruptions. On decadal and shorter timescales, discrepancies arose from record sample resolution but also from damping processes of the karst. Low spatial representativity could only in part be explained by lower resolution and hint at high heterogeneity on regional scales.

Further insight into how the variability of δ^{18}O in precipitation is recorded by speleothem records may be obtained by comparing speleothem calcite δ^{18}O variability, drip water δ^{18}O[278, 7], and observation δ^{18}O from the GNIP database [125], with monthly measurements sites worldwide in sufficient proximity to cave systems. However, drip water monitoring time series as well as those obtained from precipitation measurements are usually very short compared to the timescales that are covered by speleothem records. Instead, other climate archives of δ^{18}O such as non-polar ice cores, tropical coral records or foraminifera from marine sediments may serve as a comparison. If the archives and observations are in close proximity to each other, they must have "witnessed" a very similar climate signal that may be altered, damped or even enhanced by the specific archiving processes. Analyses of SST variability reconstructed from oceanic archives already show consistency between archives, but large discrepancy between archives and climate simulations especially on longer timescales and toward lower latitudes is found [152]. Multi-archive studies that in addition focus on terrestrial δ^{18}O archives may increase our understanding of the capability and the limitations of these paleoclimate archives of capturing the variability of isotopic compositions in precipitation.

Proxy system models that can simulate the processes that impact precipitation on its way to becoming drip water and finally a speleothem provide a different method to enhance our understanding of biases in modeled and archived signatures. Many such models of increasing complexity exist, e.g., the low-complexity model PRYSM [61] or the high-complexity speleothem chemistry model CaveCalc [200]. Maximizing the

number of global records in future analyses, the PSMs may only demand information that is available in the database and does not require local expert knowledge. A "SISAL-database-compatible" PSM of intermediate complexity, built in close cooperation with the SISAL community, is necessary to make the most use of both the large database and the PSM. Recent studies comparing δ^{18}O drip water ranges to those in speleothem records [278] or δ^{18}O drip water to precipitation δ^{18}O [7], along with the efforts of the SISAL community to compile a monitoring database, pave the first steps into building such a PSM.

Hydrological changes between the Last Glacial and present day

We thoroughly tested the capability of speleothems as archives of hydroclimate change, both in growth rates and δ^{18}O signatures, and that of climate models, in particular iHadCM3, to resolve such changes in a stable climate under high data density in Chapter 2 and Chapter 3. With the gained experience and the findings on model and data evaluation, Chapter 4 combined a large compilation of hydroclimate proxy records with climate model simulations of the LGM and the MH to analyze hydrological changes between these periods. Consistent with findings from Chapter 3, we found strong relationships between precipitation amount changes and changes in δ^{18}O for the low- to mid-latitudes (below 45°N/S). Within these latitude bands, isotopic signature changes in iHadCM3 agreed well with those obtained from speleothem records. Modeled changes in precipitation only matched in 50 % with changes archived by the compilation of lake levels, speleothem and pollen records. Here, iHadCM3 showed dry biases in Eastern Africa and potential insufficient widening of the Hadley cell in response to smaller equator-to-pole temperature gradient [143], as revealed by comparing the changes to those from the PMIP3 ensemble. However, additional detailed analysis on the extent of the Hadley cell in the LGM and MH state in different climate models are required to confirm if it drives the changes in the observed patterns. Further, the compilation of proxy records showed outliers, where δ^{18}O signatures in European records [82, 51, 63], pollen records of the West Pacific, as well as some lake levels in Eastern China may be additionally influenced by climate drivers other than precipitation amount, consistent with the findings from other studies [1, 307]. We could confirm a state dependency of δ^{18}O variability in speleothem records, but not in modeled signatures at speleothem locations. Due to the low sample size, this finding should, however, be treated cautiously and requires additional analysis.

The analysis revealed potentials and limitations in both model and data. A way of combining information of both is data assimilation, which can provide proxy-constrained, model-dynamic-constrained full-field reconstructions of climate variables [97, 65, 257]. A recently published data assimilation of surface temperature and δ^{18}O over the last 24,000 years [197] strongly improved the comparison between modeled and archived changes. Until now, speleothem records, although a valuable archive of δ^{18}O , have only been used as records for independent validation [273]. The high covariance between precipitation and δ^{18}O in Chapter 3 holds the prospect of a hydroclimate reconstruction from δ^{18}O in speleothems using data assimilation techniques. A hydroclimate-focused data assimilation may include speleothem records, additional proxy records of relative precipitation amount change [203], such as lake levels and pollen records, combined with the existing temperature proxy database [273, 197, 202]. This data assimilation could provide reconstructed fields of hydroclimate changes between the LGM and the MH that are closer to the changes observed by proxy records but consistent with model physics.

Furthermore, the presented analysis only touches the surface of what is possible with the available proxy records and the climate simulations. For example, our analysis showed disagreement between European records and modeled precipitation changes. Original studies of the records confirm that these are most likely driven by climate variables other than precipitation amount [82, 51, 63]. Regionally focused analysis using proxy and model data could help to better interpret the speleothem records from different areas. As many mismatches between modeled and recorded changes were found in transition regions of wetter and drier MH climates compared to the LGM, a more process-based approach, e.g. using paleoclimate networks [1, 221], is required to better analyze the timing and the location of changes. Our approach here was mainly restricted to the low- to mid-latitudes. As the tropical climate is strongly connected to the climate at the poles [164], further studies including high latitude proxies could provide additional insight. Accumulation rates in ice core records and high latitude pollen records from the recently published LegacyPollen1.0 database [115] could close this high latitude data gap and increase the information on global hydrological changes. Further, hydroclimate processes take place on small spatial scales, which may result in regionally complex patterns [203]. Using past hydrological changes as a reverse analog for future changes may, therefore, be regionally dependent [170]. Thus, all findings on model biases need to be carefully tested and evaluated under climatic backgrounds of future climate scenarios. This will enable us to make more reliable statements on spatial patterns of future changes.

Summary and conclusion

Paleoclimate archives are the only "witnesses" of the past climate that can give evidence of the range and rate of a changing climate. Paleoclimate model simulations are able to provide complete information on a climate system consistent with model physics outside of the historical observation range. We presented a model-data comparison that combined the information stored in speleothem records and isotope-enabled climate models. We investigated hydroclimate change between the Last Glacial Maximum around 21,000 years ago and the Holocene climate prior to the current warming period. By assessing both growth and isotopic information that is accumulated in speleothem records, we demonstrated the potential and limitations of speleothems as a terrestrial archive to reflect past hydroclimate change. To resolve the desired changes, it is recommended to adequately sample speleothem records, both with respect to age measurement as well as δ^{18}O samples. Speleothem growth rate changes can disclose changes in the hydroclimate as long as sufficient dating resolution allows detection. δ^{18}O signatures are valuable indicators of hydroclimate change in the low- to mid-latitudes, as suggested by the modeled covariance between precipitation amount and its δ^{18}O composition in these regions. Even if records are sufficiently sampled, archived climate variability on interannual timescales is likely to be damped by karst filtering processes. Modeled δ^{18}O , on the other hand, strongly underestimates variability on multi-decadal and longer timescales, even across different climate states. While modeled spatial δ^{18}O signatures at speleothem locations show reasonable agreement with archived isotopic compositions, we still found large regional differences in surface climate as resolved by different climate models. Analyzing the hydroclimate change between the Last Glacial Maximum and the Mid Holocene about 6,000 years ago showed little agreement between iHadCM3-modeled changes in precipitation amount and the changes indicated by speleothem, pollen and lake level records. Especially in transition regions, the PMIP3 multi-model comparison to hydroclimate archives showed higher agreement, encouraging the use of a multi-model approach whenever possible. The comparison between changes in the multi-model

ensemble, changes in paleoclimate archives, and those modeled by iHadCM3 was further able to reveal biases in the iHadCM3 model with respect to poleward shifts in wetter or drier transitions. This highlights the benefits and necessity of paleoclimate model-data comparisons for evaluating climate models in different climate background states. The potential of this approach can be further enhanced by including additional hydroclimate archives, especially in the higher latitudes, as well as improved statistical methods to combine information from proxy-based and model-based networks. Innovations in next generation climate models, proxy system models, and data assimilation techniques allow to infer the underlying concepts and physical causes of a changing climate, if paleoclimate archives are capable to capture and climate models to resolve them. To conclude, learning from the past can help us to understand and prepare for the changes that await us.

A Appendix

A.1 Intercomparison of age-depth models

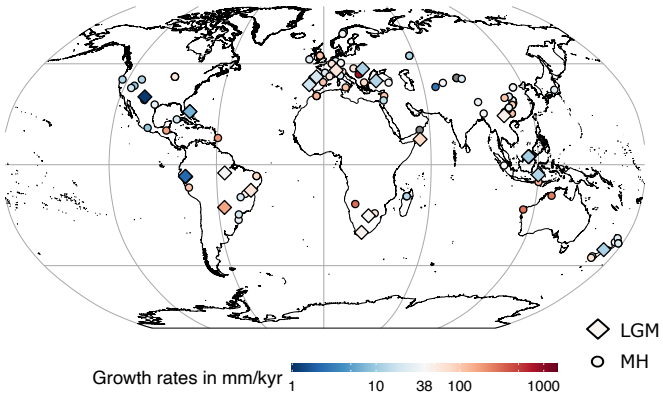

FIGURE A.1: Map of SISALv2 speleothem growth rates in the MH and LGM. Depicted are the growth rates of those LGM and MH speleothems as used in the analysis for Sec. 2.4.2. 38 mm/kyr is the median growth rate of all MH speleothems. Thus, blue indicates slower growth rates than the median MH growth, while red indicates higher growth rate. Diamonds indicate LGM records, circles the MH records.

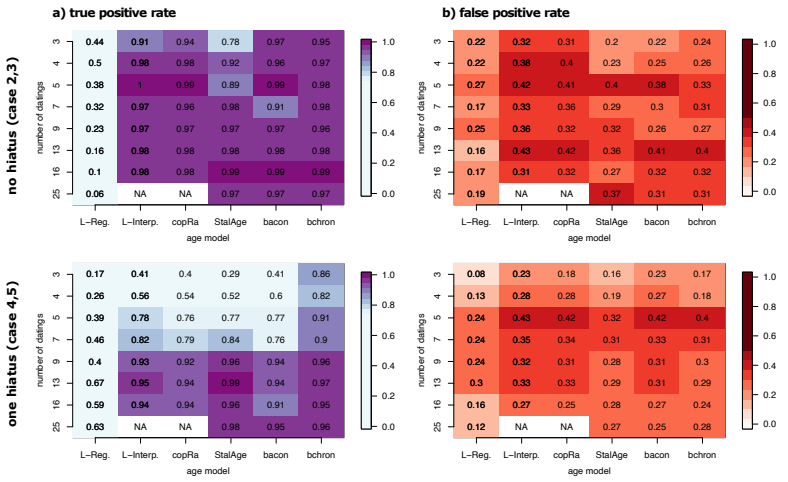

FIGURE A.2: Similar to Fig. 2.8 but separated for the cases without an hiatus (*Case 2* and *3*) in the first row, and cases including an hiatus (*Case 4* and *5*) in the second row.

A.2 Multi-model data comparison for the last millennium

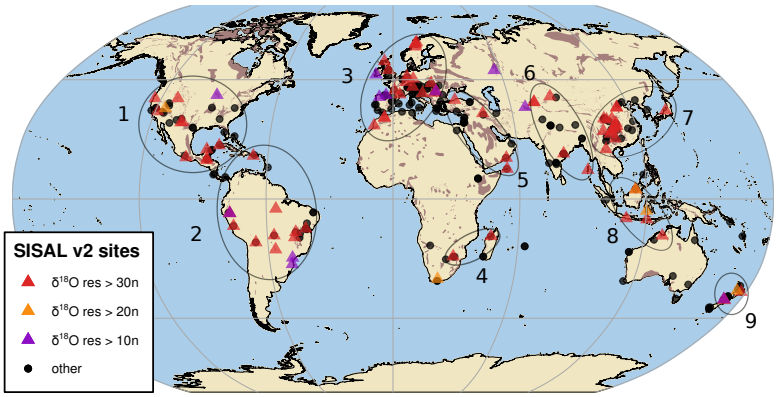

FIGURE A.3: As Fig. 3.4 but with clusters. The nine clusters used in the network analysis contain sites in North America (c1, 12 entities), South America (c2, 12 entities), Europe with North Africa (c3, 21 entities), Southern Africa (c4, 2 entities - too few for systematic analysis), Middle East (c5, 6 entities), India and Central Asia (c6, 8 entities), East Asia (c7, 18 entities), South East Asia (c8, 3 entities), and New Zealand (c9, 3 entities). Caption and Figure adapted from [24].

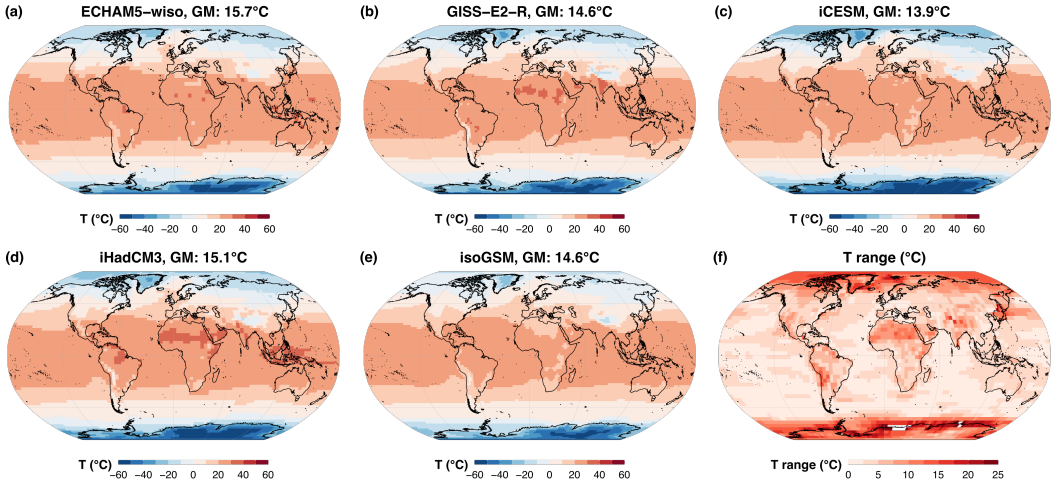

FIGURE A.4: As Fig. 3.7 but for surface air temperature. Figure and caption adapted from [25].

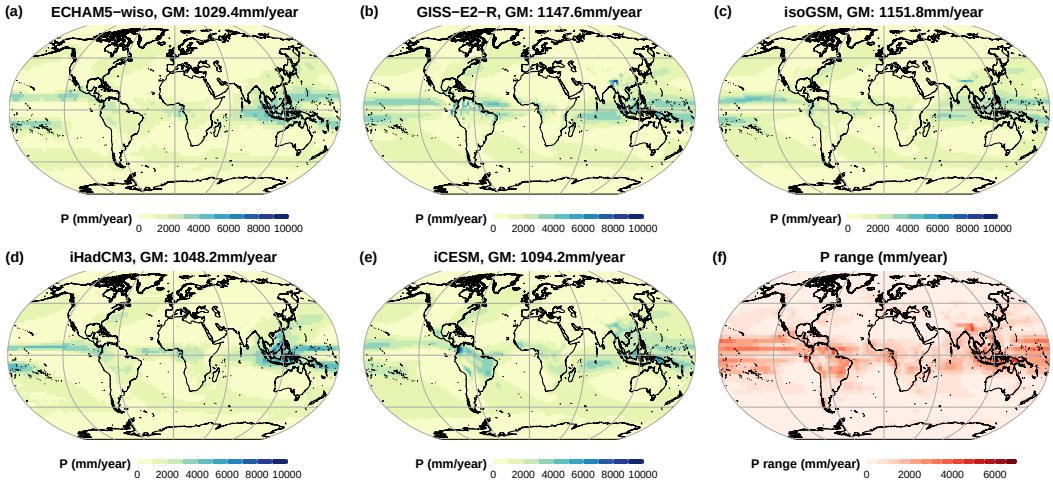

FIGURE A.5: As Fig. 3.7 but for precipitation amount. Figure and caption adapted from [25].

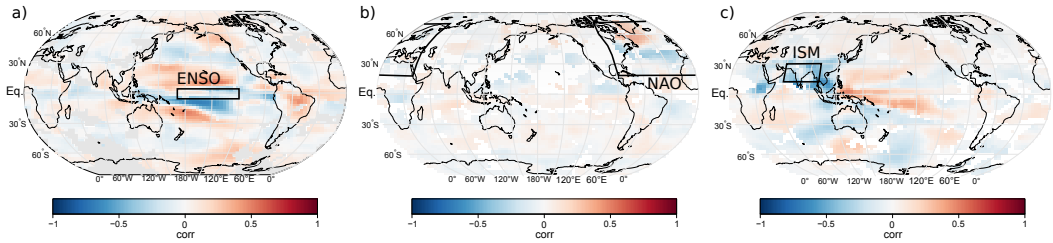

FIGURE A.6: Major climatic modes as represented in oxygen isotopes in iHadCM3 LM1. Spatial correlations of $\delta^{18}O$ and a) ENSO (average over the El-Niño box 1+2, 3.4 and 4 following [281]), b) NAO (difference between Lisbon and Reykjavik, and EOF over 20/80°N -90/40°E [119, 121])and c) ISM modes (JJAS precipitation anomaly over 10/30°N - 70/110°E [99]) in simulations covering 850-1850 CE. Figure adapted from [24].

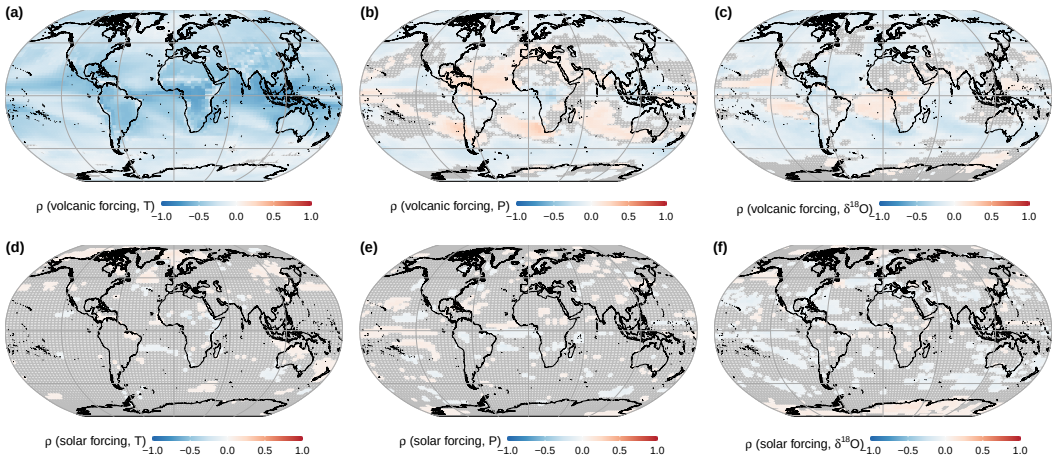

FIGURE A.7: Correlation estimate fields of a) iHadCM3 LM ensemble mean simulated temperature, b) precipitation, and c) δ^{18}O to volcanic forcing, and to solar forcing d-f). Empty tiles mask gridboxes with $p > 0.1$. The area-weighted average correlation estimates with volcanic forcing are ρ(T,volc) = -0.34 (-0.48, -0.11), ρ(P,volc) = -0.04 (-0.15, 0.05), $\rho(\delta^{18}$O,volc) = -0.08 (-0.18, 0.00). The area-weighted average correlation estimates with solar forcing are ρ(T,sol) = 0.01 (-0.004, 0.03), ρ(P,sol) = 0.003 (-0.009, 0.024), $\rho(\delta^{18}$O,sol) = -0.012 (-0.035, 0.056). The correlation estimates are calculated with 989 degrees of freedom. Figure and caption adapted from [24].

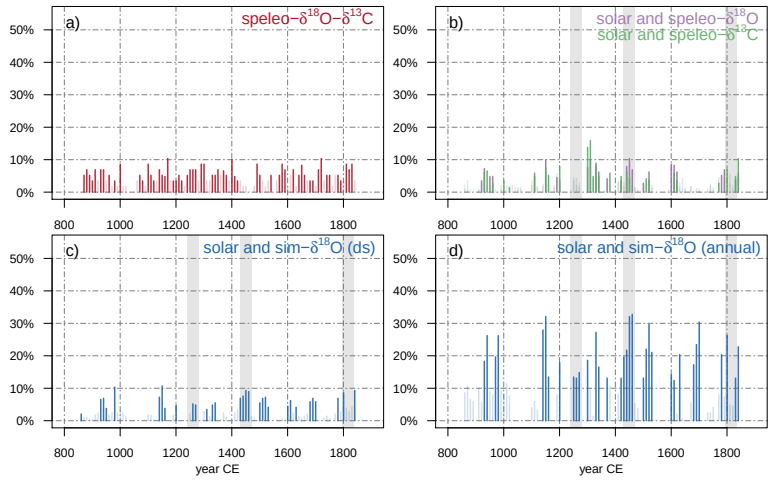

FIGURE A.8: As Fig. 3.16 but using the respective solar forcings. Figure adapted from [25].

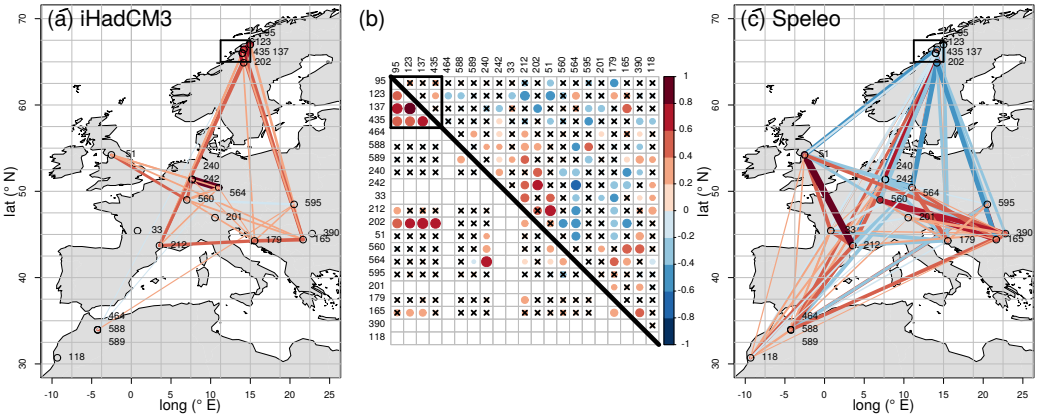

FIGURE A.9: Network map and matrix comparison for the Europe cluster: left map a) shows the correlation network with the simulation data which are represented as dots in the lower triangle of the correlation matrix in the middle (b). The upper triangle in b) and the right map in c) are based on the record to record correlation. One gridbox with 4 entities is marked in the maps and the matrix to compare directly. All links with $p < 0.1$ are shown. Figure and caption adapted from [24]. More cluster-based network analyses can be found in the supplement of [24].

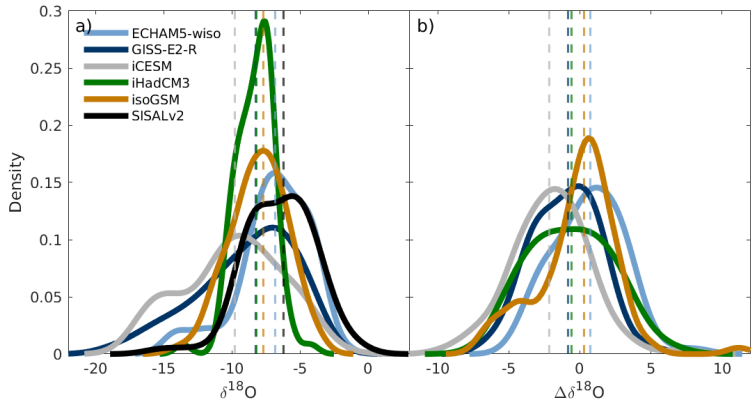

FIGURE A.10: Kernel density estimates of a) the general distributions in simulated and speleothem $\delta^{18}O$ at cave locations, b) offsets between simulated and recorded mean $\delta^{18}O$ over the last millennium ($\Delta\delta^{18}O = \delta^{18}O_{iw} - \delta^{18}O_{dweq}$). Dashed lines represent the medians. Figure and caption adapted from [25].

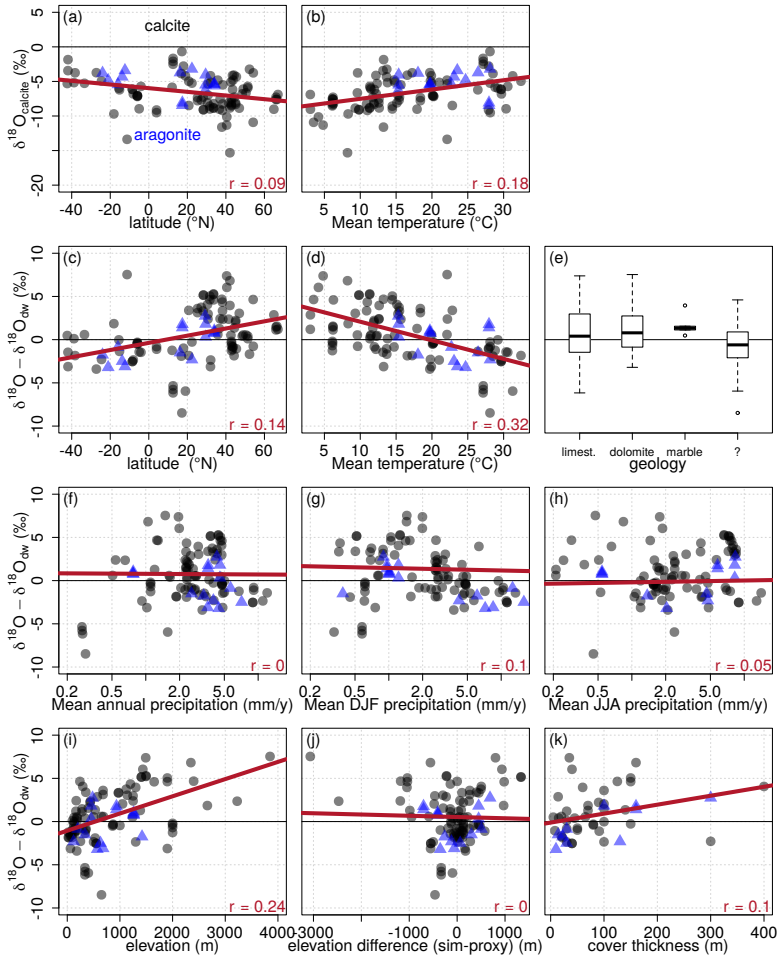

FIGURE A.11: Systematic comparison of climate variables from iHadCM3 LM1 and cave parameters on M-subset $\delta^{18}O_{dweq}$ and the offset $\Delta\ \delta^{18}O$ to the simulation. Shown are the absolute values of $\delta^{18}O_{dweq}$ against: a) site latitude, and b) simulated local annual mean temperature, and the model-data difference against c) latitude, d) simulated mean annual temperature, e) geology surrounding the cave ("?" means unknown geology), f) mean annual g) DJF and (h) JJA precipitation amount as well as i) cave elevation, j) the elevation difference between the model grid and actual cave, and k) the overall cover thickness above cave. Symbols denote calcite (black circles) or aragonite (blue triangles) specimens. An unweighted linear regression (red line) is added for illustration, but without consideration of significance. Figure and caption adapted from [24].

A.3 Hydrological changes between the Last Glacial and present day

Model	GMST ($\pm 2 * sd$) [°C]	GMPR ($\pm 2 * sd$) [mm / yr]	GM δ^{18}O ($\pm 2 * sd$) [‰]
LM1	15.12 ($\pm$0.43)	1048.24 ($\pm$15.58)	$-$8.06 ($\pm$0.19)
LMG*	9.5 ($\pm$0.39)	937.36 ($\pm$11.07)	$-$10.04 ($\pm$0.18)
LGM	9.47 ($\pm$0.26)	936.74 ($\pm$7.39)	$-$10.04 ($\pm$0.16)
LGM-	7.79 ($\pm$0.71)	902.7 ($\pm$15.62)	$-$10.5 ($\pm$0.25)
LGM+	10.01 ($\pm$0.24)	946.54 ($\pm$6.97)	$-$9.91 ($\pm$0.15)
MH	14.64 ($\pm$0.25)	1020.27 ($\pm$297.01)	$-$7.97 ($\pm$2.32)
MH*	14.67 ($\pm$0.38)	1042.99 ($\pm$10.65)	$-$8.12 ($\pm$0.37)

TABLE A.1: Global mean surface temperature, precipitation rate, and isotopic composition of precipitation for the simulations that are used in Chap. 4.

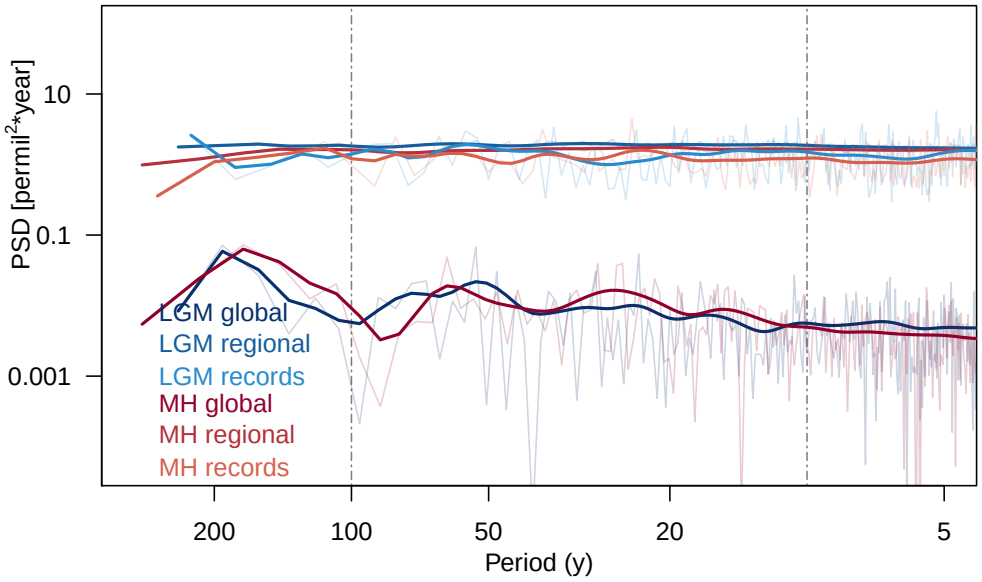

FIGURE A.12: Global, regional and local spectra in iHadCM3 for MH and LGM runs. Regional spectra show the area-weighted average of spectra produced from all grid boxes at annual resolution. Spectra at the cave site location are calculated from annual timeseries extracted from the simulations at the location of the caves as used in the analysis in Sec. 4.3.2.

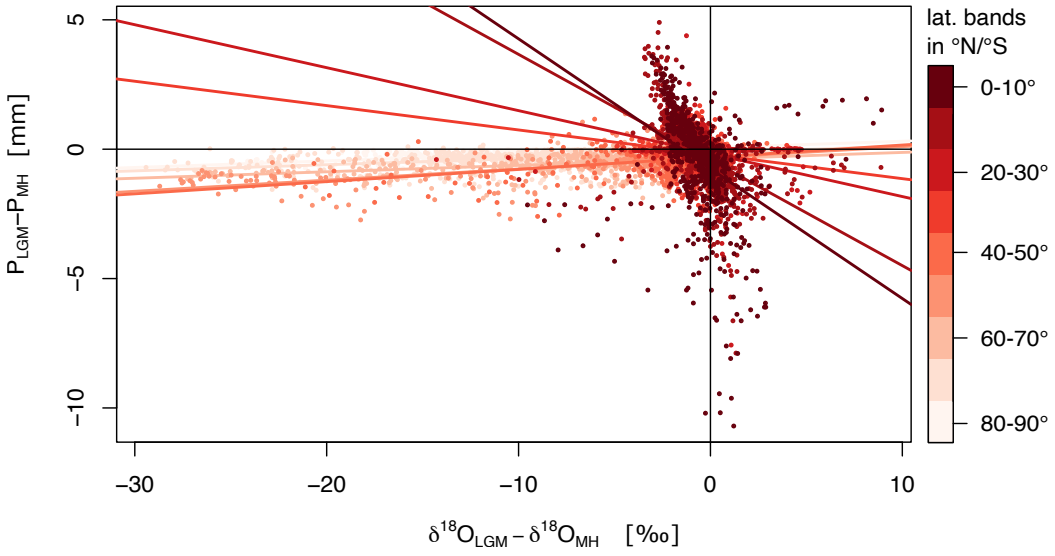

FIGURE A.13: Relationship between modeled changes in precipitation from LGM to Mid-Holocene to modeled changes in its isotopic composition in iHadCM3. Absolute changes are given in $LGM - MH$, such that changes > 0 indicate more precipitation (less depletion) in the LGM. Linear regressions are calculated for latitude bands: $80 - 90°$N/S: $0.03\frac{mm}{‰}$ (0.02, 0.02), $70 - 80°$N/S: $0.02\frac{mm}{‰}$ (-0.16, 0.02), $60 - 70°$N/S: $0.02\frac{mm}{‰}$ (-0.4, 0.02), $50 - 60°$N/S: $0.04\frac{mm}{‰}$ (-0.36, 0.04), $40 - 50°$N/S: $0.05\frac{mm}{‰}$ (-0.34, 0.04), $30 - 40°$N/S: $-0.09\frac{mm}{‰}$ (-0.24, -0.13), $20 - 30°$N/S: $-0.17\frac{mm}{‰}$ (-0.21, -0.19), $10 - 20°$N/S: $-0.41\frac{mm}{‰}$ (-0.49, -0.45), $0 - 10°$N/S: $-0.5\frac{mm}{‰}$ (-0.87, -0.58).

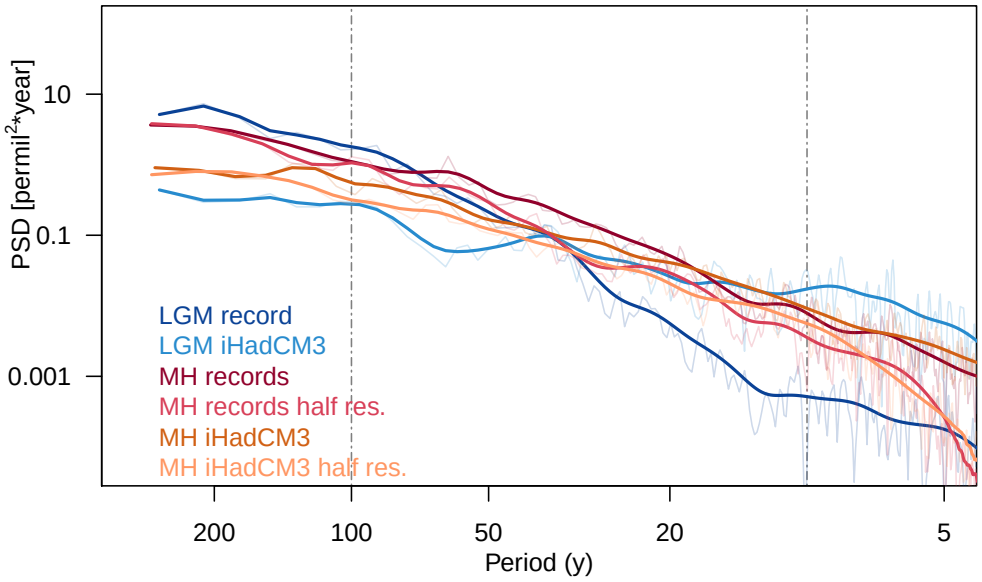

FIGURE A.14: Influence of the lower resolution in LGM records on the variability on decadal and shorter timescales. While the MH SISALv2 subset as used in the analysis in Sec. 4.3.3 shows a mean resolution of 35 yr, the LGM subset only yields 62 yr. To analyze the influence of this lower resolution, we artificially decrease the resolution in MH records, by only considering every second δ^{18}O sample in each record and the simulation. The effects are visible on decadal and shorter timescales.

Bibliography

[1] Moritz Adam, Nils Weitzel, and Kira Rehfeld. "Identifying Global-Scale Patterns of Vegetation Change During the Last Deglaciation From Paleoclimate Networks". In: *Paleoceanography and Paleoclimatology* 36.12 (2021), e2021PA004265. DOI: https://doi.org/10.1029/2021PA004265.

[2] K. K. Andersen et al. "High-resolution record of Northern Hemisphere climate extending into the last interglacial period". In: *Nature* 431.7005 (2004), pp. 147–151. DOI: 10.1038/nature02805.

[3] James Apaéstegui et al. "Precipitation changes over the eastern Bolivian Andes inferred from speleothem (d18O) records for the last 1400 years". In: *Earth and Planetary Science Letters* 494 (2018), pp. 124–134. ISSN: 0012-821X. DOI: https://doi.org/10.1016/j.epsl.2018.04.048.

[4] Kamolphat Atsawawanunt, Laia Comas-Bru, and Sahar Amirnezhad Mozhdehi. "The SISAL database: a global resource to document oxygen and carbon isotope records from speleothems". In: *Earth System Science Data Discussions* April (2018). DOI: 10.5194/essd-10-1687-2018.

[5] AR Atwood et al. "Quantifying climate forcings and feedbacks over the last millennium in the CMIP5–PMIP3 models". In: *Journal of Climate* 29.3 (2016), pp. 1161–1178.

[6] Andy Baker et al. "Elevated and variable values of 13C in speleothems in a British cave system". In: *Chemical Geology* 136.3 (1997), pp. 263–270. ISSN: 0009-2541. DOI: https://doi.org/10.1016/S0009-2541(96)00129-5.

[7] Andy Baker et al. "Global analysis reveals climatic controls on the oxygen isotope composition of cave drip water". In: *Nature Communications* 10.1 (2019), p. 2984. ISSN: 2041-1723. DOI: 10.1038/s41467-019-11027-w.

[8] Andy Baker et al. "Testing theoretically predicted stalagmite growth rate with recent annually laminated samples: Implications for past stalagmite deposition". In: *Geochimica et Cosmochimica Acta* 62.3 (1998), pp. 393–404.

[9] Andy Baker et al. "The Hekla 3 volcanic eruption recorded in a Scottish speleothem?" In: *The Holocene* 5.3 (1995), pp. 336–342.

[10] Jonathan L Baker et al. "Holocene warming in western continental Eurasia driven by glacial retreat and greenhouse forcing". In: *Nature Geoscience* 10.6 (2017), pp. 430–435. ISSN: 17520908. DOI: 10.1038/ngeo2953.

[11] J.U.L. Baldini, F. McDermott, and I.J. Fairchild. "Spatial variability in cave drip water hydrochemistry: Implications for stalagmite paleoclimate records". In: *Chemical Geology* 235.3 (2006), pp. 390–404. ISSN: 0009-2541. DOI: https://doi.org/10.1016/j.chemgeo.2006.08.005.

[12] J.U.L. Baldini et al. "Biomass effects on stalagmite growth and isotope ratios: A 20th century analogue from Wiltshire, England". In: *Earth and Planetary Science Letters* 240.2 (2005), pp. 486–494. ISSN: 0012-821X. DOI: https://doi.org/10.1016/j.epsl.2005.09.022.

[13] C. Barbante et al. "One-to-one coupling of glacial climate variability in Greenland and Antarctica". In: *Nature* 444.7116 (2006), pp. 195–198. DOI: 10.1038/nature05301.

[14] A. Berger and M.F. Loutre. "Insolation values for the climate of the last 10 million years". In: *Quaternary Science Reviews* 10.4 (1991), pp. 297–317. ISSN: 0277-3791. DOI: https://doi.org/10.1016/0277-3791(91)90033-Q.

[15] André L Berger. "Long-term variations of daily insolation and Quaternary climatic changes". In: *Journal of Atmospheric Sciences* 35.12 (1978), pp. 2362–2367.

[16] H John B Birks et al. "Strengths and weaknesses of quantitative climate reconstructions based on Late-Quaternary". In: *The Open Ecology Journal* 3.1 (2010).

[17] Maarten Blaauw and J. Andrés Christeny. "Flexible paleoclimate age-depth models using an autoregressive gamma process". In: *Bayesian Analysis* 6.3 (2011), pp. 457–474. ISSN: 19360975. DOI: 10.1214/11-BA618.

[18] Gabriel J. Bowen et al. "Isotopes in the Water Cycle: Regional- to Global-Scale Patterns and Applications". In: *Annual Review of Earth and Planetary Sciences* 47.1 (2019), pp. 453–479. DOI: 10.1146/annurev-earth-053018-060220.

[19] Pascale Braconnot et al. "Evaluation of climate models using palaeoclimatic data". In: *Nature Climate Change* 2.6 (2012), pp. 417–424. DOI: 10.1038/nclimate1456.

[20] Raymond S Bradley. *Paleoclimate: reconstructing climates of the Quaternary*. Elsevier, 1999.

[21] E. Brady et al. "The Connected Isotopic Water Cycle in the Community Earth System Model Version 1". In: *Journal of Advances in Modeling Earth Systems* 11.8 (2019), pp. 2547–2566. DOI: https://doi.org/10.1029/2019MS001663.

[22] S. F. M. Breitenbach et al. "Constructing proxy records from age models (COPRA)". In: *Climate of the Past* 8.5 (2012), pp. 1765–1779. ISSN: 18149324. DOI: 10.5194/cp-8-1765-2012.

[23] Pierre Bretagnon and Gérard Francou. "Planetary theories in rectangular and spherical variables. VSOP 87 solutions". In: *Astronomy and astrophysics* 202.1 (1988), pp. 309–315. ISSN: 0004-6361.

[24] J. C. Bühler et al. "Comparison of the oxygen isotope signatures in speleothem records and iHadCM3 model simulations for the last millennium". In: *Climate of the Past* 17.3 (2021), pp. 985–1004. DOI: 10.5194/cp-17-985-2021.

[25] J. C. Bühler et al. "Investigating oxygen and carbon isotopic relationships in speleothem records over the last millennium using multiple isotope-enabled climate models". In: *Climate of the Past Discussions* 2021 (2021), pp. 1–37. DOI: 10.5194/cp-2021-152.

[26] J. C. Bühler et al. "Supplement: Comparison of the oxygen isotope signatures in speleothem records and iHadCM3 model simulations for the last millennium". In: *Climate of the Past* 17.3 (2021), pp. 985–1004. DOI: 10.5194/cp-17-985-2021-supplement.

[27] Stephen J. Burns et al. "A 780-year annually resolved record of Indian Ocean monsoon precipitation from a speleothem from south Oman". In: *Journal of Geophysical Research: Atmospheres* 107.D20 (2002), ACL 9–1–ACL 9–9. DOI: https://doi.org/10.1029/2001JD001281.

[28] Yuval Burstyn et al. "Speleothems from the Middle East: An Example of Water Limited Environments in the SISAL Database". In: *Quaternary* 2.2 (2019). ISSN: 2571-550X. DOI: 10.3390/quat2020016.

[29] J. C. Bühler and K. Rehfeld. *iHadCM3LastMill Github Repository*. 2020, (accessed April 13, 2022). URL: https://github.com/paleovar/iHadCM3LastMill.

[30] J. C. Bühler and K. Rehfeld. *Supplement Thesis Github Repository*. 2022, (accessed April 21, 2022). URL: https://github.com/paleovar/Supplement_Thesis_JB_2022.git.

[31] Thibaut Caley, Didier M Roche, and Hans Renssen. "Orbital Asian summer monsoon dynamics revealed using an isotope-enabled global climate model". In: *Nature Communications* 5 (2014), pp. 6–11. ISSN: 20411723. DOI: 10.1038/ncomms6371.

[32] Peter Caplan et al. "Changes to the 1995 NCEP operational medium-range forecast model analysis-forecast system". In: *Weather and Forecasting* 12.3 PART II (1997), pp. 581–594. ISSN: 08828156. DOI: 10.1175/1520-0434(1997)012<0581:cttnom>2.0.co;2.

[33] M. Casado, T. Münch, and T. Laepple. "Climatic information archived in ice cores: impact of intermittency and diffusion on the recorded isotopic signal in Antarctica". In: *Climate of the Past* 16.4 (2020), pp. 1581–1598. DOI: 10.5194/cp-16-1581-2020.

[34] Chris Chatfield. *The Analysis of Time Series - An Introduction*. Sixth Edition. Chapman & Hall/CRC, 2003. ISBN: 978-0-203-49168-3.

[35] Hai Cheng et al. "Climate change patterns in Amazonia and biodiversity". In: *Nature Communications* 4.1 (2013), p. 1411. DOI: 10.1038/ncomms2415.

[36] Hai Cheng et al. "The Asian monsoon over the past 640,000 years and ice age terminations". In: *Nature* 534.7609 (2016), pp. 640–646. ISSN: 14764687. DOI: 10.1038/nature18591.

[37] Manuel Chevalier et al. "Pollen-based climate reconstruction techniques for late Quaternary studies". In: *Earth-Science Reviews* 210 (2020), p. 103384. ISSN: 0012-8252. DOI: https://doi.org/10.1016/j.earscirev.2020.103384.

[38] John C.H. Chiang et al. "Enriched East Asian oxygen isotope of precipitation indicates reduced summer seasonality in regional climate and westerlies". In: *Proceedings of the National Academy of Sciences of the United States of America* 117.26 (2020), pp. 14745–14750. ISSN: 10916490. DOI: 10.1073/pnas.1922602117.

[39] Chia Chou et al. "Increase in the range between wet and dry season precipitation". In: *Nature Geoscience* 6.4 (2013), pp. 263–267. DOI: 10.1038/ngeo1744.

[40] Intergovernmental Panel on Climate Change. "Freshwater Resources". In: *Climate Change 2014 – Impacts, Adaptation and Vulnerability: Part A: Global and Sectoral Aspects: Working Group II Contribution to the IPCC Fifth Assessment Report*. Vol. 1. Cambridge University Press, 2014, 229–270. DOI: 10.1017/CBO9781107415379.008.

[41] Intergovernmental Panel on Climate Change. "Glossary". In: *Climate Change 2013 – The Physical Science Basis: Working Group I Contribution to the Fifth Assessment Report of the Intergovernmental Panel on Climate Change*. Cambridge University Press, 2014, 1447–1466. DOI: 10.1017/CBO9781107415324.031.

[42] Sloan Coats et al. "Are simulated megadroughts in the North American Southwest forced?" In: *Journal of Climate* 28.1 (2015), pp. 124–142.

[43] Kim M Cobb et al. "El Niño/Southern Oscillation and tropical Pacific climate during the last millennium". In: *Nature* 424.6946 (2003), pp. 271–276.

[44] Matthew Collins et al. "Long-term climate change: projections, commitments and irreversibility". In: *Climate Change 2013 - The Physical Science Basis: Contribution of Working Group I to the Fifth Assessment Report of the Intergovernmental Panel on Climate Change*. Cambridge University Press, 2013, pp. 1029–1136.

[45] Christopher M Colose, Allegra N. LeGrande, and Mathias Vuille. "Hemispherically asymmetric volcanic forcing of tropical hydroclimate during the last millennium". In: *Earth System Dynamics* 7.3 (2016), pp. 681–696. ISSN: 21904987. DOI: 10.5194/esd-7-681-2016.

[46] Christopher M Colose, Allegra N. LeGrande, and Mathias Vuille. "The influence of volcanic eruptions on the climate of tropical South America during the last millennium in an isotope-enabled general circulation model". In: *Climate of the Past* 12.4 (2016), pp. 961–979. ISSN: 18149332. DOI: 10.5194/cp-12-961-2016.

[47] Laia Comas-Bru. *Karst diagram from PhD thesis of Laia Comas-Bru*. Mar. 2015. DOI: 10.5281/zenodo.6323527. URL: https://doi.org/10.5281/zenodo.6323527.

[48] Laia Comas-Bru et al. "Evaluating model outputs using integrated global speleothem records of climate change since the last glacial". In: *Climate of the Past* 15.4 (2019), pp. 1557–1579. ISSN: 18149332. DOI: 10.5194/cp-15-1557-2019.

[49] Laia Comas-Bru et al. "SISALv2: a comprehensive speleothem isotope database with multiple age–depth models". In: *Earth System Science Data* 12.4 (2020), pp. 2579–2606. DOI: 10.5194/essd-12-2579-2020.

[50] Jessica L. Conroy, Kim M. Cobb, and David Noone. "Comparison of precipitation isotope variability across the tropical Pacific in observations and SWING2 model simulations". In: *Journal of Geophysical Research Atmospheres* 118.11 (2013), pp. 5867–5892. ISSN: 21698996. DOI: 10.1002/jgrd.50412.

[51] Silviu Constantin et al. "Holocene and Late Pleistocene climate in the sub-Mediterranean continental environment: A speleothem record from Poleva Cave (Southern Carpathians, Romania)". In: *Palaeogeography, Palaeoclimatology, Palaeoecology* 243.3 (2007), pp. 322–338. ISSN: 0031-0182. DOI: https://doi.org/10.1016/j.palaeo.2006.08.001.

[52] Tyler B Coplen, Carol Kendall, and Jessica Hopple. "Comparison of stable isotope reference samples". In: *Nature* 302.21 (1983), pp. 28–30.

[53] Jason Cosford et al. "East Asian monsoon variability since the Mid-Holocene recorded in a high-resolution, absolute-dated aragonite speleothem from eastern China". In: *Earth and Planetary Science Letters* 275.3 (2008), pp. 296–307. ISSN: 0012-821X. DOI: https://doi.org/10.1016/j.epsl.2008.08.018.

[54] Peter M Cox. "Description of the "TRIFFID" dynamic global vegetation model, Hadley Centre. Technical Note 24". In: (2001), p. 17.

[55] T J Crowley and M B Unterman. "Technical details concerning development of a 1200 yr proxy index for global volcanism". In: *Earth System Science Data* 5.1 (2013), pp. 187–197. ISSN: 18663508. DOI: 10.5194/essd-5-187-2013.

[56] T. J. Crowley et al. "Volcanism and the Little Ice Age". In: *PAGES news* 16.2 (2008), pp. 22–23. ISSN: 15630803. DOI: 10.22498/pages.16.2.22.

[57] Michel Crucifix, Richard A. Betts, and Christopher D. Hewitt. "Pre-industrial-potential and Last Glacial Maximum global vegetation simulated with a coupled climate-biosphere model: diagnosis of bioclimatic relationships". In: *Global and Planetary Change* 45.4 (2005), pp. 295–312. ISSN: 0921-8181. DOI: https://doi.org/10.1016/j.gloplacha.2004.10.001.

[58] Quentin Dalaiden et al. "How useful is snow accumulation in reconstructing surface air temperature in Antarctica? A study combining ice core records and climate models". In: *Cryosphere* 14.4 (2020), pp. 1187–1207. ISSN: 19940424. DOI: 10.5194/tc-14-1187-2020.

[59] W Dansgaard. "Stable isotopes in precipitation". In: *Tellus* 16.4 (1964), pp. 436–468. ISSN: 0040-2826. DOI: 10.3402/tellusa.v16i4.8993.

[60] S. G. Dee et al. "PRYSM: An open-source framework for PRoxY System Modeling, with applications to oxygen-isotope systems". In: *Journal of Advances in Modeling Earth Systems* 7.3 (2015), pp. 1220–1247. DOI: https://doi.org/10.1002/2015MS000447.

[61] S.G. Dee et al. "Improved spectral comparisons of paleoclimate models and observations via proxy system modeling: Implications for multi-decadal variability". In: *Earth and Planetary Science Letters* 476 (2017), pp. 34–46. ISSN: 0012-821X. DOI: https://doi.org/10.1016/j.epsl.2017.07.036.

[62] R. F. Denniston et al. "A Stalagmite record of Holocene Indonesian–Australian summer monsoon variability from the Australian tropics". In: *Quaternary Science Reviews* 78 (2013), pp. 155–168. ISSN: 0277-3791. DOI: https://doi.org/10.1016/j.quascirev.2013.08.004.

[63] R. F. Denniston et al. "A stalagmite test of North Atlantic SST and Iberian hydroclimate linkages over the last two glacial cycles". In: *Climate of the Past* 14.12 (2018), pp. 1893–1913. DOI: 10.5194/cp-14-1893-2018.

[64] Clara Deser et al. "Uncertainty in climate change projections: the role of internal variability". In: *Climate Dynamics* 38.3 (2012), pp. 527–546. DOI: 10.1007/s00382-010-0977-x.

[65] Sébastien Dirren and Gregory J Hakim. "Toward the assimilation of time-averaged observations". In: *Geophysical research letters* 32.4 (2005).

[66] Sarah J. Doherty et al. "Lessons Learned from IPCC AR4: Scientific Developments Needed to Understand, Predict, and Respond to Climate Change". In: *Bulletin of the American Meteorological Society* 90.4 (2009), pp. 497 –514. DOI: 10.1175/2008BAMS2643.1.

[67] Andrew Dolman et al. "Estimating the timescale-dependent uncertainty of paleoclimate records—a spectral approach. Part II: Application and interpretation". In: *Climate of The Past Discussions* February (2020), pp. 1–38. ISSN: 1814-9340. DOI: 10.5194/cp-2019-153.

[68] Wolfgang Dreybrodt. "Chemical kinetics, speleothem growth and climate". In: *Boreas* 28.3 (1999), pp. 347–356.

[69] Wolfgang Dreybrodt. "Deposition of calcite from thin films of natural calcareous solutions and the growth of speleothems". In: *Chemical Geology* 29.1-4 (1980), pp. 89–105.

[70] Wolfgang Dreybrodt and Denis Scholz. "Climatic dependence of stable carbon and oxygen isotope signals recorded in speleothems: From soil water to speleothem calcite". In: *Geochimica et Cosmochimica Acta* 75.3 (2011), pp. 734–752. ISSN: 0016-7037. DOI: https://doi.org/10.1016/j.gca.2010.11.002.

[71] Russell N. Drysdale et al. "Palaeoclimatic implications of the growth history and stable isotope (d18O and d13C) geochemistry of a Middle to Late Pleistocene stalagmite from central-western Italy". In: *Earth and Planetary Science Letters* 227.3 (2004), pp. 215–229. ISSN: 0012-821X. DOI: https://doi.org/10.1016/j.epsl.2004.09.010.

[72] B. Efron and R. Tibshirani. "Bootstrap methods for standard errors, confidence intervals, and other measures of statistical accuracy". In: *Statistical Science* 1.1 (1986), pp. 54–75. ISSN: 08834237. DOI: 10.1214/ss/1177013815.

[73] Anja Eichler et al. "An ice-core based history of Siberian forest fires since AD 1250". In: *Quaternary Science Reviews* 30.9 (2011), pp. 1027–1034. ISSN: 0277-3791. DOI: https://doi.org/10.1016/j.quascirev.2011.02.007.

[74] Beatrice Ellerhoff et al. "State-dependent effects of natural forcing on global and local climate variability". In: *Earth and Space Science Open Archive* (2022), p. 17. DOI: 10.1002/essoar.10510620.1.

[75] M.N. Evans et al. "Applications of proxy system modeling in high resolution paleoclimatology". In: *Quaternary Science Reviews* 76 (2013), pp. 16–28. ISSN: 0277-3791. DOI: https://doi.org/10.1016/j.quascirev.2013.05.024.

[76] Veronika Eyring et al. "Overview of the Coupled Model Intercomparison Project Phase 6 (CMIP6) experimental design and organization". In: *Geoscientific Model Development* 9.5 (2016), pp. 1937–1958. ISSN: 19919603. DOI: 10.5194/gmd-9-1937-2016.

[77] Ian J Fairchild and Andy Baker. *Speleothem science: from process to past environments*. John Wiles & Sons, 2012.

[78] Ian J Fairchild and Pauline C Treble. "Trace elements in speleothems as recorders of environmental change". In: *Quaternary Science Reviews* 28.5-6 (2009), pp. 449–468. ISSN: 02773791. DOI: 10.1016/j.quascirev.2008.11.007.

[79] Ian J Fairchild et al. "Modification and preservation of environmental signals in speleothems". In: *Earth-Science Reviews* 75.1-4 (2006), pp. 105–153. ISSN: 00128252. DOI: 10.1016/j.earscirev.2005.08.003.

[80] Robert D. Field et al. "Evaluating climate model performance in the tropics with retrievals of water isotopic composition from Aura TES". In: *Geophysical Research Letters* 41.16 (2014), pp. 6030–6036. DOI: https://doi.org/10.1002/2014GL060572.

[81] Dominik Fleitmann et al. "Holocene ITCZ and Indian monsoon dynamics recorded in stalagmites from Oman and Yemen (Socotra)". In: *Quaternary Science Reviews* 26.1 (2007), pp. 170–188. ISSN: 0277-3791. DOI: https://doi.org/10.1016/j.quascirev.2006.04.012.

[82] Dominik Fleitmann et al. "Timing and climatic impact of Greenland interstadials recorded in stalagmites from northern Turkey". In: *Geophysical Research Letters* 36.19 (2009).

[83] Pascal Flohr et al. "Late Holocene droughts in the Fertile Crescent recorded in a speleothem from northern Iraq". In: *Geophysical Research Letters* 44.3 (2017), pp. 1528–1536.

[84] Jens Fohlmeister et al. "Bunker Cave stalagmites: an archive for central European Holocene climate variability". In: *Climate of the Past* 8.5 (2012), pp. 1751–1764. DOI: 10.5194/cp-8-1751-2012.

[85] Jens Fohlmeister et al. "Bunker Cave stalagmites: an archive for central European Holocene climate variability". In: *Climate of the Past* 8.5 (2012), pp. 1751–1764. ISSN: 1814-9332. DOI: 10.5194/cp-8-1751-2012.

[86] Jens Fohlmeister et al. "Carbon and oxygen isotope fractionation in the water-calcite-aragonite system". In: *Geochimica et Cosmochimica Acta* 235 (2018), pp. 127–139. ISSN: 0016-7037. DOI: https://doi.org/10.1016/j.gca.2018.05.022.

[87] Jens Fohlmeister et al. "Main controls on the stable carbon isotope composition of speleothems". In: *Geochimica et Cosmochimica Acta* 279 (2020), pp. 67–87.

[88] Jens Fohlmeister et al. "Winter precipitation changes during the Medieval Climate Anomaly and the Little Ice Age in arid Central Asia". In: *Quaternary Science Reviews* 178 (2017), pp. 24–36. ISSN: 0277-3791. DOI: https://doi.org/10.1016/j.quascirev.2017.10.026.

[89] Grant Foster and Stefan Rahmstorf. "Global temperature evolution 1979–2010". In: *Environmental Research Letters* 6.4 (2011), p. 044022. DOI: 10.1088/1748-9326/6/4/044022.

[90] Christian L. E. Franzke et al. "The Structure of Climate Variability Across Scales". In: *Reviews of Geophysics* 58.2 (2020). ISSN: 8755-1209. DOI: 10.1029/2019rg000657.

[91] Silvia Frisia, Andrea Borsato, and Jean Susini. "Synchrotron radiation applications to past volcanism archived in speleothems: An overview". In: *Journal of Volcanology and Geothermal Research* 177.1 (2008). Explosive volcanism in the central Mediterranean area during the late Quaternary - linking sources and distal archives, pp. 96–100. ISSN: 0377-0273. DOI: https://doi.org/10.1016/j.jvolgeores.2007.11.010.

[92] Chaochao Gao, Alan Robock, and Caspar Ammann. "Volcanic forcing of climate over the past 1500 years: An improved ice core-based index for climate models". In: *Journal of Geophysical Research: Atmospheres* 113.D23 (2008). DOI: https://doi.org/10.1029/2008JD010239.

[93] Lynn W. Gelhar and John L. Wilson. "Ground-Water Quality Modeling a". In: *Groundwater* 12.6 (1974), pp. 399–408.

[94] D. Genty, Andrew Baker, and B Vokal. "Inter and intra annual growth rates of European stalagmites". In: *Chemical Geology* 176 (2001), pp. 193–214.

[95] D. Genty et al. "Timing and dynamics of the last deglaciation from European and North African d13C stalagmite profiles—comparison with Chinese and South Hemisphere stalagmites". In: *Quaternary Science Reviews* 25.17 (2006), pp. 2118–2142. ISSN: 0277-3791. DOI: https://doi.org/10.1016/j.quascirev.2006.01.030.

[96] Yonaton Goldsmith et al. "Northward extent of East Asian monsoon covaries with intensity on orbital and millennial timescales". In: *Proceedings of the National Academy of Sciences* 114.8 (2017), pp. 1817–1821. DOI: 10.1073/pnas.1616708114.

[97] H. Goosse et al. "Using paleoclimate proxy-data to select optimal realisations in an ensemble of simulations of the climate of the past millennium". In: *Climate Dyn.* 27 (2006), pp. 165–184.

[98] C Gordon et al. "The simulation of SST, sea ice extents and ocean heat transports in a version of the Hadley Centre coupled model without flux adjustments". In: *Climate Dynamics* 16.2-3 (2000), pp. 147–168. DOI: https://doi.org/10.1007/s003820050010.

[99] Bhupendra Nath Goswami, V Krishnamurthy, and H Annmalai. "A broad-scale circulation index for the interannual variability of the Indian summer monsoon". In: *Quarterly Journal of the Royal Meteorological Society* 125.554 (1999), pp. 611–633.

[100] S. Goursaud et al. "Challenges associated with the climatic interpretation of water stable isotope records from a highly resolved firn core from Adélie Land, coastal Antarctica". In: *The Cryosphere* 13.4 (2019), pp. 1297–1324. DOI: 10.5194/tc-13-1297-2019.

[101] S. Goursaud et al. "Water stable isotope spatiooral variability in Antarctica in 1960-2013: Observations and simulations from the ECHAM5-wiso atmospheric general circulation model". In: *Climate of the Past* 14.6 (2018), pp. 923–946. ISSN: 18149332. DOI: 10.5194/cp-14-923-2018.

[102] Peter Greve et al. "Global assessment of trends in wetting and drying over land". In: *Nature Geoscience* 7.10 (2014), pp. 716–721. DOI: 10.1038/ngeo2247.

[103] Ethan L Grossman and Teh Lung Ku. "Oxygen and carbon isotope fractionation in biogenic aragonite: Temperature effects". In: *Chemical Geology: Isotope Geoscience Section* (1986). ISSN: 01689622. DOI: 10.1016/0168-9622(86)90057-6.

[104] Hera Guðlaugsdóttir et al. "North Atlantic weather regimes in δ18O of winter precipitation: isotopic fingerprint of the response in the atmospheric circulation after volcanic eruptions". In: *Tellus, Series B: Chemical and Physical Meteorology* 71.1 (2019), pp. 1–19. ISSN: 16000889. DOI: 10.1080/16000889.2019.1633848.

[105] Maximilian Hansen et al. "Simulating speleothem growth in the laboratory: Determination of the stable isotope fractionation (d13C and d18O) between H2O, DIC and CaCO3". In: *Chemical Geology* 509 (2019), pp. 20–44. ISSN: 0009-2541. DOI: https://doi.org/10.1016/j.chemgeo.2018.12.012.

[106] Sandy P. Harrison et al. "Ecophysiological and bioclimatic foundations for a global plant functional classification". In: *Journal of Vegetation Science* 21.2 (2010), pp. 300–317. DOI: https://doi.org/10.1111/j.1654-1103.2009.01144.x.

[107] John Haslett and Andrew Parnell. "A simple monotone process with application to radiocarbon-dated depth chronologies". In: *Journal of the Royal Statistical Society. Series C: Applied Statistics* 57.4 (2008), pp. 399–418. ISSN: 00359254. DOI: 10.1111/j.1467-9876.2008.00623.x.

[108] Waldemar Haude. "Zur praktischen Bestimmung aktuellen und potentiellen Evaporation und Evapotranspiration". In: *Mitteilungen des Deutschen Wetterdienstes* Band 1 (1954).

[109] R. Hébert, K. Rehfeld, and T. Laepple. "Comparing estimation techniques for timescale-dependent scaling of climate variability in paleoclimate time series". In: *Nonlinear Processes in Geophysics Discussions* 2021 (2021), pp. 1–26. DOI: 10.5194/npg-2021-7.

[110] Yannick E. Heiser. "Comparison of Isotopic Signatures in Ice Core and Speleothem Records to an Isotope-Enabled Climate Model Simulation for the Last Millennium". Bachelor Thesis. MA thesis. Heidelberg University: Heidelberg University, 2021.

[111] Isaac M. Held and Brian J. Soden. "Robust Responses of the Hydrological Cycle to Global Warming". In: *Journal of Climate* 19.21 (2006), pp. 5686 –5699. DOI: 10.1175/JCLI3990.1.

[112] J.C Hellstrom and M.T McCulloch. "Multi-proxy constraints on the climatic significance of trace element records from a New Zealand speleothem". In: *Earth and Planetary Science Letters* 179.2 (2000), pp. 287–297. ISSN: 0012-821X. DOI: https://doi.org/10.1016/S0012-821X(00)00115-1.

[113] C.H Hendy. "The isotopic geochemistry of speleothems—I. The calculation of the effects of different modes of formation on the isotopic composition of speleothems and their applicability as palaeoclimatic indicators". In: *Geochimica et Cosmochimica Acta* 35.8 (1971), pp. 801–824. ISSN: 0016-7037. DOI: https://doi.org/10.1016/0016-7037(71)90127-X.

[114] Michael M. Herron and Chester C. Langway. "Firn Densification: An Empirical Model". In: *Journal of Glaciology* 25.93 (1980), 373–385. DOI: 10.3189/S0022143000015239.

[115] U. Herzschuh et al. "LegacyPollen 1.0: A taxonomically harmonized global Late Quaternary pollen dataset of 2831 records with standardized chronologies". In: *Earth System Science Data Discussions* 2022 (2022), pp. 1–25. DOI: 10.5194/essd-2022-37.

[116] Linda Heusser, Cal Heusser, and Nicklas Pisias. "Vegetation and climate dynamics of southern Chile during the past 50,000 years: results of ODP Site 1233 pollen analysis". In: *Quaternary Science Reviews* 25.5 (2006), pp. 474–485. ISSN: 0277-3791. DOI: https://doi.org/10.1016/j.quascirev.2005.04.009.

[117] Max D Holloway et al. "Reconstructing paleosalinity from δ^{18} O: Coupled model simulations of the Last Glacial Maximum, Last Interglacial and Late Holocene". In: *Quaternary Science Reviews* 131 (2016), pp. 350–364. ISSN: 02773791. DOI: 10.1016/j.quascirev.2015.07.007.

[118] Max D Holloway et al. "Simulating the 128-ka Antarctic Climate Response to Northern Hemisphere Ice Sheet Melting Using the Isotope-Enabled HadCM3". In: *Geophysical Research Letters* 45.21 (2018), pp. 11,911–921,929. ISSN: 19448007. DOI: 10.1029/2018GL079647.

[119] James W. Hurrell. "Decadal trends in the North Atlantic oscillation: Regional temperatures and precipitation". In: *Science* 269.5224 (Aug. 1995), pp. 676–679. ISSN: 00368075. DOI: 10.1126/science.269.5224.676.

[120] James W. Hurrell et al. "The community earth system model: a framework for collaborative research". In: *Bulletin of the American Meteorological Society* 94.9 (2013), pp. 1339–1360.

[121] James W. Hurrell et al. "The North Atlantic Oscillation OceanSITES-Taking the pulse of the global ocean View project CoDINA-Cod: DIet and food web dyNAmics View project An Overview of the North Atlantic Oscillation". In: (2003), undefined–undefined.

[122] George C Hurtt et al. "Harmonization of land-use scenarios for the period 1500–2100: 600 years of global gridded annual land-use transitions, wood harvest, and resulting secondary lands". In: *Climatic change* 109.1 (2011), pp. 117–161.

[123] Kathleen Huybers, Summer Rupper, and Gerard H. Roe. "Response of closed basin lakes to interannual climate variability". In: *Climate Dynamics* 46.11 (2016), pp. 3709–3723. DOI: 10.1007/s00382-015-2798-4.

[124] Martin C Hänsel et al. "Climate economics support for the UN climate targets". In: *Nature Climate Change* (2020), pp. 1758–6798. DOI: 10.1038/s41558-020-0833-x.

[125] IAEA/WMO. *Global Network of Isotopes in Precipitation. The GNIP Database*. Accessible at: http://www.iaea.org/water. 2020.

[126] Miro Ivanovich and Russell S Harmon. "Uranium-series disequilibrium: applications to earth, marine, and environmental sciences. 2". In: (1992).

[127] P Jean-Baptiste et al. "Tritium dating of dripwater from Villars Cave (SW-France)". In: *Applied Geochemistry* 107.June (2019), pp. 152–158. ISSN: 18729134. DOI: 10.1016/j.apgeochem.2019.06.005.

[128] Sigfús J Johnsen et al. "Diffusion of stable isotopes in polar firn and ice: the isotope effect in firn diffusion". In: *Physics of ice core records*. Hokkaido University Press. 2000, pp. 121–140.

[129] V. E. Johnston et al. "Stable isotopes in caves over altitudinal gradients: fractionation behaviour and inferences for speleothem sensitivity to climate change". In: *Climate of the Past* 9.1 (2013), pp. 99–118. DOI: 10.5194/cp-9-99-2013.

[130] J Jouzel et al. "Magnitude of isotope/temperature scaling for interpretation of central Antarctic ice cores". In: *Journal of Geophysical Research: Atmospheres* 108.D12 (2003).

[131] J. H. Jungclaus et al. "Climate and carbon-cycle variability over the last millennium". In: *Climate of the Past* 6.5 (2010), pp. 723–737. ISSN: 18149324. DOI: 10.5194/cp-6-723-2010.

[132] J. H. Jungclaus et al. "Ocean circulation and tropical variability in the coupled model ECHAM5/MPI-OM". In: *Journal of Climate* 19.16 (2006), pp. 3952–3972. ISSN: 08948755. DOI: 10.1175/JCLI3827.1.

[133] M. Kageyama et al. "The PMIP4 contribution to CMIP6 – Part 1: Overview and over-arching analysis plan". In: *Geoscientific Model Development* 11.3 (2018), pp. 1033–1057. DOI: 10.5194/gmd-11-1033-2018.

[134] Masao Kanamitsu et al. "NCEP-DOE AMIP-II reanalysis (R-2)". In: *Bulletin of the American Meteorological Society* 83.11 (2002), pp. 1631–1644. ISSN: 00030007. DOI: 10.1175/bams-83-11-1631.

[135] Gayatri Kathayat et al. "Interannual oxygen isotope variability in Indian summer monsoon precipitation reflects changes in moisture sources". In: *Communications Earth & Environment* 2.1 (2021), pp. 1–10. DOI: 10.1038/s43247-021-00165-z.

[136] Richard W Katz and Barbara G Brown. "Extreme events in a changing climate: Variability is more important than averages". In: *Climatic Change* 21.3 (1992), pp. 289–302. ISSN: 1573-1480. DOI: 10.1007/BF00139728.

[137] Georg Kaufmann. "Stalagmite growth and palaeo-climate: the numerical perspective". In: *Earth and Planetary Science Letters* 214.1 (2003), pp. 251–266. ISSN: 0012-821X. DOI: https://doi.org/10.1016/S0012-821X(03)00369-8.

[138] Nikita Kaushal et al. "The Indian Summer Monsoon from a Speleothem d18O Perspective—A Review". In: *Quaternary* 1.3 (2018). ISSN: 2571-550X. DOI: 10.3390/quat1030029.

[139] Kenji Kawamura et al. "State dependence of climatic instability over the past 720,000 years from Antarctic ice cores and climate modeling". In: *Science Advances* 3.2 (2017), e1600446. DOI: 10.1126/sciadv.1600446.

[140] Carol Kendall and Eric A Caldwell. "Chapter 2 - Fundamentals of Isotope Geochemistry". In: *Fundamentals of Isotope Geochemistry*. Amsterdam: Elsevier, 1998, pp. 51–86. ISBN: 978-0-444-81546-0. DOI: 10.1016/B978-0-444-81546-0.50009-4.

[141] Douglas J. Kennett et al. "Development and Disintegration of Maya Political Systems in Response to Climate Change". In: *Science* 338.6108 (2012), pp. 788–791. ISSN: 0036-8075. DOI: 10.1126/science.1226299.

[142] S. Khatiwala, M. Visbeck, and P. Schlosser. "Age tracers in an ocean GCM". In: *Deep Sea Research Part I: Oceanographic Research Papers* 48.6 (2001), pp. 1423–1441. ISSN: 0967-0637. DOI: https://doi.org/10.1016/S0967-0637(00)00094-7.

[143] Yeon-Hee Kim et al. "Attribution of the local Hadley cell widening in the Southern Hemisphere". In: *Geophysical Research Letters* 44.2 (2017), pp. 1015–1024.

[144] T. Kluge et al. "Dating cave drip water by tritium". In: *Journal of Hydrology* 394.3-4 (2010), pp. 396–406. ISSN: 00221694. DOI: 10.1016/j.jhydrol.2010.09.015.

[145] T. Kluge et al. "Reconstruction of drip-water d18O based on calcite oxygen and clumped isotopes of speleothems from Bunker Cave (Germany)". In: *Climate of the Past* 9.1 (2013), pp. 377–391. ISSN: 18149324. DOI: 10.5194/cp-9-377-2013.

[146] Reto Knutti et al. "Challenges in Combining Projections from Multiple Climate Models". In: *Journal of Climate* 23.10 (2010), pp. 2739 –2758. DOI: 10.1175/2009JCLI3361.1.

[147] K.E Kohfeld and S.P Harrison. "How well can we simulate past climates? Evaluating the models using global palaeoenvironmental datasets". In: *Quaternary Science Reviews* 19.1 (2000), pp. 321–346. ISSN: 0277-3791. DOI: https://doi.org/10.1016/S0277-3791(99)00068-2.

[148] B. L. Konecky et al. "The Iso2k database: a global compilation of paleo-d18O and dH records to aid understanding of Common Era climate". In: *Earth System Science Data* 12.3 (2020), pp. 2261–2288. DOI: 10.5194/essd-12-2261-2020.

[149] T. Kunz, A. M. Dolman, and T. Laepple. "Estimating the timescale-dependent uncertainty of paleoclimate records – a spectral approach. Part I: Theoretical concept". In: *Climate of the Past Discussions* 2020 (2020), pp. 1–38. DOI: 10.5194/cp-2019-150.

[150] Matthew S. Lachniet. "Climatic and environmental controls on speleothem oxygen-isotope values". In: *Quaternary Science Reviews* 28.5-6 (2009), pp. 412–432. ISSN: 02773791. DOI: 10.1016/j.quascirev.2008.10.021.

[151] T. Laepple and P. Huybers. "Global and regional variability in marine surface temperatures". In: *Geophysical Research Letters* 41.7 (2014), pp. 2528–2534. ISSN: 19448007. DOI: 10.1002/2014GL059345.

[152] T. Laepple and P. Huybers. "Ocean surface temperature variability: Large model–data differences at decadal and longer periods". In: *Proceedings of the National Academy of Sciences* 111.47 (2014), pp. 16682–16687. ISSN: 0027-8424. DOI: 10.1073/pnas.1412077111.

[153] T. Laepple et al. "On the similarity and apparent cycles of isotopic variations in East Antarctic snow pits". In: *The Cryosphere* 12.1 (2018), pp. 169–187. DOI: 10.5194/tc-12-169-2018.

[154] J Richard Landis and Gary G Koch. "The measurement of observer agreement for categorical data". In: *biometrics* (1977), pp. 159–174.

[155] Laura Landrum et al. "Last millennium climate and its variability in CCSM4". In: *Journal of Climate* 26.4 (2013), pp. 1085–1111. ISSN: 08948755. DOI: 10.1175/JCLI-D-11-00326.1.

[156] P. M. Langebroek, M. Werner, and G. Lohmann. "Climate information imprinted in oxygen-isotopic composition of precipitation in Europe". In: *Earth and Planetary Science Letters* 311.1-2 (2011), pp. 144–154. ISSN: 0012821X. DOI: 10.1016/j.epsl.2011.08.049.

[157] Stein-Erik Lauritzen and Joyce Lundberg. "Calibration of the speleothem delta function: an absolute temperature record for the Holocene in northern Norway". In: *The Holocene* 9.6 (1999), pp. 659–669.

[158] Judith Lean. "Calculations of Solar Irradiance: monthly means from 1882 to 2008, annual means from 1610 to 2008". In: 1998 (2009), pp. 1–4. DOI: 10.1007/s00159-004.

[159] F. A. Lechleitner et al. "Climatic and in-cave influences on δ18O and δ13C in a stalagmite from northeastern India through the last deglaciation". In: *Quaternary Research* 88.3 (2017), 458–471. DOI: 10.1017/qua.2017.72.

[160] F. A. Lechleitner et al. "Stalagmite carbon isotopes suggest deglacial increase in soil respiration in western Europe driven by temperature change". In: *Climate of the Past* 17.5 (2021), pp. 1903–1918. DOI: 10.5194/cp-17-1903-2021.

[161] F. A. Lechleitner et al. "The Potential of Speleothems from Western Europe as Recorders of Regional Climate: A Critical Assessment of the SISAL Database". In: *Quaternary* 1.3 (2018), p. 30. ISSN: 2571-550X. DOI: 10.3390/quat1030030.

[162] Allegra N. Legrande and Kevin J. Anchukaitis. "Volcanic eruptions and climate". In: *PAGES Magazine* 23.2 (2015).

[163] S C Lewis and A N Legrande. "Stability of ENSO and its tropical Pacific teleconnections over the Last Millennium". In: *Climate of the Past* 11.10 (2015), pp. 1347–1360. ISSN: 18149332. DOI: 10.5194/cp-11-1347-2015.

[164] Xichen Li et al. "Tropical teleconnection impacts on Antarctic climate changes". In: *Nature Reviews Earth & Environment* 2.10 (2021), pp. 680–698. DOI: 10.1038/s43017-021-00204-5.

[165] Zhengyu Liu et al. "The Holocene temperature conundrum". In: *Proceedings of the National Academy of Sciences* 111.34 (2014), E3501–E3505.

[166] G. Lohmann et al. "A model& data comparison of the Holocene global sea surface temperature evolution". In: *Climate of the Past* 9.4 (2013), pp. 1807–1839. DOI: 10.5194/cp-9-1807-2013.

[167] G. Lohmann et al. "Simulated European stalagmite record and its relation to a quasi-decadal climate mode". In: *Climate of the Past* 9.1 (2013), pp. 89–98. ISSN: 18149324. DOI: 10.5194/cp-9-89-2013.

[168] Mahjoor Ahmad Lone et al. "Speleothem based 1000-year high resolution record of Indian monsoon variability during the last deglaciation". In: *Palaeogeography, Palaeoclimatology, Palaeoecology* 395 (2014), pp. 1–8. ISSN: 0031-0182. DOI: https://doi.org/10.1016/j.palaeo.2013.12.010.

[169] Jason A Lowe et al. "UK Climate Projections science report: Marine and coastal projections". In: (2009).

[170] Daniel P. Lowry and Carrie Morrill. "Is the Last Glacial Maximum a reverse analog for future hydroclimate changes in the Americas?" In: *Climate Dynamics* 52.7 (2019), pp. 4407–4427. DOI: 10.1007/s00382-018-4385-y.

[171] C. MacFarling Meure et al. "Law Dome CO2, CH4 and N2O ice core records extended to 2000 years BP". In: *Geophysical Research Letters* 33.14 (2006). ISSN: 00948276. DOI: 10.1029/2006GL026152.

[172] Shaun A Marcott et al. "A reconstruction of regional and global temperature for the past 11,300 years." In: *Science (New York, N.Y.)* 339.6124 (2013), pp. 1198–201. ISSN: 1095-9203. DOI: 10.1126/science.1228026.

[173] G Marland, T A Boden, and R J Andres. *Global, Regional, and National Fossil Fuel CO2 Emissions. In Trends: A Compendium of Data on Global Change*. Tech. rep. Oak Ridge, Tenn., U.S.A.: Carbon Dioxide Information Analysis Center, Oak Ridge National Laboratory, U.S. Department of Energy, 2003.

[174] John Marshall and R Alan Plumb. *Atmosphere, Ocean and Climate Dynamics: An Introductory Text (International Geophysics)*. 2007.

[175] S. J. Marsland et al. "The Max-Planck-Institute global ocean/sea ice model with orthogonal curvilinear coordinates". In: *Ocean Modelling* 5.2 (2002), pp. 91–127. ISSN: 14635003. DOI: 10.1016/S1463-5003(02)00015-X.

[176] V. Masson-Delmotte et al. "Information from paleoclimate archives". In: *Climate change 2013: the physical science basis: Contribution of Working Group I to the Fifth Assessment Report of the Intergovernmental Panel on Climate Change*. Cambridge University Press, 2013, pp. 383–464.

[177] V. Masson-Delmotte et al. "Past and future polar amplification of climate change: climate model intercomparisons and ice-core constraints". In: *Climate Dynamics* 26.5 (2006), pp. 513–529.

[178] V. Masson-Delmotte et al. "Summary for Policymakers". In: *Climate Change 2021: The Physical Science Basis. Contribution of Working Group I to the Sixth Assessment Report of the Intergovernmental Panel on Climate Change*. Cambridge University Press, 2021, pp. 383–464.

[179] J. M. McCrea. "On the isotopic chemistry of carbonates and a paleotemperature scale". In: *The Journal of Chemical Physics* 18.6 (1950), pp. 849–857. ISSN: 00219606. DOI: 10.1063/1.1747785.

[180] F. McDermott. "Palaeo-climate reconstruction from stable isotope variations in speleothems: A review". In: *Quaternary Science Reviews* 23.7-8 (2004), pp. 901–918. ISSN: 02773791. DOI: 10.1016/j.quascirev.2003.06.021.

[181] F. McDermott, D P Mattey, and C Hawkesworth. "Centennial-scale holocene climate variability revealed by a high-resolution speleothem δ18O record from SW Ireland". In: *Science* 294.5545 (2001), pp. 1328–1331. ISSN: 00368075. DOI: 10.1126/science.1063678.

[182] Martín Medina-Elizalde et al. "High-resolution speleothem record of precipitation from the Yucatan Peninsula spanning the Maya Preclassic Period". In: *Global and Planetary Change* 138 (2016). Climate Change and Archaeology in Mesoamerica: A Mirror for the Anthropocene, pp. 93–102. ISSN: 0921-8181. DOI: https://doi.org/10.1016/j.gloplacha.2015.10.003.

[183] North Greenland Ice Core Project members et al. "High resolution record of Northern Hemisphere climate extending into the last interglacial period". In: *Nature* 431.7005 (2004), pp. 147–151.

[184] M Midhun, S Stevenson, and JE Cole. "Oxygen isotopic signatures of major climate modes and implications for detectability in speleothems". In: *Geophysical Research Letters* 48.1 (2021), e2020GL089515.

[185] Glenn A. Milne, Jerry X. Mitrovica, and Daniel P. Schrag. "Estimating past continental ice volume from sea-level data". In: *Quaternary Science Reviews* 21.1 (2002). EPILOG, pp. 361–376. ISSN: 0277-3791. DOI: https://doi.org/10.1016/S0277-3791(01)00108-1.

[186] Colin P Morice et al. "Quantifying uncertainties in global and regional temperature change using an ensemble of observational estimates: The HadCRUT4 data set". In: *Journal of Geophysical Research Atmospheres* 117.8 (2012), pp. 1–22. ISSN: 01480227. DOI: 10.1029/2011JD017187.

[187] G. E. Moseley et al. "Speleothem record of mild and wet mid-Pleistocene climate in northeast Greenland". In: *Science Advances* 7.13 (2021), eabe1260. DOI: 10.1126/sciadv.abe1260.

[188] Raimund Muscheler et al. "Solar activity during the last 1000 yr inferred from radionuclide records". In: *Quaternary Science Reviews* 26.1-2 (2007), pp. 82–97. ISSN: 02773791. DOI: 10.1016/j.quascirev.2006.07.012.

[189] Raimund Muscheler et al. "The Revised Sunspot Record in Comparison to Cosmogenic Radionuclide-Based Solar Activity Reconstructions". In: *Solar Physics* 291.9-10 (2016), pp. 3025–3043. ISSN: 1573093X. DOI: 10.1007/s11207-016-0969-z.

[190] MaryLynn Musgrove et al. "Geochronology of late Pleistocene to Holocene speleothemsfrom central Texas: Implications for regional paleoclimate". In: *Geological Society of America Bulletin* 113.12 (2001), pp. 1532–1543.

[191] U Neff et al. "Strong coherence between solar variability and the monsoon in Oman between 9 and 6 kyr ago". In: *Nature* 411.6835 (2001), pp. 290–293. ISSN: 00280836. DOI: 10.1038/35077048.

[192] Raphael Neukom et al. "No evidence for globally coherent warm and cold periods over the preindustrial Common Era". In: *Nature* 571.7766 (2019), pp. 550–554. DOI: 10.1038/s41586-019-1401-2.

[193] Valdir F. Novello. personal communication. Mar. 17, 2022.

[194] Valdir F. Novello et al. "Investigating d13C values in stalagmites from tropical South America for the last two millennia". In: *Quaternary Science Reviews* 255 (2021), p. 106822. ISSN: 0277-3791. DOI: https://doi.org/10.1016/j.quascirev.2021.106822.

[195] Valdir F. Novello et al. "Vegetation and environmental changes in tropical South America from the last glacial to the Holocene documented by multiple cave sediment proxies". In: *Earth and Planetary Science Letters* 524 (2019), p. 115717. ISSN: 0012-821X. DOI: https://doi.org/10.1016/j.epsl.2019.115717.

[196] Jesse Nusbaumer et al. "Evaluating hydrological processes in the Community Atmosphere Model Version 5 (CAM5) using stable isotope ratios of water". In: *Journal of Advances in Modeling Earth Systems* 9.2 (2017), pp. 949–977. DOI: https://doi.org/10.1002/2016MS000839.

[197] Matthew B. Osman et al. "Globally resolved surface temperatures since the Last Glacial Maximum". In: *Nature* 599.7884 (2021), pp. 239–244. DOI: 10.1038/s41586-021-03984-4.

[198] Bette L Otto-Bliesner et al. "Climate variability and change since 850 CE: An ensemble approach with the Community Earth System Model". In: *Bulletin of the American Meteorological Society* 97.5 (2016), pp. 735–754.

[199] Bette L. Otto-Bliesner et al. "Last Glacial Maximum and Holocene Climate in CCSM3". In: *Journal of Climate* 19.11 (2006), pp. 2526 –2544. DOI: 10.1175/JCLI3748.1.

[200] R.A. Owen, C C Day, and G M Henderson. "CaveCalc: a new model for speleothem chemistry & isotopes". In: *Computers and Geosciences* (2018).

[201] R.A. Owen et al. "Calcium isotopes in caves as a proxy for aridity: Modern calibration and application to the 8.2 kyr event". In: *Earth and Planetary Science Letters* 443 (2016), pp. 129–138. ISSN: 0012-821X. DOI: https://doi.org/10.1016/j.epsl.2016.03.027.

[202] PAGES2k-Consortium. "Consistent multidecadal variability in global temperature reconstructions and simulations over the Common Era". In: *Nature Geoscience* 12.8 (2019), pp. 643–649. ISSN: 1752-0894. DOI: 10.1038/s41561-019-0400-0.

[203] PAGESHydro2k-Consortium. "Comparing proxy and model estimates of hydroclimate variability and change over the Common Era". In: *Climate of the Past* 13.12 (2017), pp. 1851–1900. DOI: 10.5194/cp-13-1851-2017.

[204] A K Pardaens et al. "Freshwater transports in HadCM3". In: *Climate Dynamics* 21.2 (2003), pp. 177–195. ISSN: 09307575. DOI: 10.1007/s00382-003-0324-6.

[205] S. E. Parker et al. "A data–model approach to interpreting speleothem oxygen isotope records from monsoon regions". In: *Climate of the Past* 17.3 (2021), pp. 1119–1138. DOI: 10.5194/cp-17-1119-2021.

[206] S. E. Parker et al. "A data-model approach to interpreting speleothem oxygen isotope records from monsoon regions on orbital timescales". In: *Climate of the Past Discussions* 2020 (2020), pp. 1–30. DOI: 10.5194/cp-2020-78.

[207] Judson W Partin et al. "Millennial-scale trends in west Pacific warm pool hydrology since the Last Glacial Maximum". In: *Nature* 449.7161 (2007), pp. 452–455. ISSN: 14764687. DOI: 10.1038/nature06164.

[208] J Paul, F Fortuin, and H Kélder. "An ozone climatology based on ozonesonde and satellite measurements". In: *Journal of Geophysical Research Atmospheres* 103 (1998), pp. 31709–31734. ISSN: 01480227. DOI: 10.1029/1998jd200008.

[209] PMIP3. *PMIP3 Experimental Design*. https://wiki.lsce.ipsl.fr/pmip3/doku.php. Last accessed: 2022-04-04.

[210] Daniela Polag et al. "Stable isotope fractionation in speleothems: Laboratory experiments". In: *Chemical Geology* 279.1 (2010), pp. 31–39. ISSN: 0009-2541. DOI: https://doi.org/10.1016/j.chemgeo.2010.09.016.

[211] J. Pongratz et al. "A reconstruction of global agricultural areas and land cover for the last millennium". In: *Global Biogeochemical Cycles* 22.3 (2008). ISSN: 08866236. DOI: 10.1029/2007GB003153.

[212] V. D. Pope et al. "The impact of new physical parametrizations in the Hadley Centre climate model: HadAM3". In: *Climate Dynamics* 16.2-3 (2000), pp. 123–146. ISSN: 14320894. DOI: 10.1007/s003820050009.

[213] R Core Team. *R: A Language and Environment for Statistical Computing*. R Foundation for Statistical Computing. Vienna, Austria, 2020. URL: https://www.R-project.org/.

[214] Christopher Bronk Ramsey. "Bayesian analysis of radiocarbon dates". In: *Radiocarbon* 51.1 (2009), pp. 337–360. ISSN: 00338222. DOI: 10.1017/s0033822200033865.

[215] David A Randall et al. "Climate models and their evaluation". In: *Climate change 2007: The physical science basis. Contribution of Working Group I to the Fourth Assessment Report of the IPCC (FAR)*. Cambridge University Press, 2007, pp. 589–662.

[216] Sune Olander Rasmussen, Anders Svensson, and Mai Winstrup. "State of the art of ice core annual layer dating". In: *Pages Mag* 22 (2014), pp. 26–27.

[217] K Rehfeld and J Kurths. "Similarity estimators for irregular and age-uncertain time series". In: *Climate of the Past* (2014), pp. 107–122. DOI: 10.5194/cp-10-107-2014.

[218] K. Rehfeld et al. "Assessing performance and seasonal bias of pollen-based climate reconstructions in a perfect model world". In: *Climate of the Past* 12.12 (2016), pp. 2255–2270. ISSN: 18149332. DOI: 10.5194/cp-12-2255-2016.

[219] K Rehfeld et al. "Comparison of correlation analysis techniques for irregularly sampled time series". In: *Nonlinear Processes in Geophysics* (2011), pp. 389–404. DOI: 10.5194/npg-18-389-2011.

[220] K. Rehfeld et al. "Golbal paterns of declining temperature variability from the Last Glacial Maximum to the Holocene". In: *Nature* 554 (2018), pp. 356–359. ISSN: 0028-0836. DOI: 10.1038/nature25454.

[221] K. Rehfeld et al. "Late Holocene Asian summer monsoon dynamics from small but complex networks of paleoclimate data". In: *Climate Dynamics* 41.1 (2013), pp. 3–19. ISSN: 09307575. DOI: 10.1007/s00382-012-1448-3.

[222] K. Rehfeld et al. "Variability of surface climate in simulations of past and future". In: *Earth System Dynamics* 11.2 (2020), pp. 447–468. DOI: 10.5194/esd-11-447-2020.

[223] Harriet E Ridley et al. "Aerosol forcing of the position of the intertropical convergence zone since AD 1550". In: *Nature Geoscience* 8.3 (2015), pp. 195–200.

[224] Dana Felicitas Christine Riechelmann et al. "Monitoring Bunker Cave (NW Germany): A prerequisite to interpret geochemical proxy data of speleothems from this site". In: *Journal of Hydrology* 409.3-4 (2011), pp. 682–695. ISSN: 00221694. DOI: 10.1016/j.jhydrol.2011.08.068.

[225] Camille Risi et al. "Process-evaluation of tropospheric humidity simulated by general circulation models using water vapor isotopic observations: 2. Using isotopic diagnostics to understand the mid and upper tropospheric moist bias in the tropics and subtropics". In: *Journal of Geophysical Research Atmospheres* 117.5 (2012), n/a–n/a. ISSN: 01480227. DOI: 10.1029/2011JD016623.

[226] Camille Risi et al. "Process-evaluation of tropospheric humidity simulated by general circulation models using water vapor isotopologues: 1. Comparison between models and observations". In: *Journal of Geophysical Research Atmospheres* 117.5 (2012), n/a–n/a. ISSN: 01480227. DOI: 10.1029/2011JD016621.

[227] Alan Robock. "Internally and Externally Caused Climate Change". In: *Journal of Atmospheric Sciences* 35.6 (1978), pp. 1111 –1122. DOI: 10.1175/1520-0469(1978)035<1111:IAECCC>2.0.CO;2.

[228] E Roeckner et al. *The Atmospheric General Circulation Model ECHAM5. Part I: Model description*. Tech. rep. Hamburg, Germany: Max Planck Institute for Meteorology, 2003.

[229] C. M. Roesch. "Investigating speleothem growth rates in glacial versus nterglacial climate". Master Thesis. MA thesis. Heidelberg University: Heidelberg University, 2020.

[230] C. M. Roesch and K. Rehfeld. "Automatising construction and evaluation of age-depth models for hundereds of speleothems". In: *9th International Workshop on Climate Informatics* October (2019).

[231] Christopher S Romanek, Ethan L Grossman, and John W Morse. "Carbon isotopic fractionation in synthetic aragonite and calcite: Effects of temperature and precipitation rate". In: *Geochimica et Cosmochimica Acta* 56.1 (1992), pp. 419–430. ISSN: 0016-7037. DOI: https://doi.org/10.1016/0016-7037(92)90142-6.

[232] Douchko Romanov, Georg Kaufmann, and Wolfgang Dreybrodt. "Modeling stalagmite growth by first principles of chemistry and physics of calcite precipitation". In: *Geochimica et Cosmochimica Acta* 72.2 (2008), pp. 423–437. ISSN: 0016-7037. DOI: https://doi.org/10.1016/j.gca.2007.09.038.

[233] Kazimierz Rozanski, Luis Araguãs-Araguãs, and Roberto Gonfiantini. "Relation between long-term trends of oxygen-18 isotope composition of precipitation and climate". In: *Science* 258.5084 (1992), pp. 981–985. ISSN: 00368075. DOI: 10.1126/science.258.5084.981.

[234] M. F. Sánchez Goñi et al. "The ACER pollen and charcoal database: a global resource to document vegetation and fire response to abrupt climate changes during the last glacial period". In: *Earth System Science Data* 9.2 (2017), pp. 679–695. DOI: 10.5194/essd-9-679-2017.

[235] G. A. Schmidt et al. "Climate forcing reconstructions for use in PMIP simulations of the last millennium (v1.0)". In: *Geoscientific Model Development* 4.1 (2011), pp. 33–45. DOI: 10.5194/gmd-4-33-2011.

[236] G. A. Schmidt et al. "Climate forcing reconstructions for use in PMIP simulations of the Last Millennium (v1.1)". In: *Geoscientific Model Development* 5.1 (2012), pp. 185–191. ISSN: 1991959X. DOI: 10.5194/gmd-5-185-2012.

[237] G. A. Schmidt et al. "Configuration and assessment of the GISS ModelE2 contributions to the CMIP5 archive". In: *Journal of Advances in Modeling Earth Systems* 6.1 (2014), pp. 141–184. ISSN: 19422466. DOI: 10.1002/2013MS000265.

[238] G. A. Schmidt et al. "Present-day atmospheric simulations using GISS ModelE: Comparison to in situ, satellite, and reanalysis data". In: *Journal of Climate* 19.1 (2006), pp. 153–192. ISSN: 08948755. DOI: 10.1175/JCLI3612.1.

[239] Gavin A. Schmidt et al. "Modeling atmospheric stable water isotopes and the potential for constraining cloud processes and stratosphere-troposphere water exchange". In: *Journal of Geophysical Research Atmospheres* 110.21 (2005), pp. 1–15. ISSN: 01480227. DOI: 10.1029/2005JD005790.

[240] R. Schneider et al. "A reconstruction of atmospheric carbon dioxide and its stable carbon isotopic composition from the penultimate glacial maximum to the last glacial inception". In: *Climate of the Past* 9.6 (2013), pp. 2507–2523. DOI: 10.5194/cp-9-2507-2013.

[241] D. Scholz and D. Hoffmann. "230Th/U-dating of fossil corals and speleothems". In: *Quat. Sci. J* 57.1 (2008), p. 129.

[242] D. Scholz and D. L. Hoffmann. "StalAge - An algorithm designed for construction of speleothem age models". In: *Quaternary Geochronology* 6.3-4 (2011), pp. 369–382. ISSN: 18711014. DOI: 10.1016/j.quageo.2011.02.002.

[243] D. Scholz et al. "A comparison of different methods for speleothem age modelling". In: *Quaternary Geochronology* 14 (2012), pp. 94–104. ISSN: 1871-1014. DOI: https://doi.org/10.1016/j.quageo.2012.03.015.

[244] D. Scholz et al. "Holocene climate variability in north-eastern Italy: potential influence of the NAO and solar activity recorded by speleothem data". In: *Climate of the Past* 8.4 (2012), pp. 1367–1383. DOI: 10.5194/cp-8-1367-2012.

[245] Andrew P Schurer, Simon F B Tett, and Gabriele C Hegerl. "Small influence of solar variability on climate over the past millennium". In: *Nature Geoscience* 7.2 (2014), pp. 104–108. ISSN: 17520894. DOI: 10.1038/ngeo2040.

[246] Henry P Schwarcz et al. "Stable isotope studies of fluid inclusions in speleothems and their paleoclimatic significance". In: *Geochimica et Cosmochimica Acta* 40.6 (1976), pp. 657–665. ISSN: 0016-7037. DOI: https://doi.org/10.1016/0016-7037(76)90111-3.

[247] K. Seftigen et al. "Hydroclimate variability in Scandinavia over the last millennium – insights from a climate model–proxy data comparison". In: *Climate of the Past* 13.12 (2017), pp. 1831–1850. DOI: 10.5194/cp-13-1831-2017.

[248] PR Shukla et al. "IPCC, 2019: Climate Change and Land: an IPCC special report on climate change, desertification, land degradation, sustainable land management, food security, and greenhouse gas fluxes in terrestrial ecosystems". In: (2019).

[249] Michael Sigl et al. "Insights from Antarctica on volcanic forcing during the Common Era". In: *Nature Climate Change* 4.8 (2014), pp. 693–697.

[250] L. C. Sime et al. "Antarctic isotopic thermometer during a CO2 forced warming event". In: *Journal of Geophysical Research Atmospheres* 113.24 (2008), pp. 1–16. ISSN: 01480227. DOI: 10.1029/2008JD010395.

[251] L. C. Sime et al. "Evidence for warmer interglacials in East Antarctic ice cores". In: *Nature* 462.7271 (2009), pp. 342–345. ISSN: 00280836. DOI: 10.1038/nature08564.

[252] L. C. Sime et al. "Southern Hemisphere westerly wind changes during the Last Glacial Maximum: Model-data comparison". In: *Quaternary Science Reviews* (2013). ISSN: 02773791. DOI: 10.1016/j.quascirev.2012.12.008.

[253] Jesper Sjolte et al. "Seasonal reconstructions coupling ice core data and an isotope-enabled climate model - Methodological implications of seasonality, climate modes and selection of proxy data". In: *Climate of the Past* 16.5 (2020), pp. 1737–1758. ISSN: 18149332. DOI: 10.5194/cp-16-1737-2020.

[254] Jesper Sjolte et al. "Solar and volcanic forcing of North Atlantic climate inferred from a process-based reconstruction". In: *Climate of the Past* 14.8 (2018), pp. 1179–1194. ISSN: 18149332. DOI: 10.5194/cp-14-1179-2018.

[255] Haijun Song et al. "Thresholds of temperature change for mass extinctions". In: *Nature Communications* 12.1 (2021), p. 4694. DOI: 10.1038/s41467-021-25019-2.

[256] Michael Staubwasser et al. "Climate change at the 4.2 ka BP termination of the Indus valley civilization and Holocene south Asian monsoon variability". In: *Geophysical Research Letters* 30.8 (2003).

[257] Nathan J. Steiger et al. "Assimilation of Time-Averaged Pseudoproxies for Climate Reconstruction". In: *Journal of Climate* 27.1 (2014), pp. 426 –441. DOI: 10.1175/JCLI-D-12-00693.1.

[258] F Steinhilber, J Beer, and C Fröhlich. "Total solar irradiance during the Holocene". In: *Geophysical Research Letters* 36.19 (2009), pp. 1–5. ISSN: 00948276. DOI: 10.1029/2009GL040142.

[259] Graeme L Stephens et al. "Dreary state of precipitation in global models". In: *Journal of Geophysical Research: Atmospheres* 115.D24 (2010).

[260] S. Stevenson et al. "Volcanic Eruption Signatures in the Isotope-Enabled Last Millennium Ensemble". In: *Paleoceanography and Paleoclimatology* 34.8 (2019), pp. 1534–1552. ISSN: 25724525. DOI: 10.1029/2019PA003625.

[261] Heather Stoll et al. "Interpretation of orbital scale variability in mid-latitude speleothem d18O: Significance of growth rate controlled kinetic fractionation effects". In: *Quaternary Science Reviews* 127 (2015). Novel approaches to and new insights from speleothem-based climate reconstructions, pp. 215–228. ISSN: 0277-3791. DOI: https://doi.org/10.1016/j.quascirev.2015.08.025.

[262] Heather Stoll et al. "Paleoclimate and growth rates of speleothems in the northwestern Iberian Peninsula over the last two glacial cycles". In: *Quaternary Research* 80.2 (2013), 284–290. DOI: 10.1016/j.yqres.2013.05.002.

[263] C. Sturm, Q. Zhang, and D. Noone. "An introduction to stable water isotopes in climate models: Benefits of forward proxy modelling for paleoclimatology". In: *Climate of the Past* 6.1 (2010), pp. 115–129. ISSN: 18149332. DOI: 10.5194/cp-6-115-2010.

[264] Zhe Sun et al. "Potential ENSO effects on the oxygen isotope composition of modern speleothems: Observations from Jiguan Cave, central China". In: *Journal of Hydrology* 566 (2018), pp. 164–174. ISSN: 0022-1694. DOI: https://doi.org/10.1016/j.jhydrol.2018.09.015.

[265] AS Talma and John C Vogel. "Late Quaternary paleotemperatures derived from a speleothem from Cango caves, Cape province, South Africa". In: *Quaternary Research* 37.2 (1992), pp. 203–213.

[266] Liangcheng Tan et al. "Centennial- to decadal-scale monsoon precipitation variability in the semi-humid region, northern China during the last 1860 years: Records from stalagmites in Huangye Cave". In: *The Holocene* 21.2 (2011), pp. 287–296. DOI: 10.1177/0959683610378880.

[267] Kuilian Tang and Xiahong Feng. "The effect of soil hydrology on the oxygen and hydrologen isotopic compositions of plants' source water". In: *Earth and Planetary Science Letters* 185.3-4 (2001), pp. 355–367. ISSN: 0012821X. DOI: 10.1016/S0012-821X(00)00385-X.

[268] Karl E Taylor, Ronald J Stouffer, and Gerald A Meehl. "An overview of CMIP5 and the experiment design". In: *Bulletin of the American meteorological Society* 93.4 (2012), pp. 485–498.

[269] Frank Thomas. "Grundlagen pflanzenökologischer Arbeitsmethoden". In: *Grundzüge der Pflanzenökologie*. Berlin, Heidelberg: Springer Berlin Heidelberg, 2018, pp. 60–77. ISBN: 978-3-662-54139-5. DOI: 10.1007/978-3-662-54139-5_1.

[270] DM Thompson et al. "Comparison of observed and simulated tropical climate trends using a forward model of coral δ 18O". In: *Geophysical Research Letters* 38.14 (2011).

[271] L. G. Thompson et al. "Annually Resolved Ice Core Records of Tropical Climate Variability over the Past 1800 Years". In: *Science* 340.6135 (2013), pp. 945–950. DOI: 10.1126/science.1234210.

[272] Charles Warren Thornthwaite and John Russell Mather. *Instructions and tables for computing potential evapotranspiration and the water balance*. Tech. rep. Centerton, 1957.

[273] Jessica E. Tierney et al. "Glacial cooling and climate sensitivity revisited". In: *Nature* 584.7822 (Aug. 2020), pp. 569–573. DOI: 10.1038/s41586-020-2617-x.

[274] Jessica E. Tierney et al. "Past climates inform our future". In: *Science* 370.6517 (2020), eaay3701. DOI: 10.1126/science.aay3701.

[275] Axel Timmermann and Tobias Friedrich. "Late Pleistocene climate drivers of early human migration". In: *Nature* 538.7623 (2016), pp. 92–95. DOI: 10.1038/nature19365.

[276] J. C. Tindall, P J Valdes, and L C Sime. "Stable water isotopes in HadCM3: Isotopic signature of El Niño-Southern Oscillation and the tropical amount effect". In: *Journal of Geophysical Research Atmospheres* 114.4 (2009), pp. 1–12. ISSN: 01480227. DOI: 10.1029/2008JD010825.

[277] Julia Tindall et al. "Modelling the oxygen isotope distribution of ancient seawater using a coupled ocean-atmosphere GCM: Implications for reconstructing early Eocene climate". In: *Earth and Planetary Science Letters* (2010). ISSN: 0012821X. DOI: 10.1016/j.epsl.2009.12.049.

[278] Pauline C. Treble et al. "Ubiquitous karst hydrological control on speleothem oxygen isotope variability in a global study". In: *Communications Earth & Environment* 3.1 (2022), p. 29. DOI: 10.1038/s43247-022-00347-3.

[279] Darrel M. Tremaine and Philip N. Froelich. "Speleothem trace element signatures: A hydrologic geochemical study of modern cave dripwaters and farmed calcite". In: *Geochimica et Cosmochimica Acta* 121 (2013), pp. 522–545. ISSN: 0016-7037. DOI: https://doi.org/10.1016/j.gca.2013.07.026.

[280] Darrel M. Tremaine, Philip N Froelich, and Yang Wang. "Speleothem calcite farmed in situ: Modern calibration of δ18O and δ13C paleoclimate proxies in a continuously-monitored natural cave system". In: *Geochimica et Cosmochimica Acta* (2011). ISSN: 00167037. DOI: 10.1016/j.gca.2011.06.005.

[281] K. E. Trenberth and D. P. Stepaniak. "Indices of El Niño evolution". In: *Journal of Climate* 14.8 (Apr. 2001), pp. 1697–1701. ISSN: 08948755. DOI: 10.1175/1520-0442(2001)014<1697:LIOENO>2.0.CO;2.

[282] Anastasios A. Tsonis, Kyle L. Swanson, and Paul J. Roebber. "What do networks have to do with climate?" In: *Bulletin of the American Meteorological Society* 87.5 (2006), pp. 585–595. ISSN: 00030007. DOI: 10.1175/BAMS-87-5-585.

[283] L. Tupikina et al. "Characterizing the evolution of climate networks". In: *Nonlinear Processes in Geophysics* 21.3 (2014), pp. 705–711. ISSN: 16077946. DOI: 10.5194/npg-21-705-2014.

[284] Harold C Urey. "Oxygen Isotopes in Nature and in the Laboratory". In: *Science* 108.2810 (1948), pp. 489–496.

[285] Paul J Valdes et al. "The BRIDGE HadCM3 family of climate models: HadCM3@Bristol v1.0". In: *Geoscientific Model Development* 10.10 (2017), pp. 3715–3743. ISSN: 19919603. DOI: 10.5194/gmd-10-3715-2017.

[286] David A. Vasseur et al. "Increased temperature variation poses a greater risk to species than climate warming". In: *Proceedings of the Royal Society B: Biological Sciences* 281.1779 (2014). ISSN: 14712954. DOI: 10.1098/rspb.2013.2612.

[287] Vieira, L. E. A. et al. "Evolution of the solar irradiance during the Holocene". In: *A&A* 531 (2011), A6. DOI: 10.1051/0004-6361/201015843.

[288] Annie Vincens, Yannick Garcin, and Guillaume Buchet. "Influence of rainfall seasonality on African lowland vegetation during the Late Quaternary: pollen evidence from Lake Masoko, Tanzania". In: *Journal of Biogeography* 34.7 (2007), pp. 1274–1288.

[289] B.M. Vinther et al. "Climatic signals in multiple highly resolved stable isotope records from Greenland". In: *Quaternary Science Reviews* 29.3 (2010), pp. 522 –538. ISSN: 0277-3791. DOI: https://doi.org/10.1016/j.quascirev.2009.11.002.

[290] A Wackerbarth et al. "Modelling the delta 18 O value of cave drip water and speleothem calcite". In: *Earth and Planetary Science Letters* 299.3-4 (2010), pp. 387–397. ISSN: 0012-821X. DOI: 10.1016/j.epsl.2010.09.019.

[291] A. Wackerbarth et al. "Simulated oxygen isotopes in cave drip water and speleothem calcite in European caves". In: *Climate of the Past* 8.6 (2012), pp. 1781–1799. DOI: 10.5194/cp-8-1781-2012.

[292] Jessica K. Wang et al. "Hydroclimatic variability in Southeast Asia over the past two millennia". In: *Earth and Planetary Science Letters* 525 (2019), p. 115737. ISSN: 0012-821X. DOI: https://doi.org/10.1016/j.epsl.2019.115737.

[293] Xianfeng Wang et al. "Hydroclimate changes across the Amazon lowlands over the past 45,000 years". In: *Nature* 541.7636 (2017), pp. 204–207. DOI: 10.1038/nature20787.

[294] Y. J. Wang et al. "A High-Resolution Absolute-Dated Late Pleistocene Monsoon Record from Hulu Cave, China". In: *Science* 294.5550 (2001), pp. 2345–2348. DOI: 10.1126/science.1064618.

[295] Y.-M. Wang, J L Lean, and N R Sheeley, Jr. "Modeling the Sun's Magnetic Field and Irradiance since 1713". In: *The Astrophysical Journal* 625.1 (2005), pp. 522–538. DOI: 10.1086/429689.

[296] Sophie F. Warken et al. "Solar forcing of early Holocene droughts on the Yucatán peninsula". In: *Scientific Reports* 11.1 (2021), p. 13885. DOI: 10.1038/s41598-021-93417-z.

[297] M. Werner. "Modelling stable water isotopes: Status and perspectives". In: *EPJ Web of Conferences* 9 (2010), pp. 73–82. ISSN: 2100014X. DOI: 10.1051/epjconf/201009005.

[298] M. Werner et al. "Glacial-interglacial changes in H218O, HDO and deuterium excess-results from the fully coupled ECHAM5/MPI-OM Earth system model". In: *Geoscientific Model Development* 9.2 (2016), pp. 647–670. ISSN: 19919603. DOI: 10.5194/gmd-9-647-2016.

[299] M. Werner et al. "Stable water isotopes in the ECHAM5 general circulation model: Toward high-resolution isotope modeling on a global scale". In: *Journal of Geophysical Research Atmospheres* 116.15 (2011). ISSN: 01480227. DOI: 10.1029/2011JD015681.

[300] P W Williams and D C Ford. "Global distribution of carbonate rocks". In: *Zeitschrift für Geomorphologie Supplementband* 147 (2006), p. 1.

[301] Corinne I. Wong, Jay L. Banner, and MaryLynn Musgrove. "Holocene climate variability in Texas, USA: An integration of existing paleoclimate data and modeling with a new, high-resolution speleothem record". In: *Quaternary Science Reviews* 127 (2015). Novel approaches to and new insights from speleothem-based climate reconstructions, pp. 155–173. ISSN: 0277-3791. DOI: https://doi.org/10.1016/j.quascirev.2015.06.023.

[302] Corinne I. Wong and Daniel O Breecker. "Advancements in the use of speleothems as climate archives". In: *Quaternary Science Reviews* 127 (2015), pp. 1–18. ISSN: 02773791. DOI: 10.1016/j.quascirev.2015.07.019.

[303] Xi Xi. "A Review of Water Isotopes in Atmospheric General Circulation Models: Recent Advances and Future Prospects". In: *International Journal of Atmospheric Sciences* 2014 (2014), pp. 1–16. ISSN: 2314-4122. DOI: 10.1155/2014/250920.

[304] Qingchun Yang et al. "Temperature and rainfall amount effects on hydrogen and oxygen stable isotope in precipitation". In: *Quaternary International* 519 (2019). The 3rd ASQUA Conference (Part II), pp. 25–31. ISSN: 1040-6182. DOI: https://doi.org/10.1016/j.quaint.2019.01.027.

[305] K. Yoshimura et al. "Historical isotope simulation using Reanalysis atmospheric data". In: *Journal of Geophysical Research Atmospheres* 113.19 (2008), p. D19108. ISSN: 01480227. DOI: 10.1029/2008JD010074.

[306] P. Zennaro et al. "Fire in ice: two millennia of boreal forest fire history from the Greenland NEEM ice core". In: *Climate of the Past* 10.5 (2014), pp. 1905–1924. DOI: 10.5194/cp-10-1905-2014.

[307] X. Zhang et al. "Wet–dry status change in global closed basins between the mid-Holocene and the Last Glacial Maximum and its implication for future projection". In: *Climate of the Past* 16.5 (2020), pp. 1987–1998. DOI: 10.5194/cp-16-1987-2020.

[308] Xinping Zhang et al. "GCM simulations of stable isotopes in the water cycle in comparison with GNIP observations over east asia". In: *Acta Meteorologica Sinica* 26.4 (2012), pp. 420–437. ISSN: 08940525. DOI: 10.1007/s13351-012-0403-x.

[309] Jiang Zhu et al. "Reduced ENSO variability at the LGM revealed by an isotope-enabled Earth system model". In: *Geophysical Research Letters* 44.13 (2017), pp. 6984–6992. DOI: https://doi.org/10.1002/2017GL073406.

List of Figures

List of Publications

2021 J. C. Bühler, C. Roesch, M. Kirschner, L. Sime, M. D. Holloway, and K. Rehfeld. Comparison of the oxygen isotope signatures in speleothem records and iHadCM3 model simulations for the last millennium. *Climate of the Past*, 17(3):985-1004, 2021.

2022 J. C. Bühler, J. M. Axelsson, F. A. Lechleitner, J. Fohlmeister, A. N. LeGrande, M. Midhun, J. Sjolte, M. Werner, K. Yoshimura, and K. Rehfeld. Investigating oxygen and carbon isotopic relationships in speleothem records over the last millennium using multiple isotope-enabled climate models. *Climate of the Past Discussions*, 2021:1-37, 2021.

Code to reproduce figures and analyses in this thesis is provided at `https://github.com/paleovar/iHadCM3LastMill` (last accessed: 13 April 2022 [29]) and `https://github.com/paleovar/Supplement_Thesis_JB_2022` (last accessed: 21 April 2022 [30])

Acknowledgment

First and most of all, I would like to thank Prof. Dr. Kira Rehfeld for her patience, her expertise, and her trust in me from the very beginning, even though I started in her group coming from quite a different background. Throughout the last three years, she not only managed the research "rabbit-holes" that I was digging, distinguishing dead-ends from promising treasure routes. She also provided guidance in the maze of the scientific community and made sure that all of us are well-connected and well-prepared on a soft skill level, to eventually be able to find our own way. With each accomplished challenge, she gently pushed me toward the next slightly harder one, while ensuring that I always had a safety net.

I cannot begin to express my thanks to the former STACY, now SPACY, group: to the late Friday night sessions at the otherwise empty institute, to the group hikes throughout the pandemic, to wonderful lunches and coffee breaks, to online conferences that we made fun, to vegan desserts, to teaching during the semester and last minute preparations, to hundreds of abstracts, posters, and presentations that we all polished, to climate change protest signs, and all the extensive political discussions that were usually right before someone's deadline. Especially, I want to thank Dr. Nils Weitzel, who never got tired of explaining statistical methods and tidying up the chaos in my head on possible new analyses, Elisa Ziegler who more than once saved me from a mental break-down and my code from crashing and always had time to just turn around to discuss anything, Beatrice Ellerhoff for a lot of communication input (as writing is just as much part of science as research itself), Moritz Adam who seemed to be able to tirelessly answer all my small questions on all topics within no time or at least knew where to get the answer from, Carla Roesch who we missed dearly after she left us for Scottland for all the speleothem discussions and her patient input on age-depth models, Dr. Jean-Philipp Baudouin for trilingual discussion and for saving all my files when my laptop crashed, Dr. Valdir Novello for so much input on speleothems from a hands-on expert's perspective, Dr. Mathieu Casado for all the discussions over the years and motivation of future work, and Yannick Heiser, Irene Trombini, Claudia Schiavini, Mathurin Choblet, and Laura Fink for their motivation in all of their projects that I had the pleasure to be part of. Research is a group effort and this group with its support is more than I could have wished for.

Chance and common research interest brought me together with Josefine Axelsson, who became a weekly constant throughout my pandemic home office life. Thank you so much for our Monday morning sessions, our discussions and our great project. It was an absolute pleasure working with you. Dr. Franziska Lechleitner, Dr. Jens Fohlmeister, and Prof. Dr. Denis Scholz were always available for discussion and interpretation of speleothem isotopic signatures and age-models and helped in guiding projects towards submission. Dr. Martin Werner provided the ECHAM5-wiso simulation data in multiple set ups, and provided helpful information on simulated isotopic dynamics. Thank you for being part of my supervising team, and the short stay at AWI Bremerhaven that unfortunately got interrupted by the pandemic. Dr. Allegra N. Grande, Dr. Max Holloway, Moritz Kirscher, Dr. Madhavan Midhun, Dr. Jesper Sjolte, and Prof. Dr. Kei

Yoshimura provided me with simulated datasets, which built an essential part of the multi-model comparison project.

I am very thankful for the PhD program of the HGSFP that guided me through my PhD life and their funding toward the final stage. The institute of environmental physics supported me during my complete research life in Heidelberg, in particular Prof. Dr. Werner Aeschbach and my second supervisor Prof. Dr. Norbert Frank. A special thanks goes to the secretaries of both IUP and HGSFP for patiently putting up with the administrative question marks in my head. Thank you to the PAGES community that I am glad Kira introduced me to, especially the SISAL speleothem community with Dr. Laia Comas-Bru, Dr. Yuval Burstyn, and Dr. Nikita Kaushal. Thank you for your discussion, your input, and our fun time in Jerusalem. Also thank you Summer School on Speleothem Science for giving me a kick-start into speleothem research coming from a completely different field.

A huge thank you goes to all of my proof-readers: Bea, Carla, Denis, Elisa, Irene, Joe, Josefine, Markus, Mathi, Mathieu, Mo, Nils, and Valdir - thank you for patiently finding (hopefully) every typo and splitting all the sentences that were too long. And thanks David for the final steps.

My family always supported and enabled me to pursuit this path, and never doubted my choices and abilities, even if I sometimes lacked this confidence. Thank you Opa, I know you would have been proud. Thank you to my aunt Stine and my uncles Stefan and Andi - even as a child, you proved that this is a path worth pursuing and reachable. Finally, all my love goes to Joe. You have been a constant unconditional support and never got tired of encouraging me. If one needs support, the other one will give it. Let's continue doing exactly that.

Declaration of Authorship

I, Janica Carmen Bühler, hereby declare that this thesis "Statistical assessment and modeling of spatio-temporal patterns in speleothem records from the Last Glacial to present day" is the result of my own independent work and makes use of no other sources or materials other than those referenced, and that quotations and paraphrases obtained from the work of others are indicated as such.

Heidelberg, April 22, 2022

_____